VNIVERSITAT DE VALÈNCIA

Cosmological implications of some nonstandard particle physics scenarios

Urbano França

Instituto de Física Corpuscular
Universidad de Valencia - CSIC
Departamento de Física Teórica

A thesis submitted for the degree of

Doctor of Philosophy

on September 2012.

PhD Advisor:
Dr. Sergio Pastor Carpi

À "Dona Nina" e à memória do "Seu Urbano", por estarem sempre comigo, mesmo quando longe. Obrigado! Por tudo!

"Ora (direis) ouvir estrelas! Certo
Perdeste o senso!" E eu vos direi, no entanto,
Que, para ouvi-las, muita vez desperto
E abro as janelas, pálido de espanto...

E conversamos toda a noite, enquanto
A Via Láctea, como um pálio aberto,
Cintila. E, ao vir do Sol, saudoso e em pranto,
Inda as procuro pelo céu deserto.

Direis agora: "Tresloucado amigo!
Que conversas com elas? Que sentido
Tem o que dizem, quando estão contigo?"

E eu vos direi: "Amai para entendê-las!
Pois só quem ama pode ter ouvido
Capaz de ouvir e de entender estrelas."

Olavo Bilac, XIII

Abstract

The standard cosmological model has been very successful in describing the evolution of the Universe from the first seconds until today. However, some challenges still remain concerning the nature of some of its components as well as observationally probing some of the periods of its expansion. In this thesis we discuss what are probably the three least known components of the Universe: neutrinos, dark matter, and dark energy.

In particular, concerning the neutrino sector, we place limits on the relic neutrino asymmetries using some of the latest cosmological data, taking into account the effect of flavor oscillations. We find that the present bounds are still dominated by the limits coming from big bang nucleosynthesis, while the limits on the total neutrino mass from cosmological data are essentially independent of θ_{13}. Moreover, we perform a forecast for Cosmic Origins Explorer, taken as an example of a future cosmic microwave background experiment, and find that it could improve the limits on the total lepton asymmetry. We also consider models of dark energy in which neutrinos interact with the scalar field supposed to be responsible for the acceleration of the Universe, usually implying a variation of the neutrino masses on cosmological time scales. We propose a parameterization for the neutrino mass variation that captures the essentials of those scenarios and allows one to constrain them in a model independent way, that is, without resorting to any particular scalar field model. Using different datasets we show that the ratio of the mass variation of the neutrino mass over the current mass is smaller than $\approx 10^{-2}$ at 95% C.L., totally consistent with no mass variation. Finally, we discuss how observations of the 21-cm line of the atomic hydrogen at the early universe have the potential to probe the unexplored period between the so-called dark ages and the reionization epoch of the Universe, and how it can be used to place limits on particle physics properties, in particular constraints on the mass and self-annihilation cross-section of the dark matter particles.

Resumen

El modelo cosmológico estándar ha tenido un gran éxito en la descripción del Universo desde los primeros segundos de su evolución hasta nuestros días. Sin embargo, todavía quedan desafíos respecto a la naturaleza de algunos de sus componentes, así como observacionalmente probar algunos de los períodos de su evolución. En esta tesis se discuten tres de los componentes probablemente menos comprendidos del Universo: los neutrinos, la materia oscura y la energía oscura.

En particular, en relación al sector de los neutrinos, hallamos los límites a las asimetrías primordiales de neutrinos utilizando algunos de los últimos datos cosmológicos y teniendo en cuenta el efecto de las oscilaciones de sabor. Encontramos que los límites actuales están todavía dominados por las restricciones que vienen de la nucleosíntesis del Big Bang, mientras que las cotas cosmológicas a la masa total de los neutrinos son esencialmente independientes del ángulo de mezcla θ_{13}. Además, llevamos a cabo un pronóstico para el experimento *Cosmic Origins Explorer*, tomado como un ejemplo de un futuro experimento del fondo cósmico de microondas, y encontramos que podría mejorar los límites actuales sobre la asimetría total. También consideramos modelos de energía oscura en los que los neutrinos interactúan con el campo escalar responsable de la aceleración del Universo, lo que por lo general implica una variación de la masa del neutrino en escalas de tiempo cosmológicas. Proponemos una parametrización para la variación de la masa de los neutrinos que captura los elementos esenciales de esos escenarios y que permite poner límites de una manera independiente del modelo, es decir, sin recurrir a ningún modelo particular del campo escalar. Usamos diferentes conjuntos de datos que muestran que la relación entre la variación de la masa de los neutrinos sobre la masa actual es menor que $\approx 10^{-2}$ a 95% C.L., totalmente en acuerdo con una masa que permanece constante. Finalmente, describimos cómo las observaciones de la línea de 21 cm del hidrógeno atómico en el Universo temprano tienen el potencial para sondear el período inexplorado entre la época oscura y la reionización del Universo, y cómo esas observaciones pueden ser utilizadas para poner límites a propiedades de la física de partículas, especialmente sobre la masa y la sección eficaz de auto-aniquilación de las partículas que constituyen la materia oscura.

Acknowledgments

During the course of this PhD I was very lucky: I had the opportunity to meet, work, and become friends with several awesome people that in one way or another made this work possible.

First of all, I am enormously grateful to Sergio Pastor. Besides teaching me everything I know about neutrino cosmology, he was always a source of pragmatic advice and a true mentor. I thank him for sharing his time, knowledge, and projects, what allowed me to work on a variety of areas and with many interesting people. Moreover, his ability to navigate the turbulent waters of practical things behind science is remarkable, and these acknowledgments would double or triple in size if I were to thank him for all his help with bureaucracies and other issues I faced througout the years. I am truly fortunate to have him as an advisor, friend, and also as a running mate.

I am also indebtedly thankful to José Valle for opening the doors of the Astroparticle and High Energy Physics (AHEP) group for me, giving me the possibility to join this fantastic group of people. José is responsible for creating one of the most enjoyable and immensely productive research groups I know of, and I think that anyone who have had the opportunity to be part of AHEP share with me the admiration for what he built. And of course, when we leave the group we all miss the classical "*Échame una manita*" and other typical sentences one listens when having a coffee at "La Cafetería *Valle*ncia". *Obrigado*, Valle!

Working at AHEP so many years gave me the opportunity to interact with many people which made this the best work environment one could wish for (and a place where FIA, *Federación Ificana de Apuestas*, could organize its bets). While

the list would be to big to thank everybody that spent some time here in Valencia, and under the risk of forgetting names, I was particularly lucky to spend my time here with Carolina Arbeláez, Diego Aristizábal, Sofiane Boucenna, Fernando de Campos, Lucho Doramé, Kiko Escrihuela, Andreu Esteban, Martin Hirsch, Massimiliano Lattanzi, Roberto Lineros, Michal Malinsky, Omar Miranda, Laura Molina, Stefano Morisi, Eduardo Peinado, Teguayco Pinto, Werner Porod, Laslo Reichert, Valentina de Romeri, Marco Taoso, Ricard Tomàs, Mariam Tórtola, David Vanegas, and Avelino Vicente. Thank you all for the discussions about physics and (more commonly) about life.

An important part of this thesis was done while visiting the Institute for Theory and Computation (ITC) of the Harvard-Smithsonian Center for Astrophysics (CfA), collaborating with Avi Loeb and Jonathan Pritchard. To say that the scientific atmosphere of the ITC is impressive and exciting would be an understatement, and I am sure that my scientific views and approaches were and will always be profoundly influenced by the experiences I had there. I am most grateful to Avi for giving me the opportunity to spend almost a year and a half at the ITC/CfA, and especially for always finding some time on his extremely busy schedule to discuss projects and give some pieces of advice. Moreover, it would have been impossible to enter this new field of research without the close guidance of Jonathan. He is a brilliant and humble young scientist, and working with him was a great experience that I hope continues for a long time.

While in Cambridge, I was fortunate to meet and become friends with Angélica de Oliveira Costa. Her happiness and good mood, even under stressful times, is contagious, and I am most thankful for her friendship and for the time she took to share her experience and discuss life in general over our traditional *cafezinho* in the afternoons. I miss those coffees, Angélica!

Also in Cambridge, Eric Hallman and Akshay Kulkarni were the best officemates one could wish for, and I still miss the discussions on politics and the sociology of science we had at B-216. Thanks also to Paco Villaescusa, for together we spent some good time untying the knots of the life in Cambridge and of the scientific protocols.

This thesis would be very different (and more probably it would not exist) without my collaborators. I learned a massive amount of interesting physics with them on the topics related and not related to this thesis, and that shaped the way

I think about the Universe. For that, I am grateful to Emanuele Castorina, Massimiliano Lattanzi, Julien Lesgourgues, Avi Loeb, Gianpiero Mangano, Alessandro Melchiorri, Sergio Pastor, and Jonathan Pritchard for all the discussions and for the opportunity to learn from them. Still on the scientific side, Rogerio Rosenfeld has been a mentor since the very first time I entered his office as an undergraduate student looking for a project. He has been a continuous source of advices and suggestions, and I have a lifelong debt with him for that.

Besides the CfA, I have been very fortunate to spend some time in other external research centers in which I could interact with, and learn a lot from, different people. In particular, I would like to thank Gianpiero Mangano, Gennaro Miele, and Ofelia Pisanti for hosting me at Napoli, Julien Lesgourgues for the great time in both Annecy and Lausanne, and Omar Miranda for hosting me during the month I spent at the Cinvestav in Mexico, DF. Thanks also to Omar López-Cruz for his support and help since we met in Mexico last year, and even though we have not worked together yet, I am sure that the future holds lots of mutual interesting projects.

Agradezco también a los funcionarios(as) y secretarios(as) del IFIC y del departamento de Física Teórica de la Universidad de Valencia por proporcionar el apoyo contra la burocracia local. Su ayuda fué crucial para la elaboración de ese trabajo. And, of course, I am most thankful to CSIC for funding my work in Spain through an I3P-JAE fellowship and different projects, as well as the European Particle Physics Latin American Network (EPLANET) for supporting my stay at Cinvestav.

On the personal side, I was blessed with what is, for me, the most amazing and sweet family of the World. No caso da minha mãe, não tenho palavras para agradecer o seu apoio incondicional. Estive mais ausente do que deveria, mas espero que ela saiba que independente da minha presença física ela está sempre no meu coração. Meus irmãos(ãs), sobrinhos(as) e a família em geral são sempre fonte de alegrias (e recentemente, de sobrinhos-netos!), e nunca me deixam esquecer a importância de ser fiel às nossas raízes. Obrigado a todos vocês, e saibam que levo um pedacinho de cada um de vocês comigo! É uma pena que o seu Urbano não possa compartir essa alegria com a gente, mas a lembrança dele, assim como as suas lições, são parte do que fizeram isso possível.

My friends, the ones close and the ones far away, helped maintaining my pseudo-

sanity during those years. In Valencia, besides the AHEPian mentioned before, I'd like to thank Mercedes, my ex-housemates Marta and Sebas, and too many others to be individually named; they gave me a feeling of being at home here. And speaking about home, a huge part of this thesis was written in Bailen 66, and I am very grateful to the residents of the *puerta 2* for allowing me to use their dinner table as an office space. Meus amigos no Brasil, em particular Ricardo Vêncio e os integrantes da "A Saidera", são fontes sem fim de emails sobre os mais diversos assuntos e de infinitas discussões que sempre ajudam a pôr as coisas em perspectiva e ver que existem outras coisas no mundo além da física. Thanks to you all!

Finally, words will inevitably fail to describe my gratitude to Leslie. You brought happiness, tenderness, and love to my life, and you were there to support me at every moment I needed during these last months. Without your smile and sweet eyes the difficulties would have been much larger, and I will never be able to thank you enough for showing me everyday an entirely new, more colorful, way to see the world. As the Irish proverb says, *"When I count my blessings, I count you twice"*. I look forward to a whole Universe of happy moments with you for years to come. *Gracías*, minha princesa!

Publications

This thesis is based on the following publications:

Chapter 3
E. Castorina, U. França, M. Lattanzi, J. Lesgourgues, G. Mangano, A. Melchiorri, and S. Pastor,
Cosmological lepton asymmetry with a nonzero mixing angle θ_{13},
Phys. Rev. D **86**, 023517 (2012), arXiv:1204.2510 [astro-ph.CO]

Chapter 4
U. França, M. Lattanzi, J. Lesgourgues, and S. Pastor,
Model independent constraints on mass-varying neutrino scenarios,
Phys. Rev. D **80**, 083506 (2009), arXiv:0908.0534 [astro-ph.CO]

Chapter 5
U. França, J. R. Pritchard, and A. Loeb,
The global 21 cm signal with dark matter annihilation,
Phys. Rev. D to be submitted (2012)

Papers not discussed in the thesis:

U. França,
Dark energy, curvature and cosmic coincidence,
Phys. Lett. B **641**, 351 (2006), arXiv:astro-ph/0509177 [astro-ph]

Earlier papers:

U. França and R. Rosenfeld,
Age constraints and fine tuning in variable-mass particle models,
Phys. Rev. D **69**, 063517 (2004), arXiv:astro-ph/0308149 [astro-ph]

U. França and R. Rosenfeld,
Fine tuning in quintessence models with exponential potentials,
JHEP **0210**, 015 (2002), arXiv:astro-ph/0206194 [astro-ph]

Contents

List of Figures

List of Tables

1 Introduction

> "And when you look at the sky you know you are looking at stars which are hundreds and thousands of light-years away from you. And some of the stars don't even exist anymore because their light has taken so long to get to us that they are already dead, or they have exploded and collapsed into red dwarfs. And that makes you seem very small, and if you have difficult things in your life it is nice to think that they are what is called negligible, which means they are so small you don't have to take them into account when you are calculating something."
> Mark Haddon, *The Curious Incident of the Dog in the Night-Time*

Cosmology is the science that aims at studying the origin, structure, and evolution of the entire Universe. Such an ambitious goal can only be achieved by taking into account the main physical properties of the Universe at each moment in time. On the other hand, particle physics deals with the properties and interactions of the most elementary and smaller constituents of matter, and in principle one could expect the *very small* to be not relevant in shaping the properties of the *largest scales* of the Universe. However, most of the new and fundamental ideas of the last decades in cosmology came from the sinergy between the sciences of the very small and of the very large: the very small can and *do* play a crucial role when one is calculating and understanding the Universe.

In this thesis, we describe some of our contributions towards understanding how the smaller components of the Universe can shape its global evolution on several cosmological scales and in different ways. In particular, we will discuss three of the most misterious components of the cosmic recipe: neutrinos, dark matter, and

dark energy.

For that, in the first technical chapter, *Big Bang Cosmology*, we describe in some detail the current cosmological model, known nowadays as the Standard Cosmological model, as well as its main evidences and some of its problems. In particular, we will discuss the different epochs that the Universe has been through since the Big Bang, around 13.7 Gyr ago. Initially, during the radiation dominated phase, light nuclei, mostly Hydrogen and Helium, are formed, and neutrinos are known to play a key role in the process of the so-called primordial nucleosynthesis. As the Universe expands, cold matter in the form of baryon and the hypothetical dark matter come to dominate the expansion of the Universe. During this epoch, atoms are formed in the recombination process, releasing the oldest possible picture of the Universe, the cosmic microwave background. This apparent calmness is changed when the first stars and luminous sources form under the influence of gravity, changing once again the behavior of the intergalactic medium. Finally, when the Universe was around half his current age, a new (and poorly understood) component, dark energy, changes the dynamics of its expansion. At this point, the cosmological expansion accelerates, a behavior that might hold forever or not, depending on the nature of this constituent. After discussing those epochs, we close this chapter by discussing the age of the Universe in those different models and the constraints we can place on it.

In the following chapters, we discuss in detail our contributions to understand some of the open problems in this cosmological scenario. In the chapter entitled *Cosmological Lepton Asymmetry*, we study in detail the current limits on leptonic asymmetries stored in the neutrino sector. This is important not only to help illuminating the origin of the matter-antimatter asymmetry in the Universe, but also to understand and constrain the possibility that those asymmetries could play the role of extra radiation that potentially will be precisely probed in the very near future.

In chapter 4, *Mass-Varying Neutrino Models*, we investigate a class of models for the dark energy in which the accelerated expansion of the Universe is driven by a scalar field that interacts with neutrinos, causing the masses of the latter to vary with the cosmological expansion. In particular, we parameterize the mass variation with the goal to study a set of scenarios in a model-independent way, and look for cosmological signals of the mass-variation that could help falsifying

those models. Currently, a few observational options are available for constraining dark energy models, and therefore looking for indirect ways to probe them like we do in this chapter is fundamental to reduce the number of possible candidates or even pinpoint the correct one.

Finally, in the last chapter, *Dark matter and the 21-cm global signal*, we look for potential signals of dark matter annihilation on the highly-redshifted 21-cm line of the Hydrogen atoms. This technique, known as 21-cm cosmology for short, has the potential to be a game-changer for cosmology and astrophysics, because it can open a new window to an epoch of the Universe that has never been explored before. During this time linear perturbations become nonlinear and start forming the structures that we see in the Universe today. Moreover, concerning the fundamental particles, we asses the possibility that it might shed some light on the nature of the dark matter particle, one of most important open problems in particle physics.

Because of such amount of topics and epochs covered, some topics will not be reviewed or only briefly mentioned, although they will always be defined before usage. Examples of that are structure formation issues, briefly touched upon, important in this thesis for placing constraints on the neutrino masses and for the evolution of the 21-cm signal, and cosmological perturbation theory, used for evolving the fluid perturbations that affect CMB and large scale structure.

Concerning the notations used, we tried to use the most standard notations, although in a new area like dark energy and dark matter, with many ideas appearing simultaneously, usually there is no such a thing as a standard notation. However, we hope that the notation will be clear from the context and definitions. Finally, except for parts of chapter 5, we will use all over the thesis the so-called natural units, $\hbar = c = k_b = 1$, and the reduced Planck mass, $m_p = M_p/\sqrt{8\pi} = 2.436 \times 10^{18}$ GeV, more convenient for writing the cosmological equations.

Introducción

> "Cuando nos fijamos en el cielo estamos mirando las estrellas que están a cientos y miles de años luz de distancia. Y algunas de estas estrellas ni siquiera existen ya, porque su luz ha tardado tanto en llegar a nosotros que ya han muerto, o han explotado y colapsaron a enanas rojas. Y eso te hace parecer muy pequeño, y si tienes cosas difíciles en tu vida es agradable pensar que son lo que se llaman insignificantes, o sea, que son tan pequeñas que no hay que tenerlas en cuenta cuando se calcula algo."
> Mark Haddon, *El curioso incidente del perro a medianoche*

La cosmología es la ciencia que pretende estudiar el origen, la estructura y evolución del Universo. Un objetivo tan ambicioso sólo puede llevarse a cabo tomando en cuenta las principales propiedades físicas del universo en cada momento. Por otra parte, la física de partículas se ocupa de las propiedades e interacciones de los componentes más elementales y más pequeños de la materia, y en principio se podría esperar que lo "muy pequeño" podría no ser relevante para las propiedades de las escalas más grandes del Universo. Sin embargo, la mayoría de las ideas nuevas y fundamentales de las últimas décadas en la cosmología vino de la sinergia entre las ciencias de lo muy pequeño y de lo muy grande: es decir, lo muy pequeño puede desempeñar, y desempeña, un papel crucial cuando se está tratando de calcular y comprender el Universo.

En esta tesis, se describen algunas de nuestras contribuciones a la comprensión de cómo los componentes más pequeños del Universo puede dar forma a su evolución en diferentes escalas cosmológicas y de diversas maneras. En particular,

vamos a considerar tres de los componentes más misteriosos de la receta cósmica: los neutrinos, la materia oscura y la energía oscura.

Para ello, en el primer capítulo, *Big Bang Cosmology*, se describe en detalle el modelo cosmológico actual, conocido actualmente como el modelo cosmológico estándar, así como sus principales evidencias y algunos de sus problemas. En particular, vamos a describir las diferentes épocas del Universo desde el Big Bang, hace alrededor de 13700 millones de años. Inicialmente, durante la fase dominada por la radiación, se forman núcleos ligeros, principalmente hidrógeno y helio, y se sabe que los neutrinos juegan un papel clave en el proceso de la nucleosíntesis primordial. A medida que el Universo se expande, la materia fría en forma de bariones y la hipotética materia oscura pasan a dominar la expansión del Universo. Durante esta época, los átomos se forman en el proceso de recombinación, liberando así la imagen más antigua posible del Universo, el llamado fondo cósmico de microondas. Esta calma aparente cambia cuando las primeras estrellas y las fuentes luminosas se forman bajo la influencia de la gravedad, cambiando una vez más el comportamiento del medio intergaláctico. Finalmente, cuando el Universo tenía alrededor de la mitad de su edad actual, un nuevo (y poco conocido) componente, la energía oscura, cambia la dinámica de la expansión del Universo. En este punto, comienza a acelerarse su expansión, un comportamiento que pueda mantener siempre o no, dependiendo de la naturaleza de este componente. Después de describir aquellas épocas, cerramos este capítulo hablando de la edad del Universo en los diferentes modelos y las restricciones que puede colocar sobre su valor.

En los siguientes capítulos, discutimos en detalle nuestras contribuciones para entender algunos de los problemas abiertos en este escenario cosmológico. En el capítulo titulado *Cosmological Lepton Asymmetry* se estudian en detalle los límites actuales sobre las asimetrías leptónicas almacenadas en el sector de los neutrinos. Esto es importante no sólo para ayudar a iluminar el origen de la asimetría entre materia y antimateria en el Universo, sino también para comprender y limitar la posibilidad de que esas asimetrías puedan desempeñar el papel de una radiación adicional que potencialmente puede probarse en un futuro muy próximo.

En el capítulo 4, *Mass-Varying Neutrino Models*, se investiga una clase de modelos para la energía oscura en la que la expansión acelerada del Universo es debida a un campo escalar que interactúa con los neutrinos, haciendo que las masas de esas partículas varíen con la expansión cosmológica. En particular, parametrizamos

la variación de la masa con el objetivo de estudiar un conjunto de escenarios de una manera independiente del modelo, y buscamos señales cosmológicas de dicha variación que podrían ayudar a la verificación de estos modelos. En la actualidad, se dispone de pocas opciones observacionales para restringir los modelos de energía oscura, y por lo tanto buscar formas indirectas para sondearlos como lo hacemos en este capítulo es fundamental para reducir el número de posibles candidatos o incluso determinar el modelo más correcto.

Finalmente, en el último capítulo, *Dark Matter and the Global 21-cm Signal*, buscamos señales potenciales de la aniquilación de materia oscura en el el estudio de la línea de 21 cm de los átomos de hidrógeno. Esta técnica, conocida como cosmología de 21-cm, tiene el potencial de ser muy importante para la cosmología y la astrofísica en un futuro no muy distante, ya que puede abrir una nueva ventana a una época del Universo que nunca ha sido explorada antes. Durante este tiempo, las perturbaciones lineales se tornan no lineales, formando las estructuras que vemos en el Universo actual. Por otra parte, con relación a las partículas elementales, estudiamos la posibilidad de que dicha técnica podría arrojar algo de luz sobre la naturaleza de la partícula de la materia oscura, uno de los problemas abiertos más importantes en la física de partículas actual.

Debido a tal cantidad de temas y épocas cubiertos, algunos sólo serán mencionados brevemente, a pesar de que siempre se definirán antes de su uso. Algunos ejemplos son las cuestiones de la formación de estructuras, importante en esta tesis para imponer limitaciones a las masas de los neutrinos y para la evolución de la señal de 21-cm, y la teoría de las perturbaciones cosmológicas, utilizada para la evolución de las perturbaciones que afectan la radiación de fondo y las estructuras a gran escala.

En cuanto a las notaciones utilizadas, tratamos de utilizar las notaciones más habituales, aunque en áreas nuevas como el estudio de la energía oscura y la materia oscura, en que muchas ideas aparecen al mismo tiempo, por lo general no hay una notación estándar. Sin embargo, esperamos que la notación quede clara a partir del contexto y de definiciones previas. Por último, excepto en partes del capítulo 5, vamos a utilizar a lo largo de la tesis el sistema natural de unidades, $\hbar = c = k_b = 1$, y la masa de Planck reducida, $m_p = M_p/\sqrt{8\pi} = 2{,}436 \times 10^{18}$ GeV, más convenientes a la hora de escribir las ecuaciones cosmológicas.

2

Big Bang Cosmology

In the last century cosmology became a science. Although Newton's law for gravitation worked (and still works) extremely well for several astronomical applications, a spacetime theory for gravitation, Einstein's General Relativity, was necessary to allow theorists to wonder about the behavior of the entire cosmos on a piece of paper.

However, in order to cosmology really become a branch of science, advances on the observational astronomy side were also necessary, since even the most creative theories have to be tested and shown to work in the real world. The discoveries by Edwin Hubble that our galaxy was one among many others and especially that the whole fabric of the spacetime was expanding brought to life a new area of scientific research, one that allows scientists to speculate and test their theories against cosmological observations.

In this chapter, we discuss and review some of the *main basic features* of the presently known as the standard cosmological model, the ΛCDM *Big Bang model*. As we will show, this model describes the behavior of the Universe confidently back to 0.01 seconds after the initial singularity, starting from a very hot state were the light nuclei were formed, some 13.7 Gyr in the past. Initially its energy density was dominated by relativistic particles like photons, neutrinos and (maybe) other hot relics, but cold matter in the form of baryons and especially the hypothetical dark matter (DM) eventually take over the energy density budget. During this matter domination epoch several important steps in the cosmological history take place: atoms are formed, releasing the oldest possible snapshot (in photons) of the Universe, the so-called cosmic microwave background; the first stars and galaxies

form, changing the thermal state of the Universe and reionizing the intergalactic medium, a period that still has to be better understood and that will be tested with future generations of space and ground-based telescopes.

Finally, when the Universe was approximately 10 Gyr old a new player becomes an important component of the energy density of the Universe, possibly changing its evolution forever: the so-called dark energy. The most important feature of this component is its negative pressure, that eventually becomes responsible for the observed acceleration of the Universe.

2.1. An expanding Universe

A central hypothesis for the standard cosmological model, known as the *Cosmological principle*, is that the Universe is homogeneous and isotropic beyond some scale (smaller than the horizon scale, which we are going to define later), at any time.

The cosmological principle plays a key role in the Friedmann-Robertson-Walker (FRW) model of the Universe, since the homogeneity and isotropy allows for the use of the Roberston-Walker metric. The symmetry properties of this metric reduces the ten coupled differential Einstein equations to a pair of them, the so-called Friedmann equations, which depend only on one variable, namely, the scale factor $a(t)$.

Despite of the fact that this symmetry was originally used by Einstein without observational support, nowadays a set of cosmological observations, especially the ones from the isotropy and homogeneity of the cosmic microwave background radiation (CMB), indicates that the cosmological principle is a valid approximation for the Universe in large scales [Clifton et al., 2012].

Another observational fact for the Universe is that it is expanding, as Edwin Hubble first showed in the late 1920's [Hubble, 1929]. He discovered a linear relation[1] between the distance $l(t)$ of a galaxy and its receding velocity $v(t)$,

$$v(t) = H_0\, l(t)\ , \tag{2.1}$$

[1] The linear relation is only valid for cosmologically small distances. For more distant galaxies, corrections that depend on the deceleration parameter, which we shall discuss later, have to be considered.

where the proportionality constant H_0 is nowadays known as *Hubble constant*. It is usually written in the normalized and dimensionless form

$$H_0 \;=\; 100\; h \text{ km s}^{-1} \text{ Mpc}^{-1} \;. \tag{2.2}$$

The best measurements to date on this parameter were obtained using the Hubble Space Telescope and the Wide Field Camera 3 [Riess et al., 2011],

$$h \;=\; \; 0.738 \pm 0.024 \;, \tag{2.3}$$

at 1σ of confidence level.

Notice that for the homogeneity and isotropy to be preserved in an expanding Universe, the scale factor which measures the expansion between any two points separated by a distance $l(t)$ have to be the same everywhere in the visible Universe, in such way that

$$l(t) \;=\; ra(t) \;. \tag{2.4}$$

In this way, any given galaxy sees any other galaxy located at a distance $l(t)$ recede with the velocity

$$v \;=\; \frac{dl(t)}{dt} \;=\; \frac{\dot{a}(t)}{a(t)} l(t) \;=\; H(t) l(t) \;, \tag{2.5}$$

that is, following the Hubble law. A dot here denotes a derivative with respect to the cosmic time t, and

$$H(t) \;=\; \frac{\dot{a}(t)}{a(t)} \;, \tag{2.6}$$

is the so called *Hubble parameter*, whose present value is given by the Hubble constant, equation (2.2).

The Hubble constant has a dimension of $\texttt{time}^{-1}$, and therefore it offers a natural scale for the age of the Universe,

$$H_0{}^{-1} \;=\; 9.778\; h^{-1} \text{ Gyr} \;. \tag{2.7}$$

In order to make the measurements of the receding velocities, Hubble made use of the *redshift* z suffered by the spectra of those galaxies, a quantity that can be

quantified in cosmological terms as

$$1 + z \;=\; \frac{\lambda_o}{\lambda_e} \;=\; \frac{a(t_o)}{a(t_e)} \;, \tag{2.8}$$

where λ_o corresponds to the observed wavelength of a given feature of the spectrum, and λ_e to its value when emitted.

To analyze the expansion of the Universe, it is convenient to use *comoving coordinates*, in which, by definition, the coordinate system follows the expansion, in such a way that a galaxy with no peculiar velocity keeps its coordinates constant. In those coordinates, galaxies are points at rest that follow the so-called *Hubble flow*.

Another important point is the need of a metric $ds^2 = g_{\mu\nu} dx^\mu dx^\nu$ to measure a comoving distance between any two points. As we have already commented before, a very convenient metric that incorporates the symmetries of the cosmological principle is the *Robertson-Walker (RW) metric*,

$$ds^2 \;=\; dt^2 - d\mathbf{l}^2 \;=\; dt^2 - a^2(t)\left(\frac{dr^2}{1-kr^2} + r^2 d\theta^2 + r^2 \sin^2\theta \; d\phi^2\right) \;, \tag{2.9}$$

where (t, r, θ, ϕ) are the comoving coordinates and k is $+1, 0$ or -1 depending on the geometry of the space.

2.2. Background cosmology

The Einstein's equations are given by

$$G_{\mu\nu} \;\equiv\; R_{\mu\nu} - \frac{1}{2}\mathcal{R} g_{\mu\nu} = 8\pi G \;\; T_{\mu\nu} \;, \tag{2.10}$$

where $R_{\mu\nu}$ is the so-called Ricci tensor, $\mathcal{R}$ is the Ricci scalar, both functions of the metric, and $T_{\mu\nu}$ is the energy-momentum tensor of the fluid components of the Universe. Using the RW metric and the energy-momentum tensor of a perfect fluid,

$$T^{\mu\nu} = (\rho + p) U^\mu U^\nu - p g^{\mu\nu} \;, \tag{2.11}$$

where ρ and p are the energy density and pressure measured by a comoving observer, and the 4-velocity for a comoving observer is given by $U^\mu = (1, 0, 0, 0)$, we obtain the *Friedmann equations*,

$$\frac{\dot{a}^2}{a^2} + \frac{k}{a^2} \;=\; H^2 + \frac{k}{a^2} \;=\; \frac{8\pi G}{3}\,\rho \;, \tag{2.12}$$

$$2\frac{\ddot{a}}{a} + \frac{\dot{a}^2}{a^2} + \frac{k}{a^2} \;=\; -8\pi G\; p \;. \tag{2.13}$$

Two important quantities that can be defined are the so-called *critical density*,

$$\rho_c \;\equiv\; \frac{3H^2}{8\pi G} \;, \tag{2.14}$$

and the *density parameter*

$$\Omega \;\equiv\; \frac{\rho}{\rho_c} \;=\; \frac{8\pi G}{3H^2}\,\rho \;. \tag{2.15}$$

In particular, we have that the *current critical density* is given by

$$\rho_{c0} \;=\; \frac{3H_0^2}{8\pi G} \;=\; 1.879\; h^2 \times 10^{-29}\ \text{g cm}^{-3} \;=\; 8.099\; h^2 \times 10^{-11}\ \text{eV}^4 \;. \tag{2.16}$$

That allows us to write the Friedmann equation in the form

$$H^2 \;=\; \frac{8\pi G}{3}\,\rho - \frac{k}{a^2} \;\Longrightarrow\; \frac{k}{H^2 a^2} \;=\; \Omega - 1 \;. \tag{2.17}$$

We see, therefore, that the density parameter of the Universe, given by Ω, and its spatial geometry are linked[2], yielding,

a) *open Universe*: $k \;=\; -1 \;\Longrightarrow\; \rho \;<\; \rho_c \;\Longrightarrow\; \Omega \;<\; 1$;

b) *flat Universe*: $k \;=\; 0 \;\Longrightarrow\; \rho \;=\; \rho_c \;\Longrightarrow\; \Omega \;=\; 1$;

c) *closed Universe*: $k \;=\; +1 \;\Longrightarrow\; \rho \;>\; \rho_c \;\;\Longrightarrow\; \Omega \;>\; 1$.

[2]The names, besides related to the spatial geometry, would also refer to the destiny of the Universe in case it is dominated by matter or radiation, but not a cosmological constant. For the former, an open Universe expands forever, a flat one expands forever with its velocity decreasing to zero in an infinite time, and a closed one collapses back at some time in the future. However, for a cosmological constant dominated Universe, the relation between geometry and destiny does not hold anymore [Krauss & Turner, 1999].

We can also rewrite equations (2.12) and (2.13) to obtain a more convenient form for the second Friedmann equation,

$$\frac{\ddot{a}}{a} \;=\; -\frac{4\pi G}{3}\;(\rho + 3p) \;=\; -\frac{4\pi G}{3}\;\rho\,(1+3\omega)\;, \tag{2.18}$$

where $\omega = p/\rho$ is the fluid *equation of state parameter*. Statistical mechanics tells us that for the case of a fluid composed of relativistic matter (called collectively *radiation*, or hot, matter), $\omega_r = 1/3$, while for regular baryons, whose temperature is much smaller than its mass (and also nonrelativistic, or cold, matter in general), $\omega_m \approx 0$. Soon we shall discuss the situation for more exotical fluids.

If we derive the Friedmann equation with respect to time,

$$\frac{d}{dt}\left(\dot{a}^2 + k\right) \;=\; \frac{d}{dt}\left(\frac{8\pi G}{3}\;\rho a^2\right) \;\Longrightarrow\; 2\dot{a}\ddot{a} \;=\; \frac{8\pi G}{3}\;\left(\dot{\rho}a^2 + 2\rho a\dot{a}\right)\;,$$

and use eq. (2.18), we obtain the *fluid equation*

$$-\left(\rho + 3p\right)a\dot{a} \;=\; \dot{\rho}a^2 + 2\rho a\dot{a} \;\Longrightarrow\; \dot{\rho} \;=\; -3H\left(\rho + p\right)\;, \tag{2.19}$$

which can be analogously obtained using the conservation of the energy-momentum tensor of a perfect fluid.

In this case, we can obtain the dependence of the energy density on the scale factor for a equation of state,

$$\dot{\rho}a \;=\; -3\rho\;(1+\omega)\dot{a}\;, \qquad \Rightarrow \qquad \frac{1}{3\,(1+\omega)}\int\frac{d\rho}{\rho} \;=\; \int\frac{da}{a}\;,$$

and therefore,

$$\rho \;\propto\; a^{-3(1+\omega)}\;. \tag{2.20}$$

For the above equation, we can obtain the particular well known cases of matter and radiation,

$$\rho_r \;\propto\; a^{-4}\;, \qquad\qquad \rho_m \;\propto\; a^{-3}\;. \tag{2.21}$$

These cases can also be understood from a more physical point of view. In the case of the matter density, it only implies that the density is falling as the volume of the Universe increases (that is, with the scale factor to the third power, since the number of particles is constant). In the case of radiation, there is an extra

factor coming from the fact that the wavelength also increases with the expansion, and therefore the energy density scales with the fourth power of the scale factor.

We can also consider different components for the Universe, like for instance the *cosmological constant*[3] denoted by Λ. One can show that the fluid behavior of the cosmological constant is the same of the vacuum of a quantum field, and for Lorentz invariance that amounts to saying that it has a negative pressure, equals to minus its energy density, that is, $\omega_\Lambda = -1$. Notice that this could also have been obtained from eq. (2.20) taking into account that the energy density of a cosmological constant is, by definition, constant. We will discuss the cosmological constant in much more detail in the next sections.

Solving the Friedmann equation for a given fluid allows for the determination of the behavior of the scale factor as a function of the time,

$$\frac{\dot{a}}{a} \propto a^{-3(1+\omega)/2} \quad \Rightarrow \quad \int da\, a^{3(1+\omega)/2} a^{-1} \propto \int dt \ , \tag{2.22}$$

and therefore

$$a(t) \propto t^{2/3(1+\omega)} \ . \tag{2.23}$$

In other words, during matter domination $a(t) \propto t^{2/3}$ and during radiation domination $a(t) \propto t^{1/2}$. In the case of a cosmological constant eq. (2.22) immediately leads to $a(t) \propto \exp(Ht)$, that is, an exponential expansion. Notice the latter is the case supposed to have happened very early in the history of the Universe, the so-called *inflationary epoch*, which we will see more details later.

The observed densities of baryonic matter, total (dark plus baryonic) matter, neutrinos, and photons are

$$\begin{aligned} \rho_{b0} &= 1.879 \times 10^{-29} \Omega_{b0} h^2 \text{g cm}^{-3} \\ &\approx 1.62 \times 10^{-12} \text{ eV}^4 \ , \end{aligned} \tag{2.24}$$

$$\begin{aligned} \rho_{m0} &= 1.879 \times 10^{-29} \Omega_{m0} h^2 \text{g cm}^{-3} \\ &\approx 1.21 \times 10^{-11} \text{ eV}^4 \ , \end{aligned} \tag{2.25}$$

[3]Einstein first introduced it the field equations of General Relativity in order to obtain a static Universe, according to the cosmological ideas of the time. However, as soon as Hubble discovered the expansion of the Universe, Einstein is cited by Gamow as having said that "the introduction of the cosmological term was the biggest blunder of his life." [Gamow, 1970].

$$\begin{aligned}\rho_{\nu 0}^{\text{massive}} &= 2.02 \times 10^{-31} \left(\frac{\sum_i m_{\nu i}}{1 \text{ eV}} \right) \text{ g cm}^{-3} \\ &= 8.69 \times 10^{-13} \left(\frac{\sum_i m_{\nu i}}{1 \text{ eV}} \right) \text{ eV}^4 \ , \end{aligned} \tag{2.26}$$

$$\begin{aligned}\rho_{\nu 0}^{\text{massless}} &= 8.11 \times 10^{-36} \text{ g cm}^{-3} \ , \\ &= 5.89 \times 10^{-17} \text{ eV}^4 \ , \end{aligned} \tag{2.27}$$

$$\begin{aligned}\rho_{\gamma 0} &= 4.64 \times 10^{-34} \text{ g cm}^{-3} \\ &= 3.37 \times 10^{-15} \text{ eV}^4 \ , \end{aligned} \tag{2.28}$$

We will discuss some of those in details, but just for completeness we mention here some of the ways those numbers are measured. The value of the baryonic density comes from limits on light elements production in the early Universe, the nucleosynthesis epoch, which requires $\Omega_{b0} h^2 \approx 0.02$, a result that agrees with other observational results, like CMB anisotropies. The total matter density (baryonic plus dark), $\Omega_{m0} \approx 0.3$, is essentially measured gravitationally via the rotation curves of galaxies, gravitational lensing, X-ray emission from hot gas in clusters, and the measurement of peculiar velocities in the large scale structure distribution. [Bertone et al., 2005; Bertone, 2010], and the results agree very well with the CMB anisotropy data. Neutrino density upper limit is obtained using the limits on the sum of the total masses of the three mass eigenstates obtained from cosmology [Lesgourgues & Pastor, 2006], that we will discuss more about later. Finally, the photon density is measured via the temperature of the CMB temperature.

One can see that the matter density is currently at least five orders of magnitude higher than the radiation one. However, since radiation density falls more rapidly than matter density, there should be a time in which both densities contributed equally to the density of the Universe. This time, known as *equality time*, separates an early radiation domination era from a subsequent matter domination. As we are going to see, observations confirm the scenario of an early, hot Universe in which both matter and radiation are in thermodynamical equilibrium[4].

[4]Notice that although the primordial Universe could not have been in thermodynamical equilibrium, since it was expanding, the idea of local thermodynamical equilibrium is valid for interactions whose reaction rates Γ is much larger that the expansion rate of the Universe, given by H.

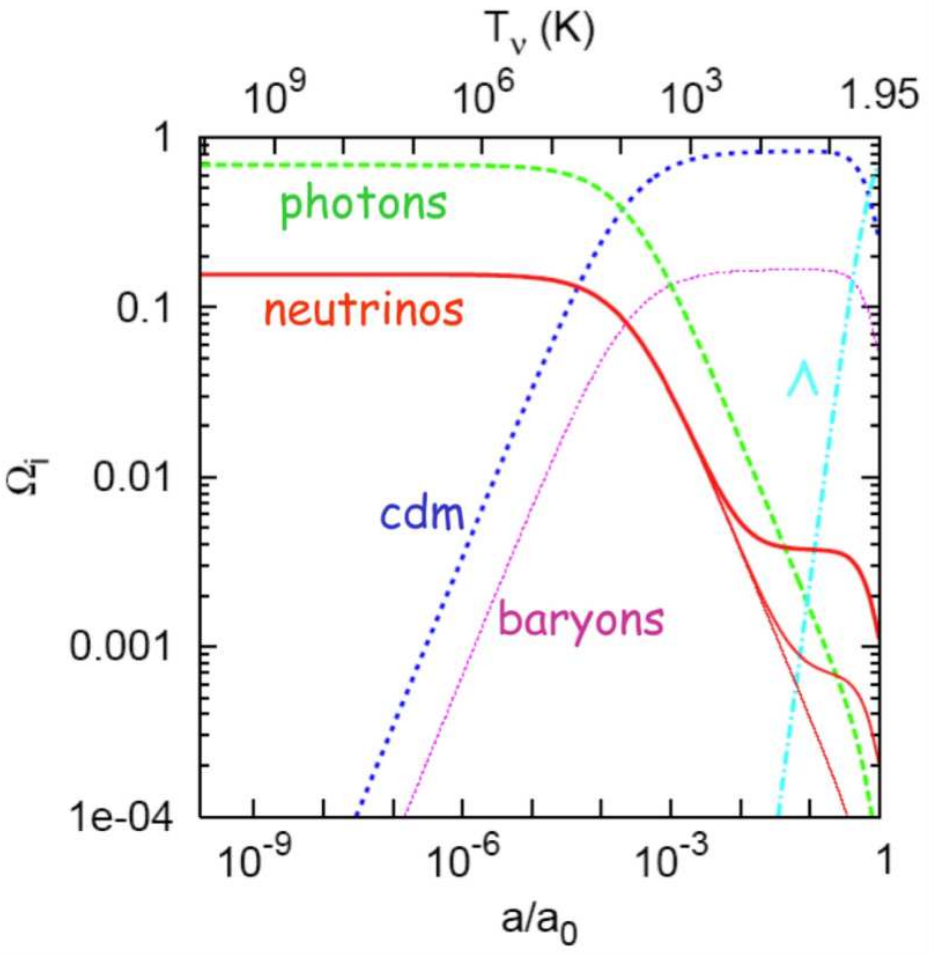

Figure 2.1: Density parameters for the different components of the Universe. From Lesgourgues & Pastor [2006].

2.3. Radiation Dominated Epoch

2.3.1. Thermodynamics of the Early Universe

In order to analyze the early Universe, it is necessary to know the species which contribute to the energy of the Universe at a given time, as well as their distribution functions, since the number and energy densities, for instance, are both dependent on them.

For a species in kinetic equilibrium, the distribution function is given by the familiar Fermi-Dirac $(+)$ or Bose-Einstein $(-)$ distributions,

$$f(\mathbf{p}) = \left[\exp\left(\frac{E-\mu}{T} \pm 1\right)\right]^{-1} , \tag{2.29}$$

Where $E^2 = |\mathbf{p}|^2 + m^2$. If the species is in chemical equilibrium, then the *chemical potential* μ is related to the other species it interacts with. Normally it is negligible compared to the energy, but in the next chapter we discuss a situation in which it might play a key role in the early Universe.

The number density, energy density, and pressure are given respectively by,

$$n = \frac{g}{(2\pi)^3}\int_m^\infty f(\mathbf{p}) d^3p , \tag{2.30}$$

$$\rho = \frac{g}{(2\pi)^3}\int_m^\infty E(\mathbf{p}) f(\mathbf{p}) d^3p , \tag{2.31}$$

$$p = \frac{g}{(2\pi)^3}\int_m^\infty \frac{|\mathbf{p}|^2}{3E} f(\mathbf{p}) d^3p . \tag{2.32}$$

While relativistic particles ($T \gg m$) show either a Fermi-Dirac or a Bose-Einstein distribution, depending on their spin, one can show that nonrelativistic particles ($m \gg T$) distribution function converges to a Maxwell-Boltzmann distribution.

In a situation of local thermodynamic equilibrium, the number density, energy density and pressure of a relativistic species are given respectively by

$$n = b_n \frac{\zeta(3)}{\pi^2} g T^3 , \tag{2.33}$$

$$\rho \;=\; b_\rho \,\frac{\pi^2}{30}\, g T^4 \;, \tag{2.34}$$

$$p \;=\; \frac{\rho}{3} \;, \tag{2.35}$$

where g corresponds to the number of degrees of freedom available for each particle species, $b_n = 1$ (3/4) and $b_\rho = 1$ (7/8) for bosons (fermions), and $\zeta(3) = 1.2026$ is the Riemann zeta function of 3. In the case of nonrelativistic particles, those thermodynamical quantities are given by

$$n \;=\; g\,\left(\frac{mT}{2\pi}\right)^{3/2} \exp(-m/T) \;, \tag{2.36}$$

$$\rho \;=\; mn \;, \tag{2.37}$$

$$p \;=\; nT \ll \rho \;, \tag{2.38}$$

from where we see that the density and pressure of nonrelativistic species are exponentially smaller than the ones of relativistic species when they are in equilibrium. Because of that, it is a good approximation to include only the contribution of the relativistic species in the early Universe, in such way that

$$\rho_r \;=\; \frac{\pi^2}{30}\, g_* T^4 \;, \tag{2.39}$$

$$p_r \;=\; \frac{\rho_r}{3} \;=\; \frac{\pi^2}{90}\, g_* T^4 \;, \tag{2.40}$$

where

$$g_* \;\equiv\; \sum_{i=\text{bosons}} g_i \left(\frac{T_i}{T}\right)^4 + \frac{7}{8} \sum_{i=\text{fermions}} g_i \left(\frac{T_i}{T}\right)^4 \;, \tag{2.41}$$

is the total number of degrees of freedom of relativistic fermions and bosons i (that is, the ones for which $m_i \ll T$), Notice that because g_* is related to the number of relativistic species in the Universe, it is a function of the cosmological temperature, as we are going to discuss later.

Deep into the radiation era, we have that

$$H \;=\; \sqrt{\frac{8\pi^3}{90}}\, g_*^{1/2} \frac{T^2}{M_P} \;=\; 1.66\, g_*^{1/2} \frac{T^2}{M_P} \;, \tag{2.42}$$

and since $a(t) \propto t^{1/2}$ for the radiation domination,

$$\frac{t}{1\ \mathrm{s}} = \frac{1}{2H} = 0.162\ g_*^{-1/2} \times 10^{-44} \left(\frac{M_P}{T}\right)^2 = 0.241\ g_*^{-1/2} \left(\frac{T}{\mathrm{MeV}}\right)^{-2} . \quad (2.43)$$

In order to estimate the different temperatures of the different species after they leave the equilibrium, we can make use of the fact that the expansion is adiabatic. We have that $3da = V^{-2/3} dV$, where V is a unitary comoving volume,

$$V d\rho = (\rho + p) dV \qquad \Rightarrow \qquad d(\rho V) = -p dV , \quad (2.44)$$

and therefore the entropy is conserved in a comoving volume, as it should be for an adiabatic expansion. The thermodynamics assures that, for a given comoving volume V,

$$T dS = d(\rho V) + p dV = V d\rho + (\rho + p) dV = d[(\rho + p)V] - V dp . \quad (2.45)$$

And using

$$dS = \left(\frac{\partial S}{\partial \rho}\right)\left(\frac{d\rho}{dT}\right) dT + \left(\frac{\partial S}{\partial V}\right) dV , \quad (2.46)$$

we have that

$$\frac{\partial S}{\partial T} = \left(\frac{\partial S}{\partial \rho}\right)\left(\frac{d\rho}{dT}\right) = \frac{V}{T}\frac{d\rho}{dT} , \quad (2.47)$$

$$\frac{\partial S}{\partial V} = \frac{\rho + p}{T} . \quad (2.48)$$

Since

$$\frac{\partial^2 S}{\partial T\ \partial V} = \frac{\partial^2 S}{\partial V\ \partial T} , \quad (2.49)$$

we have that

$$\frac{\partial}{\partial T}\left(\frac{\rho + p}{T}\right) = -\frac{1}{T^2}(\rho + p) + \frac{1}{T}\frac{d\rho}{dT} + \frac{1}{T}\frac{dp}{dT} = \frac{\partial}{\partial V}\left(\frac{V}{T}\frac{d\rho}{dT}\right) = \frac{1}{T}\frac{d\rho}{dT} , \quad (2.50)$$

and therefore,

$$\frac{dp}{dT} = \frac{\rho + p}{T} . \quad (2.51)$$

Using the above equation and equation (2.45), we can obtain the entropy, because

$$dS = \frac{1}{T}\, d[(\rho+p)V] - \frac{(\rho+p)V}{T^2}\, dT \quad \Rightarrow \quad dS = d\left[\frac{(\rho+p)V}{T} + \text{constant}\right], \tag{2.52}$$

and therefore, the entropy in a comoving volume is given by

$$S = \frac{(\rho+p)V}{T} \tag{2.53}$$

We should keep in mind that the entropy is given by the contribution of the relativistic particles, whose energy density, eq. (2.39), and pressure, eq. (2.40), results in the *entropy density s* given by

$$s \equiv \frac{S}{V} = \frac{2\pi^2}{45} g_{*S}\, T^3 , \tag{2.54}$$

where

$$g_{*S} \equiv \sum_{i=\text{bosons}} g_i \left(\frac{T_i}{T}\right)^3 + \frac{7}{8} \sum_{i=\text{fermions}} g_i \left(\frac{T_i}{T}\right)^3 . \tag{2.55}$$

Notice that $g_* = g_{*S}$ only when all the species share the same temperature. Beside that, the fact that the total entropy is constant implies that $sV \propto g_{*S} a^3 T^3$ is constant, and therefore

$$T \propto g_{*S}^{-1/3} a^{-1} , \tag{2.56}$$

that is, for epochs in which g_{*S} is approximately constant, $T \propto a^{-1}$.

However, there are several situations in which g_{*S} and g_* vary with time, as for instance when one of the species becomes nonrelativistic or annihilates and transfers its entropy to the other relativistic particles. In those cases, the temperature of the primordial plasma decreases slower than a^{-1}.

In order to obtain another important cosmological quantity, the so-called *baryon-to-photon ratio*, η_b, we can use the fact that the number density of photons, n_γ, is proportional to the entropy density,

$$s = \frac{2\pi^4}{90\zeta(3)}\, g_{*S}\, n_\gamma = 1.80\, g_{*S}\, n_\gamma , \tag{2.57}$$

where we used the fact that $g_\gamma = 2$.

Therefore, the baryon-to-photon ratio, that is, the ratio of the baryon number

density to the number density of photons is given by

$$\eta_b \;=\; \frac{n_b - n_{\bar{b}}}{n_\gamma} \;=\; 1.80\; g_{*S}\; \frac{n_b}{s}\;, \tag{2.58}$$

where n_b and $n_{\bar{b}}$ are the number density of baryons and antibaryons, respectively. Since observations indicate that $n_{\bar{b}} \approx 0$, it is usual to define $\eta_b = n_b/n_\gamma$.

Since the baryon number is conserved[5], as well as the entropy, we have that the ratio η_b varies only with g_{*S}, that is, when species annihilates generating more photons that will distribute its entropy among the other particles which are still in equilibrium.

2.3.2. Neutrino decoupling

To analyze the primordial behavior of the Universe, it is essential to know the species which are present at each time, since we have to calculate g_* and g_{*S} to be able to calculate the cosmological parameters, like H and η_b, for instance.

As we have commented before, to maintain a species in local thermodynamical equilibrium it is necessary that the interaction rate Γ be larger than H, the expansion rate of the Universe. That amounts to saying that the number of interactions between the particles that one is interested in is (much) larger than unity in a Hubble time, and therefore the expansion of the Universe can be safely ignored[6].

We can analyze, for instance, the process of neutrino decoupling. Neutrinos are kept in equilibrium via electroweak interactions with the free protons and neutrons in the early Universe. The cross section of electroweak process is given approximately by $\sigma \approx G_F^2 T^2$, where $G_F = (292.80\ \text{GeV})^{-2}$ is the Fermi constant. Since neutrinos are highly relativistic at energies around 1 MeV, its number density is proportional to T^3, and therefore their interaction rate is

$$\Gamma_{\text{EW}} \;=\; n_\nu\; \sigma\; |v| \;\approx\; G_F^2 T^5\;, \tag{2.59}$$

[5]Except, of course, if one is dealing with the very early Universe, when the baryogenesis is supposed to happen.

[6]The precise way to improve this back-of-the-envelope calculation is by numerically solving the distribution functions for the species using the Boltzmann equation [Kolb & Turner, 1990; Dodelson, 2003] and taking other effects into account, as for instance, the effect of neutrino oscillations [Mangano et al., 2005]. However, the condition $\Gamma \gtrsim H$ works as an order of magnitude estimate, and it is a good approximation in general.

where $|v| \approx 1$ simply denotes the relativistic nature of neutrinos at those energies. We can then compare the above equation with eq. (2.42), to obtain

$$\frac{\Gamma_{\rm EW}}{H} \approx \frac{M_P G_F^2 T^5}{T^2} \approx \left(\frac{T}{0.8\ {\rm MeV}}\right)^3 , \tag{2.60}$$

that is, for temperatures below 0.8 MeV, the electroweak interaction rate is not capable of keeping the neutrinos in thermodynamical equilibrium, and they decouple of the primordial plasma. A little after neutrino decoupling, the temperature falls below the electron-positron mass, they become nonrelativistic, annihilate, and their entropy is transferred to the photons. Because of that, the photon temperature falls slower than a^{-1} for a while, and the photon temperature deviates from the neutrino temperature, which is still scaling with the inverse of the scale factor.

This difference in temperature can be estimated using eq. (2.56). With the annihilation of the $e^{\pm}$ pairs, the number of eletromagnetic degrees of freedom of the primordial plasma falls from $g_* = 2 + (7/2) = 11/2$ to $g_* = 2$, correspondent to the photon. Because of that, aT_γ in eq. (2.56) increases by a factor $(11/4)^{1/3}$, while aT_ν remains constant. Because of this, we have that

$$\frac{T_\gamma}{T_\nu} = \left(\frac{11}{4}\right)^{1/3} \simeq 1.40102 . \tag{2.61}$$

After the $e^{\pm}$ annihilation, both aT_γ and aT_ν remain constant, and we expect the ratio between both temperatures to remain constant. In particular, since we measure $T_{\gamma 0} = 2.728$ K, we expect that $T_{\nu 0} \simeq 1.94$ K. Detecting such a *cosmic neutrino background* is extremely challenging and possibly not feasible in the near future (if ever), although some indirect evidences for its existence could be achievable [Trotta & Melchiorri, 2005; Gelmini, 2005; Michney & Caldwell, 2007; De Bernardis et al., 2008].

We can also calculate the present value for the number of degrees of freedom, supposed to be constant after the $e^{\pm}$ annihilation[7],

$$g_* = 2 + \frac{7}{8} \times 2 \times 3 \times \left(\frac{4}{11}\right)^{4/3} = 3.36 , \tag{2.62}$$

[7]Notice that for the evaluation of g_* and g_{*S} we have ignored here corrections to the *effective number of neutrinos* [Dicus et al., 1982; Dodelson & Turner, 1992; Mangano et al., 2002, 2005].

$$g_{*S} \;=\; 2 + \frac{7}{8} \times 2 \times 3 \times \frac{4}{11} \;=\; 3.91 \; . \tag{2.63}$$

Using the present temperature of the photons we can calculate the number density of both photons and neutrinos,

$$n_{\gamma 0} \;=\; \frac{2\zeta(3)}{\pi^2}\; T^3 \;=\; 3.153 \times 10^{-12}\ \text{eV}^3 \;\approx\; 410\ \text{cm}^{-3} \; , \tag{2.64}$$

$$n_{\nu 0} \;=\; \frac{3\zeta(3)}{2\pi^2}\; T_\nu^3 \;=\; \frac{3}{11}\; n_{\gamma 0} \;=\; 8.599 \times 10^{-13}\ \text{eV}^3 \;\approx\; 111\ \frac{\text{cm}^{-3}}{\text{flavor}} \; , \tag{2.65}$$

as well as the corresponding energy density of photons,

$$\rho_{\gamma 0} \;=\; \frac{2\pi^2}{30} T^4 \;=\; (1.43 \times 10^{-4}\ \text{eV})^4 \;=\; 4.64 \times 10^{-34}\ \text{g cm}^{-3} \; , \tag{2.66}$$

$$\Omega_{\gamma 0} h^2 \;=\; \frac{\rho_{\gamma 0}}{\rho_{c0}} \;=\; 2.47 \times 10^{-5} \; , \tag{2.67}$$

In this way, we can estimate the entropy of the Universe, as well as the baryon-to-photon ratio,

$$\eta_b \;=\; 7.04\ \frac{n_b}{s} \;=\; 7.04\ \frac{\rho_b}{m_p\ s} \;\approx\; 2.75 \times 10^{-8}\ \Omega_{b0} h^2 \; , \tag{2.68}$$

where we approximated the bayon mass to the proton mass, $m_b \approx m_p = 938.272$ MeV, and the entropy density given by (2.54). Notice finally that both the baryonic number and the entropy are conserved in a comoving volume, and therefore the ratio n_b/s is constant.

The main issue here is that the entropy of the Universe is extremely high since there are around 10^9 photons in the Universe for each baryon. Because of that, processes which involve the formation of bound states, like the primordial nucleosynthesis and the recombination, which we shall discuss next, take place at a much lower energy than one would expect, since the very small η_b assures that there are enough high energy photons to dissociate the bound states even for a low average photon temperature.

2.3.3. Primordial Nucleosynthesis

Detailed calculations [Kolb & Turner, 1990] show that nucleosynthesis might have occurred at energies around $T \approx 0.1$ MeV. Essentially, two factors are responsible for such a low temperature: the huge entropy of the Universe and the dubbed "deuterium bottleneck". In what follows, we are going to make a brief summary of the main physical process that take place during nucleosynthesis, although one should keep in mind that in order to track precisely the light elements abundance[8], obviously the work should be done numerically including the full nuclear reaction chain [Iocco et al., 2009].

The first step in the formation of the light elements, Deuterium, has a binding energy of 2.22 MeV, what allows for a significant amount of those nuclei only when the temperature of the Universe is around 0.1 MeV. Therefore, the whole primordial nucleosynthesis process happens only below this energy.

When the weak interactions rate falls below the Hubble rate and the neutrinos fall off out the equilibrium, the weak reactions

$$\nu_e + n \rightleftarrows p + e^- \ ,$$

$$e^+ + n \rightleftarrows p + \bar{\nu}_e \ ,$$

that interconvert protons and neutrons stop, and the proton-to-neutron ratio basically freezes, except for the slow β-decay,

$$n \rightleftarrows p + e^- + \bar{\nu}_e \ . \tag{2.69}$$

Taking the Maxwell-Boltzmann distribution, eq. (2.36), at $T = 0.8$ MeV, when $\Gamma_{EW} < H$, we have that

$$\frac{n_n}{n_p} \approx e^{-(m_n - m_p)/T} \approx \frac{1}{5} \ , \tag{2.70}$$

where $m_n = 939.565$ MeV and $m_p = 938.272$ MeV. This fraction does not remain constant, since some neutrons still are converting into protons via β decay (2.69). Therefore, at the temperature of 0.1 MeV, the ratio reaches its final value $n_n/n_p \approx$

[8] As it is known for several decades [Burbidge et al., 1957], heavy elements are synthesized much later in the history of the Universe.

1/7, since after that the reactions that form $^3He^{++}$ and especially $^4He^{++}$ also become efficient. In particular, the ^{4}He nucleus has a high binding energy of 28.3 MeV, much larger than the photon temperature at that time, and therefore remains stable.

The fact the nucleosynthesis essentially stops after the formation of ^{4}He, except for a small portion of ^{7}Li (^{7}Li/H $\approx 10^{-10}$ - 10^{-9}), is due mainly to the lack of stable isotopes with mass $A = 5$ and $A = 8$ and to the low temperature in which the process starts. Therefore, besides the H (essentially all the protons that were left), ^{4}He and ^{7}Li, a small portion of D (D/H $\approx 10^{-3} - 10^{-4}$) and ^{3}He (^{3}He/H $\approx 10^{-4} - 10^{-5}$) not used for the production of ^{4}He is present when nucleosynthesis finishes.

A back-of-the-envelope calculation can then be used to estimate the fraction X_P of ^{4}He over H nuclei, keeping in mind that helium is composed by 2 neutrons and 2 protons. For that, we are going to assume that the two were the only light nuclei produced during the nucleosynthesis process, what is a good approximation.

When this happens, all neutrons are used to form helium nuclei, and the excess of protons is left as hydrogen nuclei. In this way,

$$X_P = \frac{n_{\mathrm{He}}}{n_{\mathrm{H}}} = \frac{n_n/2}{7n_n - n_n} \approx \frac{1}{12} . \tag{2.71}$$

And the *mass fraction* Y_P of ^{4}He over the total mass is (using $m_p \approx m_n$)

$$Y_P = \frac{4n_{\mathrm{He}}}{n_{\mathrm{H}} + 4n_{\mathrm{He}}} = \frac{4X_P}{1 + 4X_P} \approx 0.25 . \tag{2.72}$$

Those primordial abundances depend on some physical quantities like the neutron half-life $\tau_{1/2}(n)$ (important to know the exact ratio between neutrons and protons after weak interactions cease), the number of degrees of freedom g_* (which directly affect the Hubble parameter) and the baryon-to-photon ratio η_b (the abundances with respect to the hydrogen X_A of a given nucleus is proportional to η_b^{A-1}). From the last one it is possible, using equation (3.1) constrain the present baryon density using the abundance of light nuclei.

Figure 2.2 shows the abundances as a function of the baryonic density. ^{4}He corresponds to its mass fraction Y_P, while the other nuclei show their abundances relative to the hydrogen. The vertical strip shows the region of concordance for the

3 of the 4 nuclei [Lesgourgues et al., 2012]. The apparent issue with the primordial abundance of ^{7}Li is currently being studied very intensively [Fields, 2011]. In summary, the fact that there is a concordant strip is a strong evidence for the big bang model until 10^{-2} second after the initial singularity. It is also striking that the value $\Omega_{b0}h^2 \approx 0.02$ agrees extremely well with the CMB measurements. The concordance makes of nucleosynthesis one of the main pillars of the standard cosmological model.

2.4. Matter Dominated Epoch

As we have discussed before, matter and radiation densities evolve differently with time, in such way that

$$\frac{\rho_r}{\rho_m} = \frac{\rho_{r0}}{\rho_{m0}} \left(\frac{a_0}{a}\right) = \frac{\rho_{r0}}{\rho_{m0}} (1+z) . \tag{2.73}$$

And the equality time can be calculated to be

$$1 + z_{\text{eq}} = \frac{\rho_{m0}}{\rho_{r0}} = 24000\ \Omega_{m0}h^2 \approx 3600 , \tag{2.74}$$

$$T_{\text{eq}} = T_0 (1 + z_{\text{eq}}) = 65425\ \Omega_{m0}h^2\ \text{K} \approx 9800\ \text{K} \approx 0.85\ \text{eV} . \tag{2.75}$$

That is, for temperatures below 0.8 eV matter is the leading component in the right-hand-side of Friedmann equation[9].

However, matter and radiation still behave like plasma, since they still are coupled due to the Thomson scattering. Only after the capture of the electrons by the ionized nuclei, the process known as *recombination*, radiation can travel freely through the spacetime in the form of the *cosmic background radiation* (CMB).

[9] The process, however, is not instantaneous, and is strongly complicated by the fact that at least one of the neutrinos is supposed to become nonrelativistic around the same epoch.

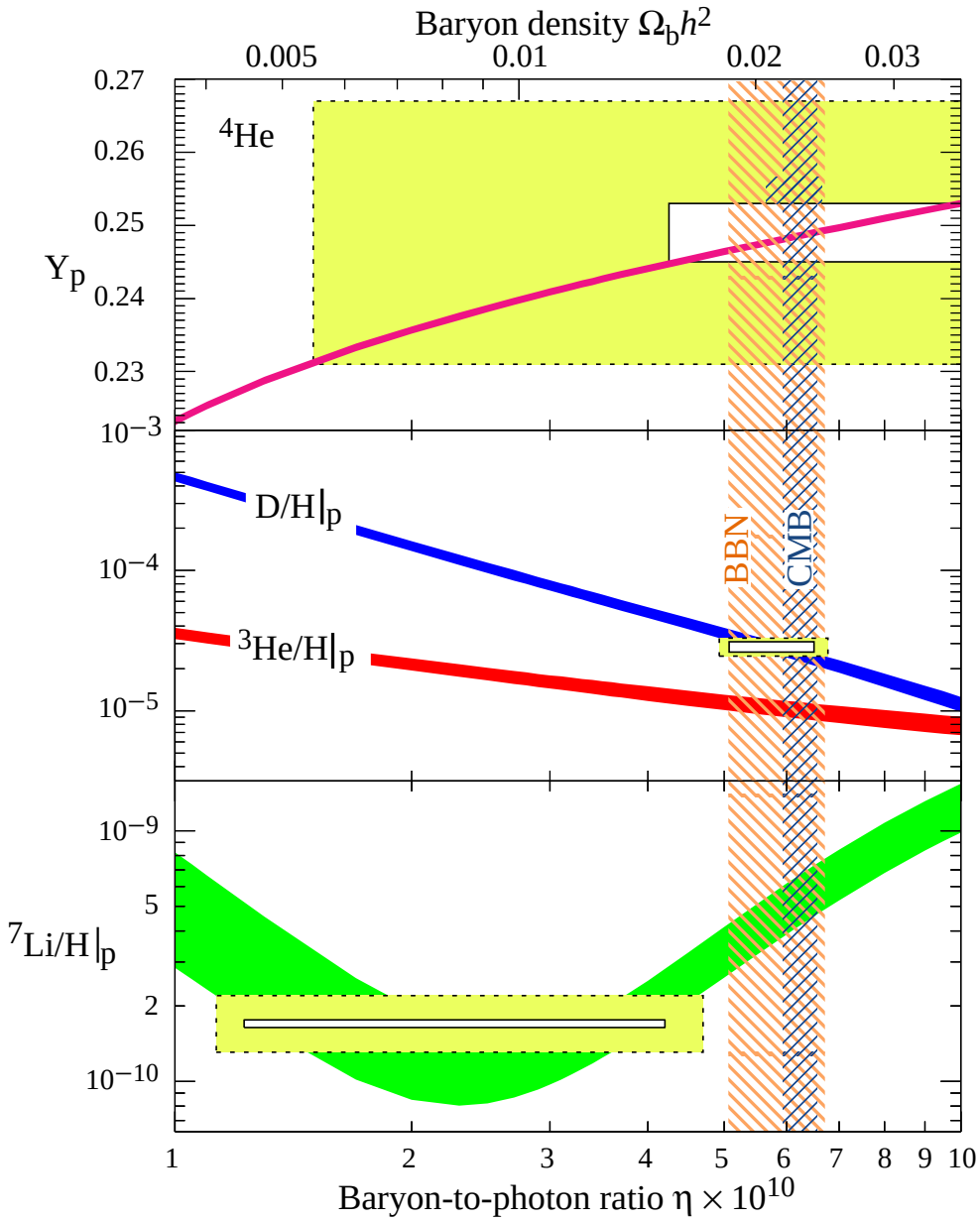

Figure 2.2: The abundances of ^{4}He, D, ^{3}He, and ^{7}Li as predicted by the standard model of BBN - the bands show the 95% C.L. range. Boxes indicate the observed light element abundances (smaller boxes: $\pm 2\sigma$ statistical errors; larger boxes: $\pm 2\sigma$ statistical and systematic errors). The narrow vertical band indicates the CMB measure of the cosmic baryon density, while the wider band indicates the BBN concordance range (both at 95% C.L.). From Fields & Sarkar [2012].

2.4.1. Cosmic background radiation

The hydrogen bound state has an energy corresponding to the difference between the free proton and electron masses with respect to the bound state,

$$m_H - m_p - m_e \;=\; -13.59 \text{ eV} \;,$$

and therefore neutral atoms could be formed below this temperature, at least in principle[10]. However, again due to the high entropy of the Universe, electron capture is delayed until the temperature of the Universe of the order of 0.3 eV. When the electrons and nuclei recombine, Thomson scattering ceases. One can show that the *last scattering surface* (LSS) is located at $z \approx 1100$, when the Universe was around 300.000 years old.

Since the whole plasma of nuclei, electrons and photons was in local thermodynamical equilibrium, the distribution of the photons have to follow a blackbody radiation distribution, simply redshifted after the last scattering surface.

In 1948, Gamow, Alpher and Herman [Alpher et al., 1948; Gamow, 1948b] for the first time estimated the temperature of the present Universe to be $T \approx 5$ K, using for that a hot big bang model[11] [Alpher & Herman, 1948; Gamow, 1948a; Alpher & Herman, 1950].

A naive estimative of the present temperature of the cosmic background radiation can be done assuming the present age of the Universe to be $t_0 = 13.5$ Gyr and matter dominated since recombination,

$$\frac{T_0}{T_{LSS}} \;=\; \left(\frac{t_{LSS}}{t_0}\right)^{2/3} \;\Longrightarrow\; T_0 \;\approx\; 2.5 \text{ K} \;. \tag{2.76}$$

Despite of this striking result, the calculation did not receive much attention, since it was considered highly speculative, and the detection of such a background, technologically unfeasible.

However, two engineers working at the Bell Labs, Penzias and Wilson [Penzias & Wilson, 1965], discovered such radiation in 1964. At Princeton, a group led by Robert Dicke (and with Jim Peebles and David Wilkinson) was preparing an

[10] The recombination process is obviously far more complicated than discussed here, where again our intention is only to present a qualitative idea of the process in which the CMB is released. For more detailed accounts, see for instance [Kolb & Turner, 1990; Dodelson, 2003].

[11] Historical details can be found in [Alpher & Herman, 1988; Brush, 1992].

experiment to search for this radiation [Peebles et al., 2009] when they learned about the results, and immediately realized the cosmological importance of what Penzias and Wilson have discovered [Dicke et al., 1965]. Interestingly enough, the discover rendered the 1978 Nobel prize to Penzias and Wilson, but not for Gamow or Dicke.

The full confirmation of the blackbody spectrum came only in the 90's, as measured by the FIRAS (Far Infrared Absolute Spectrophotometer) instrument on board of COBE (Cosmic Background Explorer) satellite [Mather et al., 1994], what awarded John Mather the 2006 Nobel prize. George Smoot was awarded the same year for the discovery of the anisotropies of the cosmic background radiation [Wright et al., 1992; Smoot et al., 1992], that we will discuss later.

COBE's curve (figure 2.3) show an amazing agreement with a blackbody curve, and therefore, with the predictions of the hot Big Bang model. The errors can be hardly seen on the theoretical curve (in the figure, the errors were multiplied by a factor of 400 in order to be visible). The present temperature of the Universe is [Fixsen et al., 1996]

$$T_0 = 2.728 \pm 0.001 \text{ K} . \tag{2.77}$$

The radiation is homogeneously and isotropically distributed in all directions (in agreement with the cosmological principle), with fluctuations (or anisotropies) of the order of 10^{-5}.

2.4.2. The dark ages

After the recombination of the hydrogen atoms and the release of the cosmic microwave background the Universe entered a period that became known as the *dark ages*, in which the potential wells seeded by dark matter start atracting the baryons (that at this point can collapse gravitationally as the Compton scattering ceased) to form what will later become the first galaxies and stars.

The evolution of the small density perturbations

$$\delta(\mathbf{l}) = \frac{\rho(\mathbf{l})}{\bar{\rho}} - 1 , \tag{2.78}$$

where $\bar{\rho}$ is the average density of the Universe, can be described by the continuity and Euler equations, and feel the gravitational atraction described by the Newto-

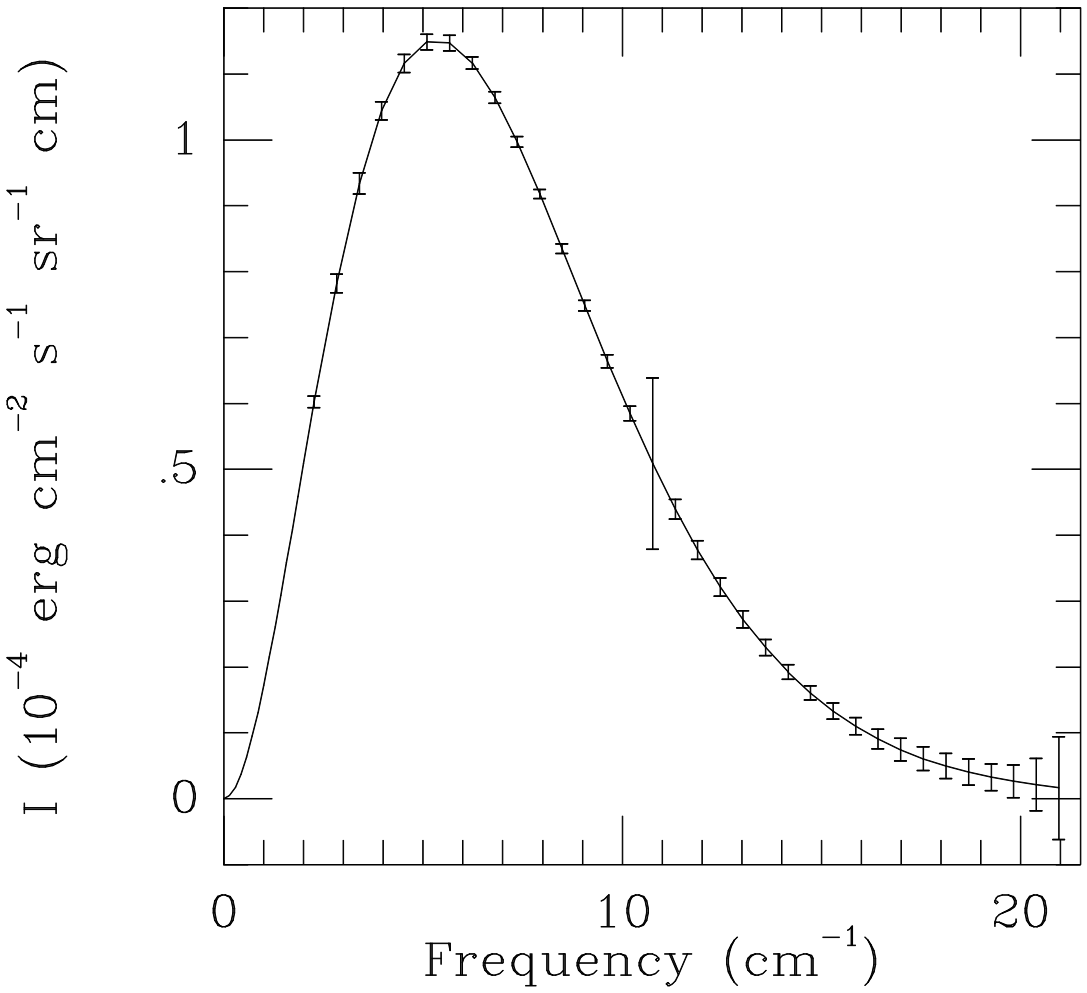

Figure 2.3: Cosmic microwave background radiation (CMBR) spectrum as measured by FIRAS instrument on COBE. The error bars were increased by a factor of 400 to be visible. From Turner & Tyson [1999].

nian Poisson equation [Loeb, 2010]. For small perturbations we can linearize the density perturbations, take its Fourier transform and combine those equations to obtain, to leading order in δ,

$$\frac{\partial^2\delta}{\partial t^2} + 2H\frac{\partial\delta}{\partial t} = 4\pi G\bar{\rho}\delta - \frac{c_S^2 k^2}{a^2}\delta \ , \tag{2.79}$$

where c_s^2 is the sound speed, dependent on each species present in the cosmological fluid. The fluid approach is valid for collisionless dark matter particles until there is the so-called cross-streaming, when distinct fluid elements encounter each other. In the cosmological case this occurs normally at a much later time, when the perturbations become nonlinear, and therefore this approach is valid for small perturbations. The wavenumber $k = 2\pi/\lambda$ is obtained when we expand the density field as a sum over periodic Fourier modes, each with its corresponding comoving wavelength λ. The precise calculation of the evolution of the perturbations needs to take into account other subtle effects as, for instance, the impact on the formation of the first structures due to the relative velocity of dark matter and baryons when the photons decouple from the baryons [Tseliakhovich & Hirata, 2010; Visbal et al., 2012].

To understand statistically the properties of those perturbations the standard procedure is to use two measures. The first is the *correlation function*

$$\xi(\mathbf{r}) = \langle\delta(\mathbf{x}+\mathbf{r})\delta(\mathbf{x})\rangle \ , \tag{2.80}$$

where the average is taken over the entire statistical ensemble of points with a comoving distance $\mathbf{r}$ from the point $\mathbf{x}$. Notice that for the isotropic and homogeneous distribution, ξ is a function of only $r = |\mathbf{r}|$. The second one is the corresponding Fourier transform, the so-called *power spectrum*,

$$P(k) = (2\pi)^{-3}\langle\delta_{\mathbf{k}}\delta^*_{\mathbf{k}'}\rangle \ . \tag{2.81}$$

One could obviously construct higher powers of the perturbation correlation function. However, if the density field is a Gaussian random field its statistical properties are entirely described by the power spectrum only [Lyth & Liddle, 2009]. However, in the case of non-gaussianities the higher order correlations are necessary for understanding the properties and origin of the fields [Bartolo et al., 2004].

In the current standard cosmological model, the origin of those perturbations is ascribed to inflationary fields (that will be discussed in the next section), but for our purposes it is enough to know that most models predict a simple primordial power-law spectrum of perturbations,

$$P(k) \propto k^n \ , \qquad n \approx 1 \ , \qquad \text{(Primordial)} \tag{2.82}$$

where n is the *scalar spectral index*, and for a value around unity the power spectrum is said to be nearly scale invariant, meaning that the gravitational potential fluctuations have the same amplitude over all scales when they enter the horizon.

Nonetheless, this primordial shape changes and develops features as the Universe evolves. A particular transition takes place at the matter-radiation equality discussed above, and it develops a small-scale shape of

$$P(k) \propto k^{n-4} \ , \qquad \text{(Small} - \text{scale)} \tag{2.83}$$

due to the fact that perturbations experience no growth during radiation domination. Those modes therefore have an amplitude much smaller than the extrapolation of long wavelength modes. This can be encoded in the so-called *transfer function* that describes the evolution of the perturbations from the inflationary era to the matter-radiation equality.

In any case, all of this is true for linear perturbations, when their density is much smaller than the average density of the Universe, eq. (2.78). To form the luminous sources that will change the physical state of the Universe forever one needs to go for the nonlinear evolution of the perturbations and the theory behind formation of structures.

2.4.3. The first luminous objects

To understand the formation of the first objects in the Universe as well as their impact on the evolution of the cosmos one needs to model the nonlinear evolution of the perturbations, as the halos of dark matter are going to seed the formation of galaxies and stars.

Nowadays numerical simulations of structure formation can be performed over a wide range of scales, and help us to understand the behavior of the cosmic

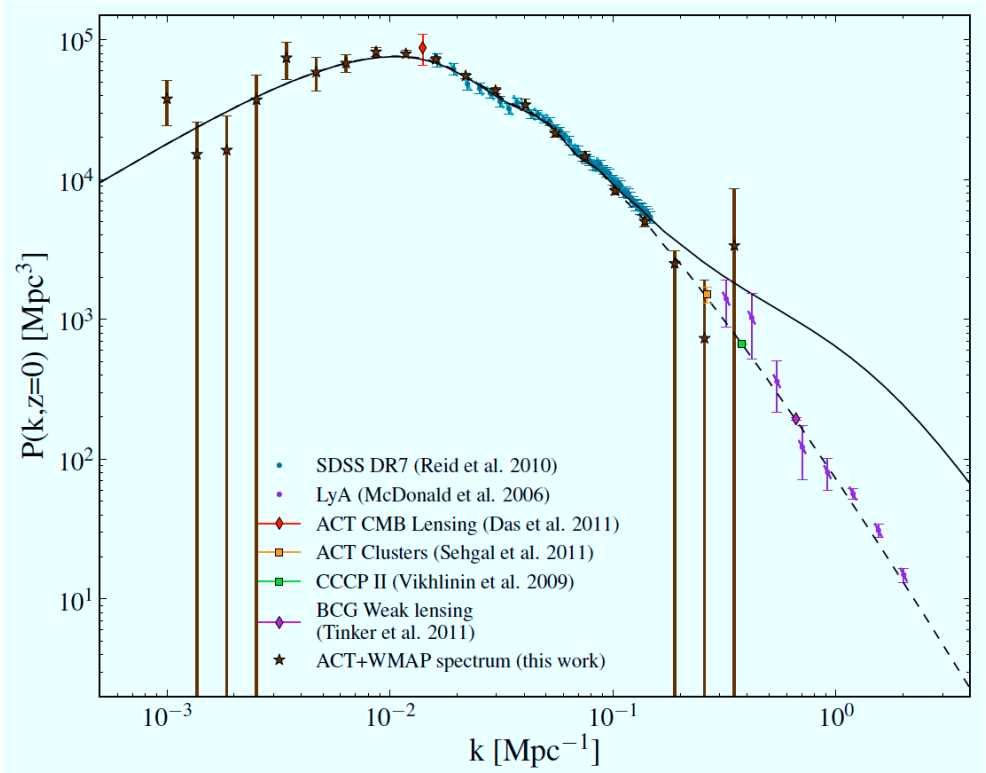

Figure 2.4: Reconstructed matter power spectrum: the stars show the power spectrum from combining the Atacama Cosmology Telescope (ACT) and WMAP data, compared to a serie of measurements of the power spectrum at different scales. The solid and dashed lines show the nonlinear and linear power spectra, respectively, from the best-fit ACT ΛCDM model with spectral index of $n_S = 0.96$. From Hlozek et al. [2012].

web throughout the history of the Universe [Springel et al., 2006]. While those numerical studies allow for precise predictions and understanding of the evolution, much of the physics can also be understood with simpler analytical models, and this interplay between analytical and numerical results allow for a better understanding of the formation of structures in the Universe.

Using the collapse model, for instance, one can analytically calculate the fully nonlinear solution for a purely spherical top-hat perturbation and show that the linearized density contrast of a shell of (dark) matter collapsing at redshift z_c had an overdensity, extrapolated to the present day, of [Padmanabhan, 1993; Stiavelli, 2009]

$$\delta_{\rm crit}(z_c) \approx 1.686(1+z_c) \ , \tag{2.84}$$

meaning that overdensities with $\delta > \delta_{\rm crit} \approx 1.686$ at redshift z_c will collapse and virialize.

Using the Press-Schechter formalism [Press & Schechter, 1974] we can predict the fraction of halos with mass above M that has collapsed at a given redshift, and find the number density of comoving halos with mass between M and $M+dm$ [Barkana & Loeb, 2001],

$$n(M,z) = \sqrt{\frac{2}{\pi}}\frac{\rho_m}{M}\frac{-d[\ln\sigma(M)]}{dM}\nu_c \exp\left[-\frac{\nu_c^2}{2}\right] \ , \tag{2.85}$$

where $\nu_c = \delta_{\rm crit}(z)/\sigma(M)$ and $\sigma(M)$ is the root mean square (rms) of the smoothed density field (at radius $R = (3M/4\pi\bar{\rho})^{1/3}$). This scenario has been improved by taking into account more realistic non-spherical collapses: in particular, Sheth & Tormen [1999] allowed for ellipsoidal collapse, allowing for the three different collapsing times (one for each axis), and some years later they fitted simulations in the context of ellipsoidal collapse to obtain more accurate values for the parameters of the model [Sheth & Tormen, 2002].

One extra piece needed for understanding the physics behind the halo properties and formation of structure is the role played by the baryons. As the halos of dark matter form, baryons fall into them due to gravity. However, since baryons are not collisionless, the pressure of the infalling gas becomes important, and the balance between gravity and pressure changes the simple picture of the spherical collapse

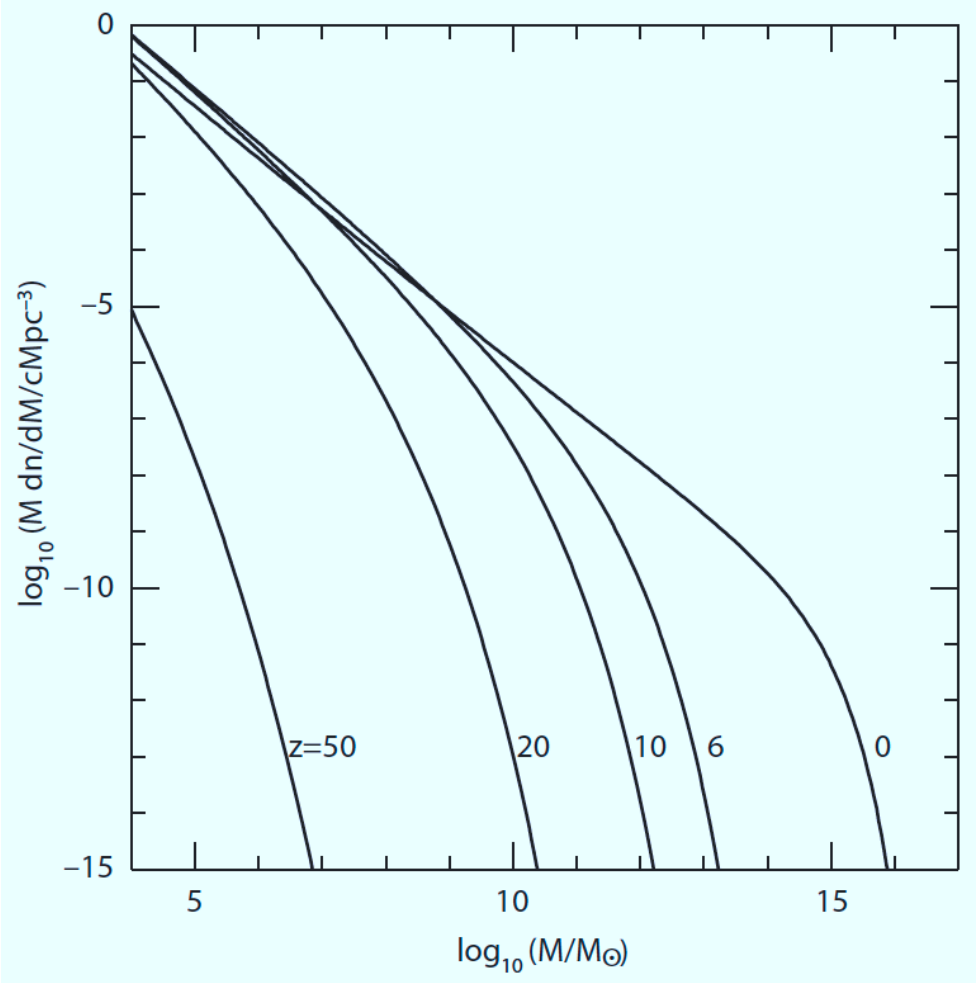

Figure 2.5: Number density of halos per logarithmic bin of halo mass, Mdn/dM (in units of comoving Mpc^{-3}), at various redshifts. From Loeb [2010].

model.

In particular, one can show that there is a scale that separates the stable perturbations from the ones that collapse. This scale is set by the *Jeans mass*, that can be estimated to be, for $z \lesssim 100$, [Barkana & Loeb, 2001]

$$M_J \approx 5.73 \times 10^3 \left(\frac{\Omega_m h^2}{0.15}\right)^{-1/2} \left(\frac{\Omega_b h^2}{0.022}\right)^{-3/5} \left(\frac{1+z}{10}\right)^{3/2} M_\odot \ . \qquad (2.86)$$

When an object with $M > M_J$ collapses, the gas can cool inside this dark matter halo (that cannot condense or cool for being effectively collisionless), eventually condensing to the center and fragmenting into stars. This is the physical mechanism that generates a extended dark matter halo with a core dominated by cold gas and stars.

The evolution and formation of galaxies is a topic of very intensive research nowadays as the computer power increases, allowing for more detailed simulations. In what concerns the rest of this work, we will be interested in the effect that this first luminous sources play in the intergalactic medium (IGM) [Meiksin, 2009; Loeb, 2010]. Although it has not yet been probed directly, it is theoretically expected that the photons produced by the first generation of stars will heat and reionize the intergalactic gas at lower redshifts, producing a significant impact in the properties of the IGM.

2.4.4. Reionization

Observations of the CMB, spectra of early quasars, and other cosmological probes indicate that the intergalactic medium went through a transition at redshifts around 10 in which most of the atomic hydrogen of the Universe was reionized [Fan et al., 2006]. Studies of the Gunn-Peterson effect, an absorption trough seen in the spectra of quasars bluewards of the Lyman-α line [Gunn & Peterson, 1965], for instance, indicate a rapid increase of the neutral fraction between the redshifts 5.5 and 6 [Fan, 2008], and current CMB experiments indicate that $(8.8 \pm 1.5)\%$ (68% C.L.) of the CMB photons were scattered by free electrons after the recombination epoch [Komatsu et al., 2011], implying that the reionization of the Universe took place at $z \approx 10$.

To understand how the first stars were able to ionize the entire IGM one needs to

take into account that as the first stars start burning hydrogen they produce UV and X-ray photons that escape the dark matter halos and interact with the surrounding intergalactic medium. In particular, the description of those spherically symmetric *ionization fronts* needs to include the cosmological expansion, recombinations, and properties of the ionizing sources,

$$\bar{n}_{\rm H}\left(\frac{dV_p}{dt} - 3HV_p\right) = \frac{dN_\gamma}{dt} - \alpha_B C \bar{n}_{\rm H}^2 V_p \ , \tag{2.87}$$

where $\bar{n}_{\rm H}$ is the mean number density of atomic hydrogen, V_p is the physical volume of the ionized sphere, α_B is the coefficient for the case-B recombination, adequate for the optically thick regime [Draine, 2011; Osterbrock & Ferland, 2006], and C is the so-called clumping factor. The first term in the RHS is proportional to the emissivity of the source of photons. It has been shown that those bubbles of ionized hydrogen grow with time, and the IGM goes from a phase in which most hydrogen is atomic to one in which it is basically all ionized [Stiavelli, 2009; Loeb, 2010; Loeb & Furlanetto, 2012].

Finally, it should be mentioned that this period is potentially going to be probed very accurately by forthcoming 21-cm cosmology observations [Furlanetto et al., 2006a; Morales & Wyithe, 2010; Pritchard & Loeb, 2012], a topic we are going to discuss in much more detail in chapter 5.

2.5. Dark Energy Dominated Epoch

Over the last two decades a new cosmological scenario emerged (for some reviews see, for instance, Bahcall et al. [1999]; Freedman & Turner [2003]; Ratra & Vogeley [2008]; Frieman et al. [2008]) thanks to a set of different cosmological observations, especially the precise measurements of the anisotropies of the cosmic microwave background, and of the expansion rate of the Universe using distant Type Ia supernovae back from the time the Universe was about half of its present age.

As we discussed before, the cosmic microwave background is essentially homogeneous and isotropic, with fluctuations of the order $\delta T/T \approx 10^{-5}$. Those small fluctuations carry important cosmological information concerning the status of the baryon-photon coupled fluid in the early Universe, just before the release of

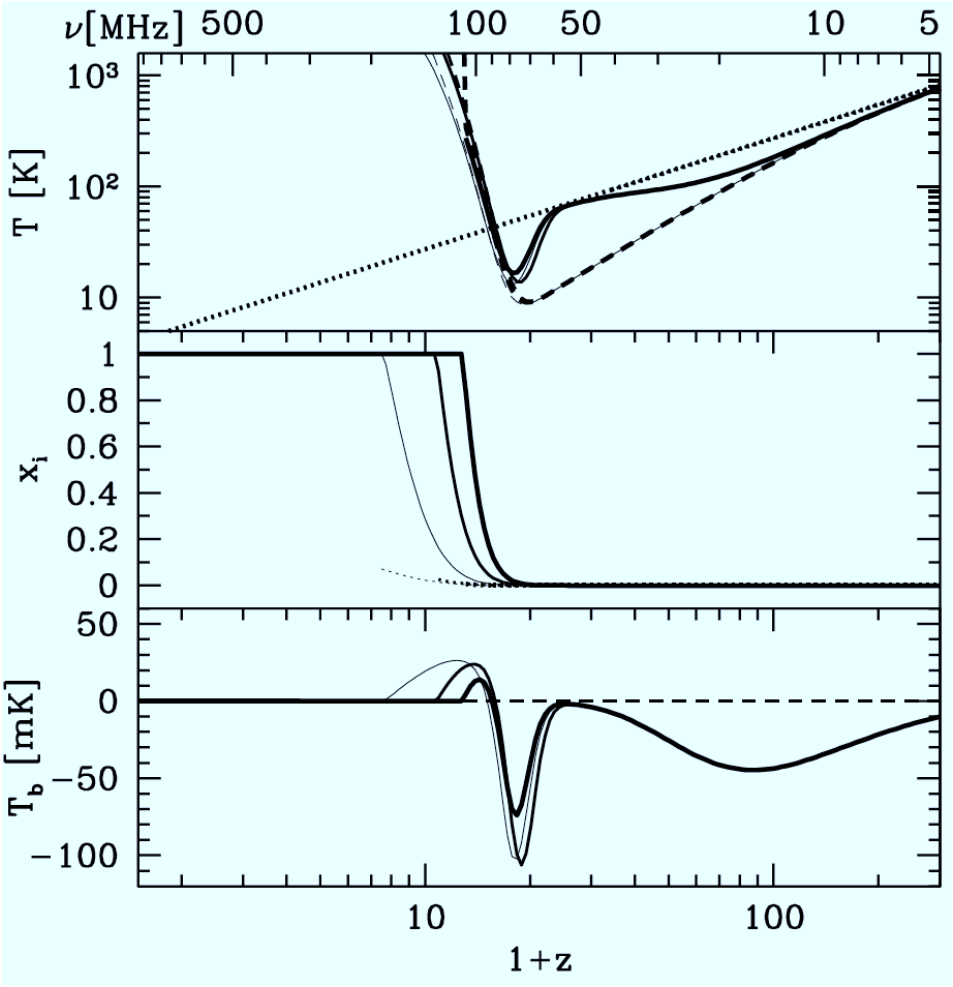

Figure 2.6: From top to bottom: temperature of the IGM, ionized fraction, and global 21-cm signal for different reionization models as a function of redshift. The first population of stars heat and ionize the medium at $z \approx 10$. From Pritchard & Loeb [2012].

the CMB. Using them properly allows for putting constraints on some of the cosmological parameters, like the spatial curvature of the Universe and the baryonic density [Dodelson, 2003].

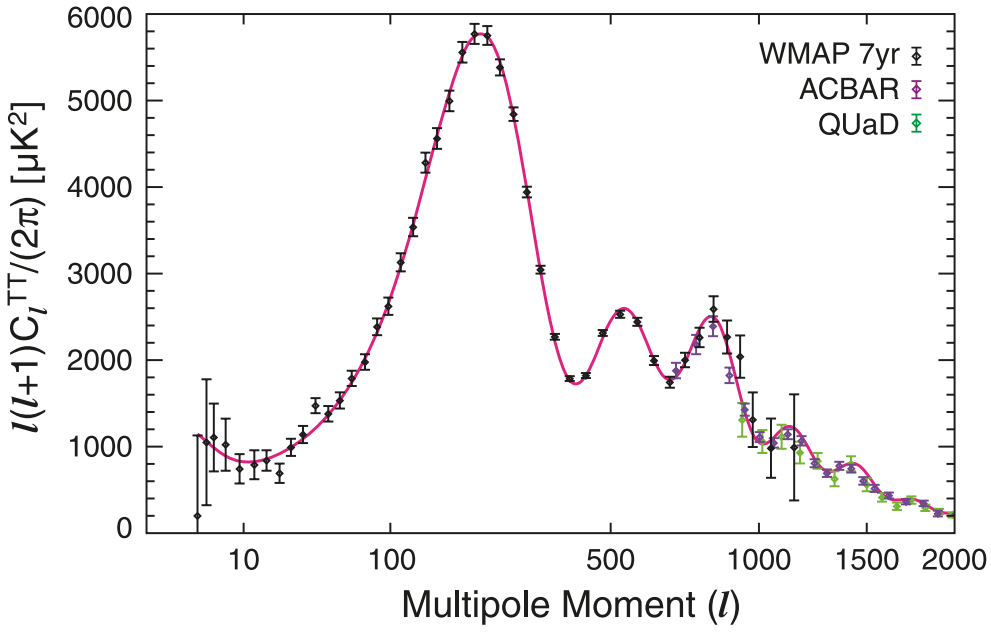

Figure 2.7: The WMAP 7-year temperature power spectrum [Komatsu et al., 2011], along with the temperature power spectra from the ACBAR [Reichardt et al., 2009] and QUaD [Brown et al., 2009] experiments. We show the ACBAR and QUaD data only at $l \geq 690$, where the errors in the WMAP power spectrum are dominated by noise. The solid line shows the best-fitting 6-parameter flat ΛCDM model to the WMAP data alone. From Komatsu et al. [2011].

Nowadays, the most precise data of CMB anisotropies come from the WMAP 7yr data (Wilkinson Microwave Anisotropy Probe) satellite[12], shown in Figure 2.7. In the particular case of the spatial curvature, the recent results of the combination between several CMB, Type Ia supernovae, BAO, and the two point function of the BOSS-CMASS galaxy sample [Sanchez et al., 2012] indicate that

$$10^3\ \Omega_K \equiv 10^3\ (1 - \Omega_0)\ =\ -4.5^{+4.3}_{-4.2}\ , \tag{2.88}$$

that is, the energy density of the Universe is very close to the critical one. However, as we discussed earlier, baryonic density cannot be larger than around 4% of the

[12] `http://map.gsfc.nasa.gov/`

present critical density [Sanchez et al., 2012],

$$100\ \Omega_{b0}h^2\ =\ 2.223^{+0.039}_{-0.037}\ , \tag{2.89}$$

a result that agrees extremely well with light element abundances.

Even including the dark matter contribution, the total matter density amounts to [Sanchez et al., 2012]

$$100\ \Omega_{m0}h^2 = 11.13 \pm 0.40\ . \tag{2.90}$$

Therefore, CMB alone results in the need of a smooth component that dominates currently the energy density of the Universe.

On top of that, in the late 90's two independent groups observing Type Ia supernovae gathered evidence [Riess et al., 1998; Perlmutter et al., 1999] for the astonishing result that the expansion of the Universe is *accelerating*, indicating the presence of a cosmological constant-like fluid that contributes to about 70% of the present energy of the Universe, figure 2.8).

Supernovae data [Shapiro & Turner, 2006] indicate with 5σ confidence level that there was a recent period of acceleration for the Universe, corresponding to a negative *deceleration parameter*,

$$q_0\ \equiv\ -\frac{\ddot{a}_0}{a_0H_0^2}\ =\ \frac{4\pi G}{3H_0^2}\ \sum_i \rho_i\,(1+3\omega_i)\ =\ \frac{\Omega_0}{2}+\sum_i \frac{3}{2}\ \Omega_i\omega_i\ , \tag{2.91}$$

where i correspond to the different fluids, as well as evidence for an earlier decelerated period. Moreover, as the number of supernovae observed increases the error bars keep shrinking towards a cosmological constant [Conley et al., 2011], especially when combined with different cosmological datasets (see, *e.g.*, Figure 2.9).

Those results lead to a cosmological paradigm in which this negative pressure fluid, coined *dark energy* (DE) [Peebles & Ratra, 2003; Copeland et al., 2006; Caldwell & Kamionkowski, 2009; Amendola & Tsujikawa, 2010], is the dominant component of the energy of the Universe, driving its dynamics nowadays.

Moreover, different pieces of evidence for the existence of dark energy come from several other cosmological observations. We just cite here some of them,

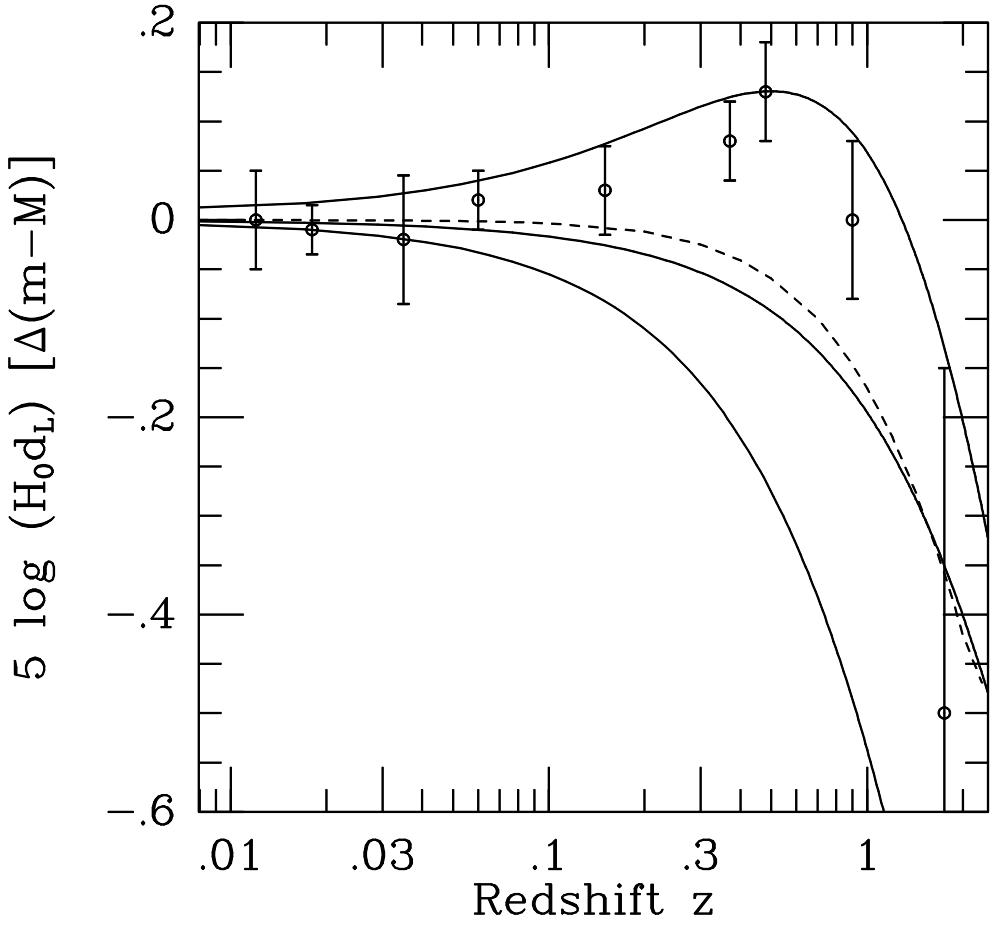

Figure 2.8: Hubble diagram for around 200 Type Ia supernovae. From top to bottom, $(\Omega_{m0} = 0.3; \Omega_{\Lambda 0} = 0.7)$, $(\Omega_{m0} = 0.3; \Omega_{\Lambda 0} = 0)$ and $(\Omega_{m0} = 1; \Omega_{\Lambda 0} = 0)$. The dashed curve represents an Universe in which $q = 0$ over all its evolution, and therefore points above it indicate a period of acceleration. From Freedman & Turner [2003].

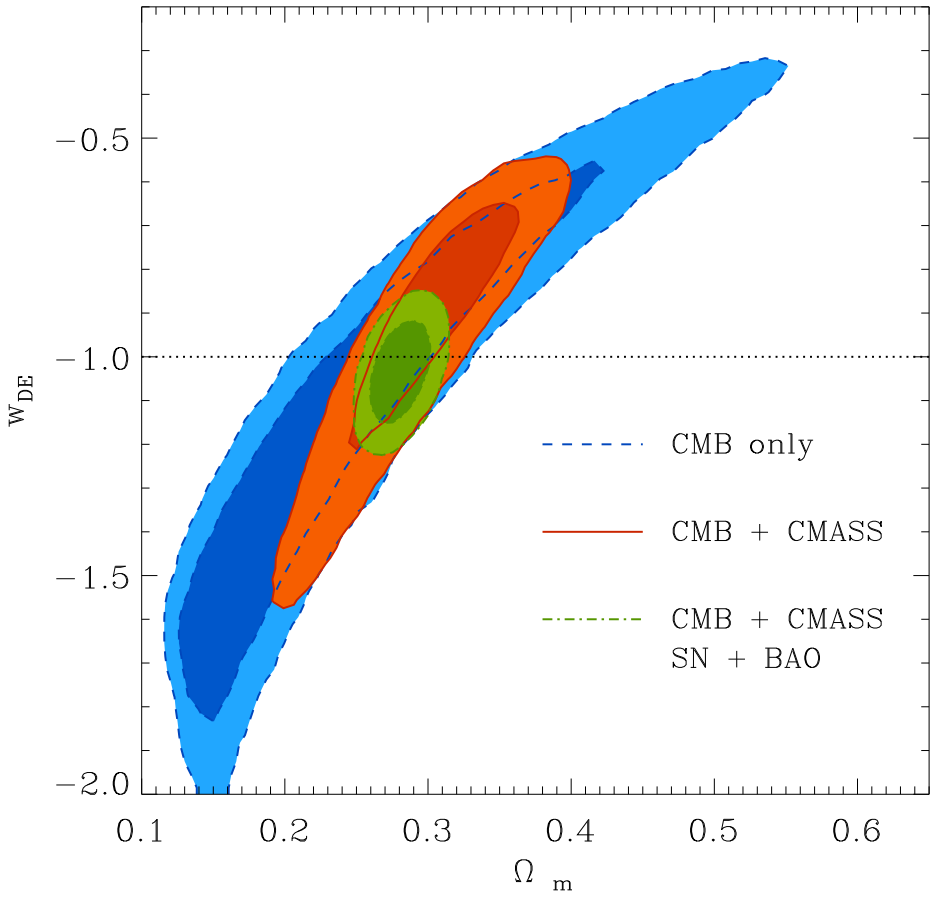

Figure 2.9: The marginalized posterior distribution in the $\Omega_m - w_{DE}$ ($w_{DE} \equiv \omega_\phi$ in our notation) plane for the ΛCDM parameter set extended by including the redshift-independent value of w_{DE} as an additional parameter. The dashed lines show the 68% and 95% contours obtained using CMB information alone. The solid contours correspond to the results obtained from the combination of CMB data plus the shape of the redshift-space correlation function (CMASS). The dot-dashed lines indicate the results obtained from the full dataset combination (CMB+CMASS+SN+BAO). The dotted line corresponds to the ΛCDM model, where $w_{DE} = -1$. From Sanchez et al. [2012].

especially the ones which are important currently to pinpoint the nature of the dark energy, and the ones that probably will become important during the next years, like baryonic acoustic oscillations (BAO) [Seo & Eisenstein, 2003, 2007; Beutler et al., 2011; Xu et al., 2012; Padmanabhan et al., 2012], weak lensing [Huterer, 2002; Zhan et al., 2009; Vanderveld et al., 2012], 21-cm cosmology [Pritchard et al., 2007; Wyithe et al., 2008; Chang et al., 2008; Masui et al., 2010], and others [Seljak et al., 2006; Cunha et al., 2009].

The number of possible candidates for dark energy that emerged in the last few years is enormous [Amendola & Tsujikawa, 2010], and we are going to review only two of them: the *cosmological constant*, important not only for historical reasons, but also because the data seems to be narrowing the results towards it, and the scalar field models for dark energy, the dubbed *quintessence models*. But before that, we should take a brief look at another period in which the Universe supposedly had its expansion accelerated, the so-called *inflationary period*.

2.5.1. A short digression: Inflation

The standard cosmological model, although sucessful, presents some problems with its "initial conditions". Within the context of the standard big bang model, there is no explanation for the observed homogeneity and isotropy of the Universe on large scales, what was known in the early 1980's as the *horizon problem*: as the Universe expands, regions that were not in causal contact before become accessible. An example of that is, for instance, that during the decoupling time the horizon corresponded to a size of around 1° in the present sky. Therefore, we would not expect the homogeneity and isotropy of the CMB on scales larger than that.

In the same way, one can show that a flat Universe, that is $\Omega = 1$, is the only stable point for the equations of regular matter in the Universe. If the Universe was slightly closed or open during its early stages, it rapidly evolves away from $\Omega \sim 1$, since

$$\begin{aligned} (\Omega - 1)_{\mathrm{RD}} &= (\Omega_i - 1) \left(\frac{t}{t_i}\right)^{2/3} , \\ (\Omega - 1)_{\mathrm{MD}} &= (\Omega_i - 1) \frac{t}{t_i} , \end{aligned}$$

during radiation and matter domination, respectively, and for an open or closed

Universe. Since observations indicate that $\Omega_0 \sim 1$, it implies that for the nucleosynthesis epoch $\Omega_{\rm nuc} - 1 \sim t_{\rm nuc}/t_0 \sim 10^{-18}$. Therefore, in order to obtain the present dynamics of the Universe, the initial density had to be fine-tuned to be *extremely* close to the critical density, what became known as the *flatness problem*.

Alan Guth [Guth, 1981] noticed, in a seminal paper, that phase transitions very early in the history of the Universe would lead to a period of *early accelerated expansion*. He called this period inflation, and noticed that it would solve the issues discussed above and other problems (like the overabundance of heavy relics) if it lasted long enough. Although the original model was known to have problems in percolating the bubbles of the phase transition, the importance of an accelerated phase to explain the initial conditions of the Universe was rapidly recognized, and soon enough new models without the problems of the original one were proposed [Linde, 1982, 1983; Albrecht & Steinhardt, 1982].

To see how a period of acceleration can solve some of the problems discussed above, we can analyze again the Friedmann equation,

$$\Omega - 1 \;=\; \frac{k}{H^2 a^2} \;.$$

Since one can show that in general $H \propto t^{-1}$, H is always decreasing in value, and therefore Ω would being taken away from 1. However, if $d(Ha)/dt > 0$, what would take Ω towards 1. One can show that a condition for that is,

$$\frac{d(Ha)}{dt} \;>\; 0 \;\Rightarrow\; \ddot{a} \;>\; 0 \;.$$

An accelerating Universe leads the Universe towards flatness. Moreover, if this inflation happens early and lasts enough, the whole observable Universe will have expanded from a small region that *was in causal contact* before inflation, explaining the homogeneity and isotropy, as well as diluting away any unwanted relic abundance [Lyth & Liddle, 2009].

Therefore, one can define inflation as the time when the Universe is accelerating expanding,

$$\frac{d(Ha)}{dt} \;>\; 0 \qquad \Longleftrightarrow \qquad \ddot{a} \;>\; 0 \qquad \Longleftrightarrow \qquad \omega < -\frac{1}{3} \;,$$

where we have used eq. (2.18). Notice that a cosmological constant like fluid is

the candidate for causing the inflation, since $\omega_\Lambda = -1$. However, inflation needs to finish and a reheating process [Bassett et al., 2006] to take place (populating the Universe with radiation and baryons, since inflation dilutes strongly any previous particle abundance that could exist). Therefore, one needs a "cosmological constant" behavior, but with a fluid that after inflation either decays into photons to start the "standard big bang", or that at least decays faster than any subdominant component and leaves place for gravitational reheating to happen.

In terms of the Friedmann equation, for a constant energy density ρ_Λ,

$$H = \frac{\dot{a}}{a} = \sqrt{\frac{8\pi G}{3}\,\rho_\Lambda} = \text{const} \qquad \Rightarrow \qquad a(t) = a(t_i)\exp\left[H(t-t_i)\right] \ , \quad (2.92)$$

where t_i is the initial time for the inflation. Therefore, in the case a constant energy density dominates the energy density of the Universe, the scale factor increases exponentially, being that the reason Guth called this expansion inflationary.

2.5.2. Cosmological constant

Arguably the most natural candidate for dark energy is the so-called *cosmological constant*. As we have discussed in the previous chapter, the cosmological constant has been revived several times in the last decades, mostly motivated by cosmological problems [Carroll et al., 1992], like the age of the Universe (section 2.6), and theoretical prejudices for a flat Universe [Turner et al., 1984; Ostriker & Steinhardt, 1995; Krauss & Turner, 1995].

However, the fact its energy density is constant and of the order of the *present critical density* brings several unanswered questions [Weinberg, 1989]. One of them is the *coincidence problem*: why the dark energy and the matter densities have the same order of magnitude in the present, even if they scale differently for the whole history of the Universe. We shall come back to this problem in the end of the chapter.

Another conundrum as complicated as this one is the *cosmological constant problem*. The cosmological constant turns out to be a measure of the energy density of the vacuum and although we cannot calculate the vacuum energy with any confidence, this identification allows us to consider the scales of various contributions to the cosmological constant.

The configuration with the lowest energy density in a theory (if it exists) will be one in which there is no contribution from kinetic or gradient energy in the Lagrangian of the theory, like the minimum in the Higgs potential, for instance. Therefore, the vacuum energy-momentum tensor is given by

$$T^{\Lambda}_{\mu\nu} = -\rho_{\Lambda} g_{\mu\nu} \ , \tag{2.93}$$

with ρ_{Λ} given by the minimum of the potential energy for each theory. Notice that this form for the vacuum energy-momentum tensor can also be argued for on the more general grounds that it is the only Lorentz-invariant form for $T^{\Lambda}_{\mu\nu}$ of a perfect fluid, eq. (2.11).

The vacuum can therefore be thought of as a perfect fluid with

$$\omega_{\Lambda} = \frac{p_{\Lambda}}{\rho_{\Lambda}} = -1 \ . \tag{2.94}$$

The vacuum energy is also equivalent to writing in the right-hand side of Einstein's equations a new term of the form $\Lambda g_{\mu\nu}$, for

$$\rho_{\Lambda} \equiv \frac{\Lambda}{8\pi G} \ . \tag{2.95}$$

This equivalence is the origin of the identification of the cosmological constant with the energy of the vacuum, and shows that we can also think about the cosmological constant in gravitational terms. In fact, the action for general relativity in the presence of a "bare" cosmological constant Λ_0

$$S = \frac{1}{16\pi G} \int d^4x \sqrt{-g}(R - 2\Lambda_0) \ , \tag{2.96}$$

leads to Einstein's equations (2.10) plus a cosmological constant term like the one discussed above. Thus, the cosmological constant can be thought of as simply a constant term in the Lagrange density of the theory. Indeed, eq. (2.96) is the most general covariant action we can construct out of the metric and its first and second derivatives [Carroll, 2001].

Classically, then, the effective cosmological constant is the sum of a bare term Λ_0 and the potential energy V of the fields present in the Universe. But there is still another contribution, coming from quantum fluctuations in the fields.

A (free) quantum field can be understood as a collection of an infinite number of harmonic oscillators in momentum space. Formally, the zero-point energy of such an infinite collection will be infinite [Weinberg, 1989; Carroll et al., 1992]. If, however, we discard the very high-momentum modes on the grounds that we trust our theory only up to a certain ultraviolet momentum cutoff k_{max}, we find that the resulting energy density is of the form

$$\rho_\Lambda \sim \hbar k_{\mathrm{max}}^4 \ . \tag{2.97}$$

In flat spacetime, this energy has no effect, and is traditionally discarded by a process known as "normal-ordering". However, when one is dealing with curved spacetimes, like FRW, the actual value of the vacuum energy has important consequences.

The "net" cosmological constant, therefore, is the sum of all those contributions, including potential energies from scalar fields, zero-point fluctuations of each field theory, and the bare cosmological constant Λ_0.

In the particular case of the first of them, we can consider the Weinberg-Salam electroweak model, where the phases of broken and unbroken symmetry are distinguished by a potential energy difference of approximately $M_{\mathrm{EW}} \sim 200$ GeV. Therefore, except for some incredible coincidence, we would expect a contribution for the cosmological constant coming from the electroweak symmetry breaking of order

$$\rho_\Lambda^{\mathrm{EW}} \sim (200 \text{ GeV})^4 \sim 3.7 \times 10^{26} \text{ g cm}^{-3} \ . \tag{2.98}$$

In the case of fluctuations, we should choose our cutoff at the energy past which we no longer trust our field theory. If we are confident that we can use ordinary quantum field theory all the way up to the Planck scale $m_{\mathrm{p}} = (8\pi G)^{-1/2} \sim 10^{18}$ GeV, we would obtain

$$\rho_\Lambda^{m_{\mathrm{p}}} \sim (10^{18} \text{ GeV})^4 \sim 2.3 \times 10^{89} \text{ g cm}^{-3} \ , \tag{2.99}$$

far beyond any reasonable value for the observed cosmological constant,

$$\rho_\Lambda^{(\mathrm{obs})} \leq (10^{-12} \text{ GeV})^4 \sim 2.3 \times 10^{-31} \text{ g cm}^{-3} \ , \tag{2.100}$$

The ratio of eq. (2.99) to eq. (2.100) is the origin of the famous discrepancy of 120 orders of magnitude between the theoretical and observational values of the cosmological constant [Weinberg, 1989], what became known as *the cosmological constant problem*.

The practical approach that most people take is to assume that the cosmological constant is zero, by some (yet to be discovered) reason, and try to attack the dark energy using different tools. One of them is using scalar fields to explain the current acceleration of the Universe, very much like they are used for primordial inflation. In the next section, we are going to review briefly the use of scalar fields in cosmology, initially for inflationary models, and then in the scenarios known as quintessential models.

2.5.3. The potential of scalar fields

As we mentioned earlier, the idea of inflation was born in the context of phase transitions in the early Universe. However, Guth's original model suffer from a problem known as *graceful exit*, a problem already pointed out in the original paper. Inflation in this model was caused by the supercooling of the Universe during a phase transition. Bubbles of the new phase should form and percolate. But because of the exponential expansion of the horizon, bubbles will never percolate, and the whole scenario is spoiled.

However, soon enough new models appeared, like the *New inflation* models [Linde, 1982; Albrecht & Steinhardt, 1982] and the *Chaotic models* [Linde, 1983]. They were based on the idea of using different scalar field (dubbed *inflaton*) potentials, and after that essentially all inflationary models were based on the same approach.

The overall idea is that the early Universe is homogeneously filled with a scalar field Φ (or more than one in the *Hybrid models* [Lyth & Liddle, 2009]) dominated by its potential $V(\Phi)$. The action of this field in curved spacetime is given by

$$S = \int d^4x \sqrt{-g} \left[\frac{1}{2} g^{\mu\nu} \partial_\mu \Phi \partial_\nu \Phi - V(\Phi) \right] \tag{2.101}$$

(where g is the determinant of the metric tensor $g_{\mu\nu}$), and the corresponding

energy-momentum tensor is

$$T_{\mu\nu} = \frac{1}{2}\partial_\mu\Phi\partial_\nu\Phi + \frac{1}{2}(g^{\alpha\beta}\partial_\alpha\Phi\partial_\beta\Phi)g_{\mu\nu} - V(\Phi)g_{\mu\nu} \ . \tag{2.102}$$

Comparing the above equation with the one of a perfect fluid, eq. (2.11), for a homogeneous field, we have that the 0-0 component is given by

$$T^0_0 = \rho_\Phi = \dot{\Phi}^2 - \frac{1}{2}\dot{\Phi}^2 + V(\Phi) \qquad \Rightarrow \qquad \rho_\Phi = \frac{1}{2}\dot{\Phi}^2 + V(\Phi) \ , \tag{2.103}$$

and the spatial components correspond to

$$(-1)(-T^i_i) = p_\Phi = \frac{1}{2}\dot{\Phi}^2 - V(\Phi) \qquad \Rightarrow \qquad p_\Phi = \frac{1}{2}\dot{\Phi}^2 - V(\Phi) \ . \tag{2.104}$$

The equation of state of ω_Φ is given by

$$\omega_\Phi \ = \ \frac{p_\Phi}{\rho_\Phi} \ = \ \frac{\frac{1}{2}\dot{\Phi}^2 - V(\Phi)}{\frac{1}{2}\dot{\Phi}^2 + V(\Phi)} \ \Rightarrow \ -1 \ \leq \ \omega_\Phi \ \leq \ 1 \ . \tag{2.105}$$

As one can see from the above equation, when the potential energy dominates over the kinetic one, the field behaves like a cosmological constant, as we have commented in the beginning of the section. In the opposite situation, when the kinetic energy dominates, the energy density of the inflaton scales as a^{-6}, much faster than matter and radiation.

The equation of motion for the scalar field can be obtained by varying its action with respect to the field, and analogously to the flat spacetime case, this corresponds to the Klein-Gordon equation,

$$\Box\Phi = -\frac{dV}{d\Phi} \tag{2.106}$$

where the covariant d'Alembertian is $\Box = \nabla^\nu\nabla_\nu = g^{\mu\nu}\nabla_\mu\nabla_\nu$. Therefore, in an expanding Universe, a spatially homogeneous scalar with potential $V(\Phi)$ and minimal coupling to gravity has the equation of motion given by

$$\ddot{\Phi} + 3H\dot{\Phi} + \frac{dV}{d\Phi} = 0 \ , \tag{2.107}$$

where H is the Hubble parameter, and overdots indicate time derivatives. Notice

that the Hubble parameter acts as a friction term: the field will be overdamped (and thus approximately constant) when $H > \sqrt{d^2V/d\Phi^2}$, and underdamped (and thus free to roll) when $H < \sqrt{d^2V/d\Phi^2}$.

This equation of motion could also be obtained from the fluid equation eq. (2.19) of the scalar field,

$$\dot{\rho_\Phi} = -3H\left(\rho_\Phi + p_\Phi\right) , \tag{2.108}$$

using equations (2.103) and (2.104).

There are a lot more about inflation discussed elsewhere, like its key role in seeding the perturbations of structure formation [Dodelson, 2003; Lyth & Liddle, 2009], how the models can be probed by current observations [Dodelson et al., 1997; Lidsey et al., 1997; Dvorkin & Hu, 2010; Mortonson et al., 2011], and on the construction of particle physics models of inflation [Lyth & Riotto, 1999; Lyth & Liddle, 2009]. However, as stated before, our main interest here is the fact that recent observations indicates that the Universe is again in an accelerated period, and that scalar field models can also be used to explain the current acceleration of the Universe, the so-called *quintessence models*.

Quintessence

As we just discussed, a scalar field[13] ϕ only gravitationally coupled to the matter content of the Universe can be an alternative to the cosmological constant the dark energy if its energy density is similar to the present critical density of the Universe [Peebles & Ratra, 1988; Ratra & Peebles, 1988; Wetterich, 1988; Frieman et al., 1995; Ferreira & Joyce, 1998].

Caldwell, Dave and Steinhardt [Caldwell et al., 1998] coined the term *quintessence* for the scalar field, and proposed that it could have small perturbations that, in principle, could be probed in the CMB and matter power spectrum. Different quintessence models correspond to different choices of the scalar field potential.

Two classes of particular solutions, called *tracker* and *scaling* solutions [Copeland et al., 1998; Liddle & Scherrer, 1999; Steinhardt et al., 1999; Zlatev et al., 1999], were soon discovered. Those solutions correspond to stable dynamical fixed points [Copeland et al., 2006] for the coupled system of equations given by

[13] We will use ϕ for the quintessence field, in order to distinguish it from the inflaton field Φ.

$$\begin{aligned} \dot{H} &= -\frac{\kappa^2}{2}\left(\gamma_{\mathrm{bf}}\rho_{\mathrm{bf}} + \dot{\phi}^2\right) , \\ \ddot{\phi} &= -3H\dot{\phi} - \frac{dV}{d\phi} , \\ \dot{\rho}_{\mathrm{bf}} &= -3\gamma_{\mathrm{bf}}H\rho_{\mathrm{bf}} , \end{aligned} \tag{2.109}$$

where $\gamma_i \equiv 1+\omega_i$, and the index *bf* denotes the dominant background fluid (matter or radiation) when the system reaches the fixed point.

Both the tracker and scaling solutions are characterized by the fact that the quintessence equation of state, eq. (2.105) becomes constant in the fixed point, that is, the system reaches a point in which the ratio between the kinetic and potential energies becomes constant. In the next section, we are going to discuss why those solutions are interesting, the differences between them, and what kind of quintessence potentials generate each of the solutions.

Tracker and scaling quintessence

The idea of using quintessential tracker solutions first emerged as a tentative to address the *coincidence problem*: why are dark energy and dark matter energy densities of the same order of magnitude in the present epoch? This problem arises because dark energy must have a negative pressure to accelerate the Universe, and cold dark matter (as well as baryons) has vanishing pressure. Therefore, the ratio of their energy densities ρ, for a constant equation of state ω_ϕ of dark energy, must vary as

$$\frac{\rho_m}{\rho_\phi} = \frac{\rho_{m0}}{\rho_{\phi 0}}(1+z)^{-3\omega_\phi} \approx \frac{(1+z)^3}{2} , \tag{2.110}$$

what makes the current epoch a very special one, when both terms contribute almost equally to the energy density of the Universe.

As we are going to discuss, tracker models cannot solve the coincidence problem. In this sense, what models of quintessence do, in general, is to fine tune the overall scale of the potential of dark energy (or the scale in which modifications of general relativity become important) to be of order of the present critical density, a fine tuning that emerges even when one is using tracking or scaling solutions.

More recent tentatives to solve this problem include scalar fields with non-

canonical kinetic terms where the equation of state of the field changes to a cosmological constant-like as the background changes from radiation to matter domination (see, e.g., Armendariz-Picon et al. [2000, 2001]), and (spatial) curvature coupled quintessence, where the existence of a small spatial curvature of the Universe, $\Omega_K \lesssim 10^{-3}$, triggers the recent dark energy domination [França, 2006]. However, the former apparently have a very small parameter space that can generate relevant cosmological solutions, and the latter still is a phenomenological model, to be obtained from a more fundamental theory, and also has to be compared to different data sets to check its consistency. The coincidence problem still is a tricky problem to be solved by any serious dark energy candidate.

Tracker solutions were initially though to be able to solve the problem because in the fixed point (fp) regime, both quintessence and matter densities scale on the same way, and therefore the ratio between the densities after the stable solution is reached is given by

$$\frac{\rho_m^{\rm fp}}{\rho_\phi^{\rm fp}} = \frac{\Omega_m^{\rm fp}}{\Omega_\phi^{\rm fp}} = \text{ constant } . \tag{2.111}$$

In fact, one can show that the fixed point is stable and can be reached from a wide range of initial conditions, and therefore could, at least in principle, address the coincidence. However, the constant ratio implies that the quintessence *tracks* the behavior of the background fluid, and even when the ratio is the correct one ($\sim 3/7$), the quintessence equation of state is very close to the matter one, and therefore cannot accelerate the Universe.

Nonetheless, even though the coincidence problem cannot be solved by those solutions, they still are interesting because for them the *dark energy equation of state remains constant*. Therefore, assuming a constant equation of state when fitting the data is a well motivated fact *in the context of those solutions*, although surely one has to keep an open mind and test for other possibilities [Linder, 2008b], like varying equations of state [Albrecht et al., 2006; Albrecht & Bernstein, 2007].

In this way, we will discuss how to obtain the kind of potentials that generate such solutions [Liddle & Scherrer, 1999], although we are not going to discuss their dynamical stability [Copeland et al., 2006]. Before that, we have to stop and clarify an issue on the notation of the solutions, since the *tracker* solutions have been defined differently in the almost simultaneous works [Steinhardt et al., 1999; Zlatev et al., 1999] and [Liddle & Scherrer, 1999]. In the former, they define a

tracker solution as the one in which

$$\omega_\phi \approx \frac{\omega_{\rm bf} - 2(\Gamma - 1)}{1 + 2(\Gamma - 1)}, \qquad \Gamma \equiv \frac{V'' V}{(V')^2} ,$$

for $\Gamma > 1$ and approximately constant. Prime in this equation denotes derivatives with respect to the field ϕ, and $\omega_{\rm bf}$ corresponds to the background equation of state.

The same kind of solution has been defined in [Liddle & Scherrer, 1999] as a scaling one. In this work, a tracker solution is one in which $\Gamma = 1$, leading to $\omega_\phi = \omega_{\rm bf}$. This is the definition we are going to use here and in the other chapters.

To obtain the potentials, we have to write the equations in a more convenient form. Using the definition of the energy density for a spatially homogeneous scalar field, we have that

$$\dot{\rho}_\phi = \dot{\phi}\left(\ddot{\phi} + \frac{dV}{d\phi}\right) = -3H\dot{\phi}^2 , \tag{2.112}$$

where for the last equality we have used the Klein-Gordon equation. Then, assuming the constant behavior for both the equations of state of the background, $\rho_{\rm bf} \propto a^{-m}$, and quintessence, $\rho_\phi \propto a^{-n}$, we have that

$$\dot{\rho}_\phi + 3H\gamma_\phi\rho_\phi = 0 \quad \Rightarrow \quad \frac{\dot{\rho}_\phi/2}{\rho_\phi} = -\frac{3}{2}H\gamma_\phi = -\frac{nH}{2} , \tag{2.113}$$

that is,

$$\frac{\dot{\phi}^2/2}{\rho_\phi} = \frac{n}{6} . \tag{2.114}$$

Assuming that the initial density of the background fluid is much larger than the quintessence, $\rho_\phi \ll \rho_{\rm bf}$, we have that the scale factor evolves as $a(t) \propto t^{2/m}$, and therefore

$$H = \frac{\dot{a}}{a} = \frac{2}{m}\frac{t^{(2-m)/m}}{t^{2/m}} = \frac{2}{m}\, t^{-1} . \tag{2.115}$$

That leads to the field equation,

$$\ddot{\phi} = -\frac{6}{m}\frac{\dot{\phi}}{t} - \frac{dV}{d\phi} , \tag{2.116}$$

and since

$$\rho_\phi \propto a^{-n} \propto t^{-2n/m} , \tag{2.117}$$

we finally obtain that eq. (2.114) reads

$$\dot{\phi} \propto \sqrt{\rho_\phi} \propto t^{-n/m} \ . \tag{2.118}$$

That set of equations is now in a very suitable form, since plugging eq. (2.118) in eq. (2.116), we can integrate the equations to obtain the scalar field potential $V(\phi)$. That is what we are going to do next for both tracker and scaling solutions.

a) Tracker solutions

For $n = m$, eq. (2.118) gives

$$\int d\phi \propto \int \frac{dt}{t} \propto \ln t \quad \Rightarrow \quad \phi(t) = A \ \ln(t/t_\star), \tag{2.119}$$

where A is a constant, and the field is written in units of m_p, and one can show from the equation of motion of the scalar field, eq. (2.116), that

$$V(\phi) = \frac{2t_\star}{\lambda^2}\left(\frac{6}{m} - 1\right) e^{-\lambda\phi} \equiv V_0 \ e^{-\lambda\phi} \ , \tag{2.120}$$

that is, the tracker solutions happen for the "famous" exponential potential, [Ratra & Peebles, 1988; Wetterich, 1988; Ferreira & Joyce, 1998; Copeland et al., 1998]. This tracker solution is a stable fixed point for $\lambda^2 > 3\gamma_{\rm bf}$, with the density parameter of the quintessence given by

$$\Omega_\phi^{\rm fp} = \frac{3\gamma_{\rm bf}}{\lambda^2} \ . \tag{2.121}$$

In fact, one can show [Liddle & Scherrer, 1999; Copeland et al., 1998] that the exponential potential is the only one which presents tracker solutions for the uncoupled quintessence. However, as we discussed before, *tracker solutions* cannot accelerate the Universe, and therefore we know that those kind of solutions are excluded, although one can consider different behaviors of the exponential potential, like its scaling solutions [França & Rosenfeld, 2002] to look for cosmologically interesting solutions.

b) Scaling solutions

A scaling solution is the one in which the positive constants $m = 3\gamma_{\rm bf}$

and $n = 3\gamma_\phi$ are different. As we are going to see, this kind of solutions arise naturally in inverse law potentials [Ratra & Peebles, 1988], also called *Ratra-Peebles potentials*, for obvious reasons.

For $n \neq m$, we have from eq. (2.118) that

$$\int d\phi \propto \int t^{-n/m} dt \quad \Rightarrow \quad \phi(t) = A\ t^{1-n/m}\ , \tag{2.122}$$

where A is simply a constant. The field equation in this case gives

$$V(\phi) = A^2 \left(1 - \frac{n}{m}\right)^2 \frac{(6-n)}{2n} \left(\frac{\phi}{A}\right)^\alpha \equiv V_0\ \phi^\alpha\ , \tag{2.123}$$

where

$$\alpha = \frac{2n}{n-m} \quad \Rightarrow \quad n = \frac{\alpha}{\alpha - 2}\ m\ . \tag{2.124}$$

Therefore, scaling solutions happen for inverse law potentials.

We have two particular solutions of interest: $\alpha > 2$ and $\alpha < 0$. Notice that $0 < \alpha \leq 2$ is not included, since we assumed that n and m are positive constants. Moreover, if $\alpha = 0$, then the potential is simply a constant and does not depend on ϕ.

Moreover, in the attractor regime, we have that the two equations of state can be related,

$$\gamma_\phi = \frac{\alpha}{\alpha - 2}\ \gamma_{\rm bf} \quad \Rightarrow \quad \omega_\phi = \frac{2}{\alpha - 2} + \frac{\alpha}{\alpha - 2}\ \omega_{\rm bf}\ . \tag{2.125}$$

In the present epoch, the background fluid is composed by nonrelativistic matter, and therefore,

$$\omega_\phi = \frac{2}{\alpha - 2}\ , \tag{2.126}$$

which is negative for $\alpha < 0$.

Summing up, we see that the scaling solution can in principle provide the observed acceleration of the Universe, with the ratio of densities given by

$$\frac{\rho_\phi}{\rho_m} \propto a^{-n/3}\ , \tag{2.127}$$

from where one can clearly see that the coincidence problem still is present,

since one has to fine tune the parameters of the potential (V_0, α) in order to obtain reasonable cosmological histories. Moreover, it should be noted that, as in the case of the exponential potentials, one can always evade the attractor conditions for those potentials [Kneller & Strigari, 2003].

To conclude this section, it should be said that scaling solutions are far more common than tracker ones [Copeland et al., 2005]. The exponential potential, for instance, also presents a stable scaling regime [Copeland et al., 1998], valid for $\lambda^2 < 3\gamma_{\rm bf}$, with the equation of state given by

$$\omega_\phi = -1 + \frac{\lambda^2}{3} \tag{2.128}$$

that can explain the current acceleration of the the Universe and the dark energy density with the same level of fine tuning required in more elaborate models [França & Rosenfeld, 2002]. Those models were later shown to be totally consistent with M / String Theory [Kallosh et al., 2002; Gutperle et al., 2003], and therefore gained an interesting appeal from the theoretical point of view.

2.5.4. Dark energy and the rest of the Universe

Quintessence is modelled by a scalar field whose excitations are very light,

$$m_\phi = \sqrt{\frac{V''(\phi)}{2}} \sim H_0 \sim 10^{-33}\ \text{eV}\ . \tag{2.129}$$

From the point of view of particle physics, the exchange of very light fields gives rise to forces of very long range, a *fifth force*, what makes interesting to consider the direct interaction of the quintessence field ϕ to ordinary matter. Although it is traditional to neglect (or set to zero) the couplings of this light scalar to the standard model particles, we expect such couplings to be present. As an example, they could be present in the form [Copeland et al., 2004]

$$\mathcal{L}_{\phi F} = -\frac{1}{4g^2(\phi(t))} F_{\mu\nu}\tilde{F}^{\mu\nu} = -\frac{1}{4} B(\phi(t)) F_{\mu\nu}\tilde{F}^{\mu\nu} \tag{2.130}$$

where $\tilde{F}^{\mu\nu}$ is the dual of the electromagnetic strength tensor, $2\tilde{F}^{\mu\nu} = \epsilon^{\alpha\beta\mu\nu}F_{\alpha\beta}$.

That kind of couplings leads to a variation in the fine structure constant α [Uzan, 2003, 2011], and assuming a coupling of the form $B(\phi) = 1 - \zeta(\phi - \phi_0)/m_p$, for most quintessence potentials one can obtain a limit in which $\zeta < 10^{-5}$ [Copeland et al., 2004]. The robust limit $\zeta < 10^{-3}$ comes only from the equivalence principle [Olive et al., 2002], obtained comparing the differential acceleration of light and heavy elements, and therefore is also valid for the coupling of this field with baryons in the Universe. Moreover, astrophysical and cosmological bounds on density dependent couplings strongly constrains those couplings [Ellis et al., 1989; Dent et al., 2009].

Moreover, tests of the gravitational inverse square law found no evidence for a deviation of the standard gravity [Adelberger et al., 2009] down to the scale $\lambda = 56$ μm [Kapner et al., 2007], smaller than the dark energy scale, given by $\rho_{\phi 0}^{1/4} \sim 2.2 \times 10^{-3}$ eV $\sim (90\ \mu\text{m})^{-1}$.

Yet another scenario was proposed [Khoury & Weltman, 2004a,b] using self-interactions of the scalar-field to avoid the most restrictive of the current bounds. They dubbed such scalars *chameleon fields* due to the way in which the mass of the field depends on the density of matter in the local environment. A chameleon field might be very heavy in relatively high density environments, such as the Earth and its atmosphere, but almost massless cosmologically where the density is much lower. This feature allows for the field to evade local constraints on fifth force effects. However, the linearised equations have been probed and a lot of the parameter space has been excluded [Upadhye et al., 2012; Adelberger et al., 2007], although there are claims that nonlinear effects play an important role [Mota & Shaw, 2006, 2007] and can change those conclusions. In this sense, we see that even in more exotical scenarios the coupling to baryons seems to be severely constrained.

Nonetheless, there is still another possibility to be studied: the coupling between dark energy and dark matter. Those, obviously, can be probed only cosmologically, since none of them has been directly detected yet, although one should keep in mind that the stability of the quintessence potentials severely constrains the coupling, as is usual for scalar potentials [Doran & Jäckel, 2002], unless one assumes (as we will do in the rest of the text) to be already dealing with the "quantum corrected potential". This interaction leads, in general, to radically different predictions for the dark sector, and also to distinct properties of the dark matter

particle, like the variation of its mass. That idea is the main responsible behind several models that arose later, in particular the idea of neutrino as a mass-varying particle that we are interested in.

Coupled dark energy

In this section we are going to consider the modifications on the background equations that arise from the coupling between quintessence and dark matter. Both components, as discussed in the previous chapters, have their behaviors dictated by the conservation of the energy momentum tensors $T^{(\phi)}_{\mu\nu}$ and $T^{(C)}_{\mu\nu}$, respectively (hereafter the index C refers to the cold dark matter component).

General covariance requires the conservation of their sum, so that it is possible to consider a coupling such that,

$$\begin{aligned} \nabla^\mu T^{(\phi)}_{\nu\mu} &= -\delta(\phi)\, T^{\alpha(C)}_{\alpha} \nabla_\nu \phi \ , \\ \nabla^\mu T^{(C)}_{\nu\mu} &= \delta(\phi)\, T^{\alpha(C)}_{\alpha} \nabla_\nu \phi \ , \end{aligned} \tag{2.131}$$

where δ is a free parameter, normally taken to be a constant, although it can be a function of the field ϕ.

Such a coupling arises for instance in string theory, or after a conformal transformation of Brans-Dicke theory [Amendola, 1999, 2000], although one should keep in mind that the specific coupling (2.131) is only one of the possible forms, and more complicated functions are also possible, as well as more phenomenological approaches [Mangano et al., 2003; Quartin et al., 2008].

The coupling to relativistic particles like photons (and neutrinos in the early Universe, as we will discuss later) in this case vanish, since

$$T^{\beta(r)}_{\beta} \equiv T^{(r)} = \rho_r - 3p_r = 0 \ . \tag{2.132}$$

The equations (2.131) for a homogeneous quintessence can be written as

$$\begin{aligned} \dot{\rho}_\phi + 3H\rho_\phi(1+\omega_\phi) &= -\delta(\phi)\rho_C\dot{\phi} \ , \\ \dot{\rho}_c + 3H\rho_c &= \delta(\phi)\rho_C\dot{\phi} \ , \end{aligned} \tag{2.133}$$

that is, the usual fluid equation plus a right-hand side dependent on the coupling.

Notice that this amounts to saying that the usual scaling of the energy densities with the scale factor, $\rho \propto a^{-3(1+\omega)}$ for constant ω, does not hold here. In fact, one can rewrite the above equations in the form

$$\begin{aligned} \dot{\rho}_\phi + 3H\rho_\phi(1+\omega_\phi^e) &= 0, \\ \dot{\rho}_c + 3H\rho_c(1+(1+\omega_c^e)) &= 0\ , \end{aligned} \tag{2.134}$$

where the effective equations of state are given by

$$\begin{aligned} \omega_\phi^e &= \omega_\phi + \frac{\delta(\phi)\rho_C\dot{\phi}}{3H\rho_\phi} = \omega_\phi + \frac{\mathcal{I}}{3H\rho_\phi}\ , \\ \omega_c^e &= -\frac{\delta(\phi)\dot{\phi}}{3H} = -\frac{\mathcal{I}}{3H\rho_c}\ , \end{aligned}$$

where we define $\mathcal{I} = \delta(\phi)\rho_C\dot{\phi}$, and this fact holds for *any interaction term* $\mathcal{I}$.

The Klein-Gordon equation is given by,

$$\ddot{\phi} + 3H\dot{\phi} = -\frac{dV}{d\phi} - \delta(\phi)\rho_c\ , \tag{2.135}$$

and clearly shows the effect on the field of the coupling with the dark matter: it inserts an extra piece in the potential of the quintessence.

The rest of the fluids (baryons, neutrinos and photons) follow the same standard equations, as well as the Friedmann equation,

$$H^2 = \frac{1}{3m_p^2}\left(\rho_c + \rho_b + \rho_\gamma + \rho_\nu + \frac{1}{2}\dot{\phi}^2 + V(\phi)\right)\ . \tag{2.136}$$

In what follows we are going to consider a particular model as an example, but before doing it, we shall describe another way to interpret the above equations, in the context of mass-varying cold dark matter particles.

2.5.5. Mass-varying particles

In general, when one considers two interacting species, like in eq. (2.133), we are interested in interactions that happen via quantum field theory creation and/or annihilation of particles, like models in which the dark matter particles [Lattanzi &

Valle, 2007] or massive neutrinos [Beacom et al., 2004] decay, leading their number density to be

$$n(t) = n_i \left(\frac{a_i}{a}\right)^3 \exp[-t/\tau] \ , \tag{2.137}$$

to fall faster than a^{-3}, where n_i is the initial number density when the decay starts, and τ is the mean lifetime of the particle [Kolb & Turner, 1990].

However, here we will be interested in a less standard form of interaction: one in which the mass of the particle depends on the vacuum expectation value (vev) of the quintessence field,

$$m_c(\phi) = m_{c0} f(\phi) \ . \tag{2.138}$$

In this case the particle is not decaying into quintessence or any other particle, and its number is conserved,

$$\dot{n}_c + 3Hn_c = 0 \ . \tag{2.139}$$

Therefore, the energy density $\rho_c = m_c n_c$ obeys the equation

$$\dot{\rho}_c + 3H\rho_c = \frac{d\ln[f(\phi)]}{d\phi}\rho_c\dot{\phi} \ . \tag{2.140}$$

Comparing equations (2.133) and (2.140), one can clearly see that the former can be interpreted as a set of equations of a mass-varying particle coupled to the quintessence field, with an interaction term

$$\delta(\phi) = \frac{d\ln[f(\phi)]}{d\phi} \ . \tag{2.141}$$

The idea of a cosmological important mass-varying particle has been investigated initially in the context of scalar-tensor theories [Casas et al., 1992]. The term "VaMPs" for those scenarios was coined by Anderson & Carroll [1998], which also analyses some cosmological consequences of a particular coupling, and brings into attention the fact that with an extra contribution to the potential, eq. (2.135), it is possible to define a minimum for the sum of the two, and therefore to obtain a cosmological constant behavior for the field stuck in the bottom of the potential.

In order to analyse in more detail this class of models, we are going to take a particular potential and mass variation, the so-called exponential VaMP model [Comelli et al., 2003; França & Rosenfeld, 2004].

The potential of the DE scalar field ϕ is given by

$$V(\phi) = V_0 \; e^{\beta\phi/m_p}, \tag{2.142}$$

where V_0 and β are positive constants. Dark matter is modelled by a particle of mass

$$m_c = m_{c0} \; e^{-\lambda(\phi-\phi_0)/m_p} \; , \tag{2.143}$$

where m_{c0} is the current mass of the dark matter particle and λ a constant parameter. Comparing with previous equations, we see that in this case $\delta(\phi)$ is given by,

$$\delta = -\frac{\lambda}{m_p} = \text{ constant} \; . \tag{2.144}$$

The fluid equations become,

$$\begin{aligned} \dot{\rho}_c \; &+ \; 3H\rho_c = -\frac{\lambda\dot{\phi}}{m_p} \; \rho_c \; , \\ \dot{\rho}_\phi \; &+ \; 3H\rho_\phi(1+\omega_\phi) = \frac{\lambda\dot{\phi}}{m_p} \; \rho_c \; , \end{aligned} \tag{2.145}$$

where $\omega_\phi = p_\phi/\rho_\phi = (\frac{1}{2}\dot{\phi}^2 - V)/(\frac{1}{2}\dot{\phi}^2 + V)$ is the usual equation of state parameter for a homogeneous scalar field.

Thus, we have that

$$\begin{aligned} \omega_c^{(e)} \; &= \; \frac{\lambda\dot{\phi}}{3Hm_p} = \frac{\lambda\phi'}{3m_p} \; , \\ \omega_\phi^{(e)} \; &= \; \omega_\phi - \frac{\lambda\dot{\phi}}{3Hm_p} \; \frac{\rho_c}{\rho_\phi} = \omega_\phi - \frac{\lambda\phi'}{3m_p} \; \frac{\rho_c}{\rho_\phi} \; , \end{aligned} \tag{2.146}$$

are the effective equation of state parameters for dark matter and dark energy, respectively. Primes denote derivatives with respect to $u = \ln(a) = -\ln(1+z)$, and $a_0 = 1$.

The Klein-Gordon equation reads

$$\ddot{\phi} + 3H\dot{\phi} = \frac{\lambda\rho_\chi}{m_p} - \frac{\beta V}{m_p} \; . \tag{2.147}$$

The Klein-Gordon and the Friedmann equations become, in terms of u,

$$H^2\phi'' \;+\; \frac{1}{3m_p^2}\left[\frac{3}{2}(\rho_b+\rho_c)+\rho_r+3V\right]\phi' = \frac{\lambda\rho_c}{m_p} - \frac{\beta V}{m_p}\ , \qquad (2.148)$$

$$H^2 = \frac{(1/3m_p^2)\ (\rho_c+\rho_b+\rho_r+V)}{1-(1/6m_p^2)\ \phi'^2}\ , \qquad (2.149)$$

where we have neglected the mass of the neutrinos, and their contribution is summed with the photons one, denoted by radiation (r).

Using the fact that the right-hand side of eq. (2.148) is the derivative with respect to the field ϕ of an effective potential [Hoffman, 2003],

$$V_{\rm eff}(\phi) = V(\phi)+\rho_c(\phi)\ , \qquad (2.150)$$

one can show that there is a fixed point value for the field, given by $dV_{\rm eff}(\phi)/d\phi = 0$:

$$\frac{\phi}{m_p} = -\ \frac{3}{(\lambda+\beta)}\ u\ +\ \frac{1}{(\lambda+\beta)}\ln\left(\frac{\beta V_0}{\lambda\rho_{c0}e^{\lambda\phi_0/m_p}}\right)\ . \qquad (2.151)$$

At the present epoch the energy density of the Universe is divided essentially between dark energy and dark matter. In this limit, using the above solution, one obtains

$$\Omega_\phi = 1-\Omega_c = \frac{3}{(\lambda+\beta)^2}+\frac{\lambda}{\lambda+\beta}\ , \qquad (2.152)$$

$$\omega_c^{(e)} = \omega_\phi^{(e)} = -\ \frac{\lambda}{\lambda+\beta}\ , \qquad (2.153)$$

which is a stable attractor for $\beta > -\lambda/2+(\sqrt{\lambda^2+12})/2$. The equality between ω_c and ω_ϕ clearly denotes a tracker solution coming from the behavior of the exponential potential [Amendola, 1999; Comelli et al., 2003; França & Rosenfeld, 2004] in this regime.

The density parameters for the components of the Universe and the effective equations of state for the DE and DM for a typical solution are shown in Fig. 2.10. Notice that the transition to the tracker behavior in this example is currently occurring.

Moreover, in those models, the cosmological predictions are in general much different when compared with the "standard cases" of a cosmological constant or

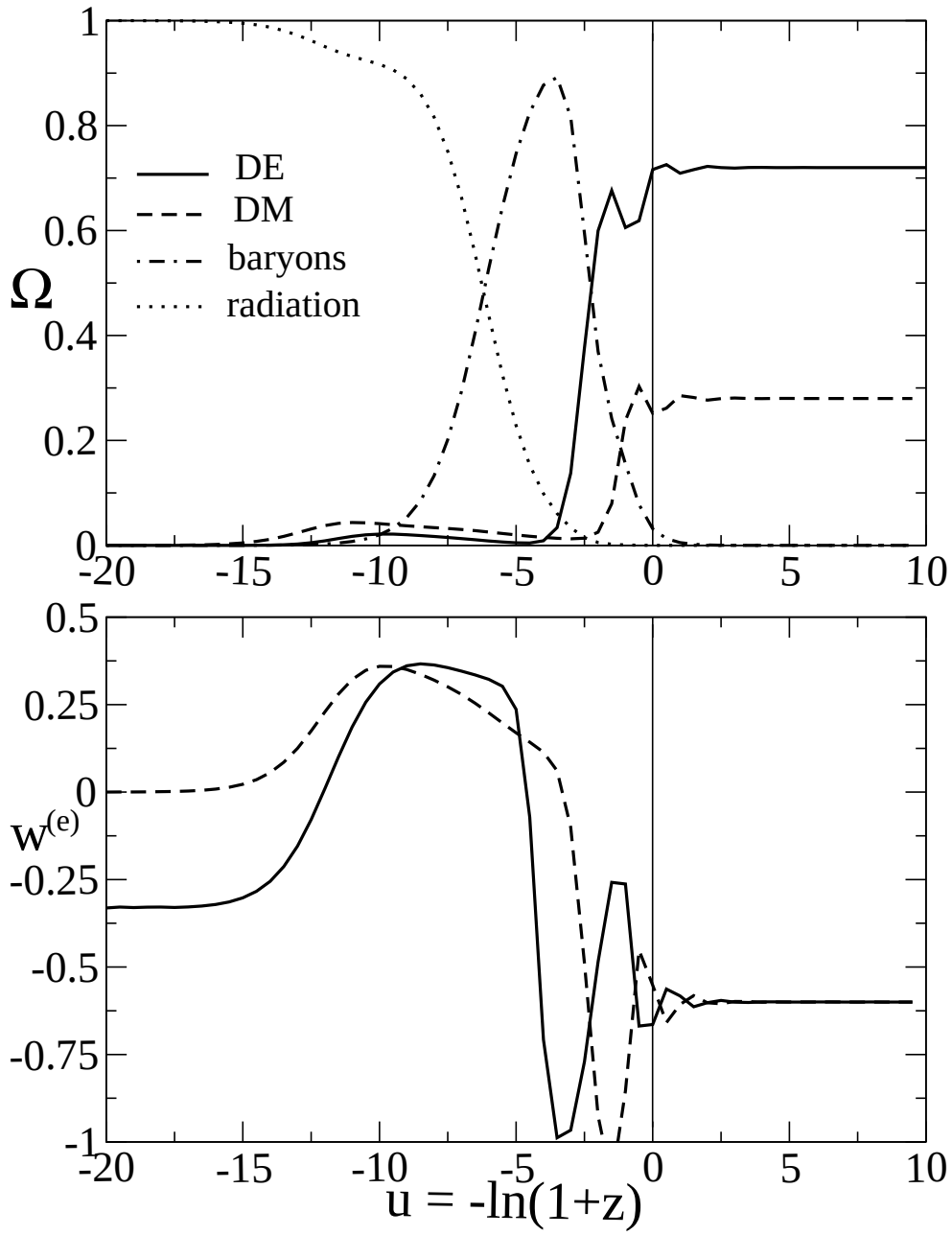

Figure 2.10: *Top panel*: Density parameters of the components of the Universe as a function of $u = -\ln(1+z)$ for $\lambda = 3$, $\beta = 2$ and $V_0 = 4.2 \times 10^{-48}$ GeV^4. After a transient period of baryonic matter domination (dot-dashed line), DE comes to dominate and the ratio between the DE (solid line) and DM (dashed line) energy densities remains constant. *Bottom panel*: Effective equations of state for DE (solid line) and DM (dashed line) for the same parameters used in top panel. In the tracker regime both equations of state are negative. From França & Rosenfeld [2004].

an uncoupled quintessence. The acceleration of the Universe could have started as early as $z \sim 3$ [Amendola, 2003; Amendola et al., 2006], the relic abundance of cold dark matter could be altered by as much as 40% [Rosenfeld, 2005], and a possible super-acceleration of the Universe that violates the weak energy condition, $\omega_\phi < -1$, could be accomodated without problems [Das et al., 2006].

Therefore, the message is that even background quantities like the abundance of dark matter and the expansion history could be severely changed if we allow for different models of the dark sector. Because of that, it was initially thought that in this case a tracker solution would be able to solve the coincidence problem [Comelli et al., 2003], although later it became clear that the level of fine tuning needed for such potentials was even stronger than in normal quintessence models [França & Rosenfeld, 2004]. Notice that, also in this case, non-attractor solutions [França & Rosenfeld, 2002] might be cosmologically relevant [Farrar & Peebles, 2004].

2.6. The age of the Universe

To close this chapter, we include here a note on what was probably one of the first indications of the existence of the dark energy: the age of the Universe [Turner et al., 1984; Ostriker & Steinhardt, 1995; Krauss & Turner, 1995].

Although the model independent measures of the age of the Universe still give larger errors, they can exclude some models for the Universe based on the lower limit for the age of the Universe. Assuming that besides matter, there is an extra component in the Universe, which we shall denote by ϕ,

$$\rho \;=\; \rho_m + \rho_r + \rho_\phi \;\Longrightarrow\; \Omega \;=\; \Omega_m + \Omega_r + \Omega_\phi \;.$$

with an equation of state ω_ϕ, we have that

$$\frac{\dot{a}^2}{a^2} + \frac{k}{a^2} \;=\; \frac{8\pi G}{3}\;\left(\rho_m + \rho_r + \rho_\phi\right)\;,$$

Using eq. (2.20), we have that

$$\frac{\dot{a}^2}{a^2} + \frac{k}{a^2} \;=\; \frac{8\pi G}{3}\;\left[\rho_{m0}\left(\frac{a_0}{a}\right)^3 + \rho_{r0}\left(\frac{a_0}{a}\right)^4 + \rho_{\phi 0}\left(\frac{a_0}{a}\right)^{3(1+\omega_\phi)}\right]\;.$$

That can be rewritten as,

$$\dot{a}^2 + k \;=\; a_0^2 H_0^2 \;\left[\Omega_{m0}\left(\frac{a_0}{a}\right) + \Omega_{r0}\left(\frac{a_0}{a}\right)^2 + \Omega_{\phi 0}\left(\frac{a_0}{a}\right)^{1+3\omega_\phi}\right] \;.$$

Notice that we can use the Friedman equation, $k = a_0^2 H_0^2\,(\Omega_0 - 1)$, in such a way that

$$\dot{a} \;=\; a_0 H_0 \,\sqrt{1 - \Omega_0 + \Omega_{m0}\left(\frac{a_0}{a}\right) + \Omega_{r0}\left(\frac{a_0}{a}\right)^2 + \Omega_{\phi 0}\left(\frac{a_0}{a}\right)^{1+3\omega_\phi}} \;.$$

Changing the variables, $y = a/a_0$ and $dy/da = a_0^{-1}$, we have that $da/dt = a_0(dy/dt)$, and

$$t_0 \;=\; H_0^{-1} \int_0^1 \frac{dy}{\sqrt{1 - \Omega_0 + \Omega_{m0}\; y^{-1} + \Omega_{r0}\; y^{-2} + \Omega_{\phi 0}\; y^{-(1+3\omega_\phi)}}} \;, \qquad (2.154)$$

where we assumed that $a_i \approx 0 \ll a_0$. Therefore, this is the equation to be solved to calculate for the age of the Universe.

In a *flat matter dominated Universe* we have, for instance, that

$$t_0 \;=\; H_0^{-1} \int_0^1 dy\; y^{1/2} \;\Longrightarrow\; t_0 \;=\; \frac{2}{3} H_0^{-1} \;\approx\; 6.52\; h^{-1}\;\text{Gyr} \;. \qquad (2.155)$$

WMAP collaboration [Komatsu et al., 2011] has given a stringent value for the age of the Universe, $t_0 = 13.7 \pm 0.2$ Gyr at 68% C.L. However, this result is model dependent and obtained from direct integration of the Friedmann equation for the running spectral index ΛCDM model. More conservative are the observations that indicates as lower limit for the age of the oldest globular clusters (and consequently for the age of the Universe) $t_0 = 10.4$ Gyr at 95% C.L. [Krauss & Chaboyer, 2003].

Notice that this value is far too large when compared with the value given by eq. (2.155). One way to solve those problems is using a cosmological constant plus matter flat Universe. In this case, the age is given by

$$\begin{aligned} t_0 \;&=\; H_0^{-1} \int_0^1 \frac{dy}{\sqrt{(1 - \Omega_{\Lambda 0})\; y^{-1} + \Omega_{\Lambda 0} y^2}} \\ &=\; -\frac{2}{3} H_0^{-1} \int_\infty^1 \frac{du}{u^{5/3}\sqrt{(1 - \Omega_{\Lambda 0}) u^{2/3} + \Omega_{\Lambda 0} u^{-4/3}}} \;, \end{aligned}$$

where $y = u^{-2/3}$ and $dy/du = -2/3\ u^{-5/3}$. Since

$$\int \frac{dx}{x\sqrt{ax^2+bx+c}} = -\frac{1}{\sqrt{c}} \ln\left(\frac{2\sqrt{c}}{x}\sqrt{ax^2+bx+c} + \frac{2c}{x} + b\right) , \qquad c > 0$$

we have that (for $a = 1 - \Omega_\Lambda$, $b = 0$, $c = \Omega_\Lambda$),

$$t_0 = -\frac{2}{3}H_0^{-1}\int_\infty^1 \frac{du}{u\sqrt{(1-\Omega_{\Lambda 0})u^2+\Omega_{\Lambda 0}}} \Longrightarrow t_0 = \frac{2}{3}H_0^{-1}\Omega_{\Lambda 0}^{-1/2} \ln\left[\frac{1+\Omega_{\Lambda 0}^{1/2}}{(1-\Omega_{\Lambda 0})^{1/2}}\right] . \tag{2.156}$$

That is, the age of the Universe depends on the contribution of the cosmological constant $\Omega_{\Lambda 0}$. As one can see in figure 2.11, for a flat Universe the age is always higher when a non-negligible cosmological constant is present. For $\Omega_{\Lambda 0} = 0.7$, for instance,

$$t_0 \approx 1.45 \times \frac{2}{3}H_0^{-1} \approx 9.45\ h^{-1}\ \text{Gyr} \approx 13.5\ \text{Gyr} . \tag{2.157}$$

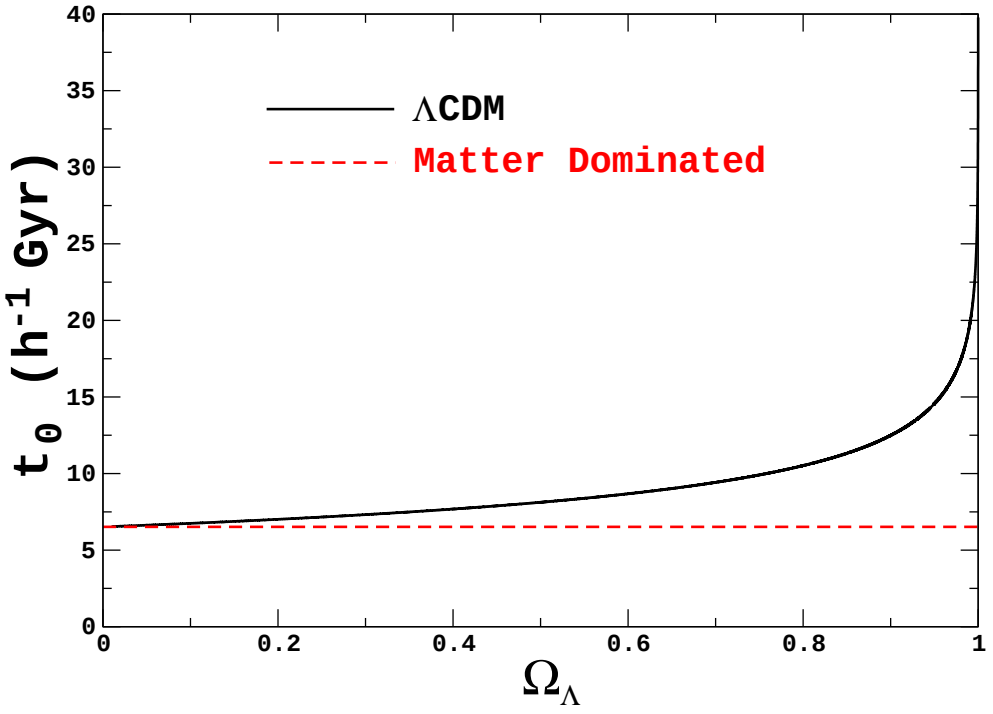

Figure 2.11: Age of the Universe in units of h^{-1} Gyr for a flat Universe with and without a cosmological constant. Dotted line shows $t_0 = \frac{2}{3H_0}$ for comparison only.

In fact, using the limits discussed above and the position of the first Doppler peak in WMAP experiment it is possible to put an upper limit on the equation of state (assumed constant) of the dark energy, $\omega_\phi < -0.67$ at 90% confidence level [Jimenez et al., 2003]. However, current upper limits on the age of the Universe can not constrain the lower value of the equation of state, since for large values of the age ($t_0 \gtrsim 18$ Gyr) the cosmology is essentially independent on the value of the equation of state [Krauss, 2004], unless we assume that reionization took place too early in the Universe history (as indicated by WMAP data), and consequently the upper limit for the age of the Universe is close to the upper limits coming from globular cluster, $t_0 \approx 16$ Gyr, as in the case discussed in [Jimenez et al., 2003].

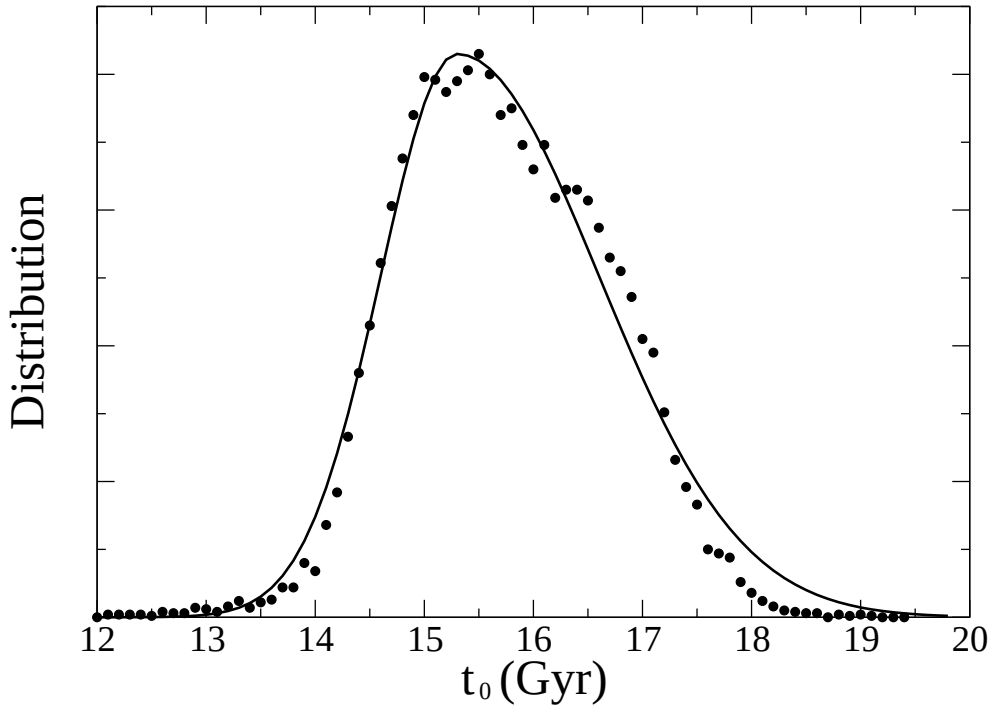

Figure 2.12: Distribution of models that satisfy Hubble parameter ($h = 0.72 \pm 0.08$) and DE parameter density ($\Omega_\phi = 0.7 \pm 0.1$) constraints as a function of age of the Universe for the coupled dark energy-dark matter models. A fit to the points gives $t_0 = 15.3^{+1.3}_{-0.7}$ Gyr at 68% C.L. From França & Rosenfeld [2004].

In the case of a varying dark energy equation of state, a model independent approach to calculate the age of the Universe has been performed [Kunz et al., 2004], and using CMB and supernovae data the age of the Universe was found to

be $t_0 = 13.8 \pm 0.3$ Gyr at 68% C.L., showing that this result seems robust, at least for the simpler dark energy models.

For coupled models, the age of the Universe is in general much higher than the one in standard cosmological models, as one can see from figure 2.12. In particular, comparing with the estimates we have just discussed, $t_0 = 13.8 \pm 0.3$ Gyr at 68% C.L., we have that in the coupled scenario $t_0 = 15.3^{+1.3}_{-0.7}$ Gyr at 68% C.L. [França & Rosenfeld, 2004].

2.7. Summary and Open Problems

In this chapter we discussed briefly the main aspects of the standard cosmological model. We discussed some of the well established results of the model, like the expansion of the Universe, the abundance of light elements, the blackbody spectrum for the CMB, and the age of the Universe, as well as some relatively more recent results that shed some light on the components that constitute the Universe we live in, like the CMB anisotropies, the observation of distant supernovae, and the power spectrum of galaxies.

We also mentioned some of the theoretical developments to explain the evolution of the Universe, from the inflationary early Universe to the recent period of acceleration, passing through the still unexplored dark ages, when the cosmic dawn took place thanks to the formation of the first stars.

Such a model obviously leaves many questions unanswered, and in the rest of this thesis we will focus on our contribution to answer three particular questions concerning the field of astroparticle physics.

Chapter 3 is concerned with the matter-antimatter asymmetry in the early Universe, in the context of leptonic asymmetries. Our goal is to constrain with current cosmological datasets the amount of asymmetries that can be stored in the neutrino sector, and forecast what some of the future experiments might be able to say about it.

Chapter 4 studies in detail a model that could explain the acceleration of the Universe and have some impact on the cosmic neutrino background. In this model, the dark energy is modeled by a scalar field that interacts with neutrinos via their masses. We analyze this model at the background and linear perturbation level to constrain its parameters and its possible impact on the relic neutrinos.

Finally, Chapter 5 deals with the question of the impact of dark matter on cosmological observables and how we can use them to constrain the nature of this particle. In particular, we focus on 21-cm cosmology, a new observational technique that has the potential to play a key role in the understanding of the dark ages and the accurate determination of cosmological paramters. We aim to understand the role played by dark matter in the cosmic dawn, and how we can hope to use this future dataset to constrain dark matter properties.

3

Cosmological Lepton Asymmetry

In the previous chapter we briefly mentioned that observations indicate that the amount of antimatter in the Universe is observed to be small. Probes of the anisotropies of the cosmic microwave background (CMB) together with other cosmological observations have measured the cosmological baryon asymmetry η_b to the percent level thanks to very precise measurements of the baryon density, as η_b is derived through eq. (2.58) [Komatsu et al., 2011]. Quantifying this asymmetry between matter and antimatter of the Universe is crucial for understanding some of the particle physics processes that might have taken place in the early Universe, at energies much larger than the ones that can be reached currently in particle accelerators.

Nonetheless, whereas the lepton asymmetries are expected to be of the same order of the baryonic one due to sphaleron effects [Kolb & Turner, 1990] that equilibrate both asymmetries, it could be the case that other physical processes lead instead to leptonic asymmetries much larger than η_b, eq. (2.58), (see, *e.g.*, Casas et al. [1999]; March-Russell et al. [1999]; McDonald [2000]), with consequences for the early Universe phase transitions [Schwarz & Stuke, 2009], cosmological magnetic fields [Semikoz et al., 2009], and the dark matter relic density [Shi & Fuller, 1999; Laine & Shaposhnikov, 2008; Stuke et al., 2012].

In particular, neutrino asymmetries are also bound to be nonzero in the presence of neutrino isocurvature perturbations, like those generated by curvaton decay [Lyth et al., 2003; Gordon & Malik, 2004; di Valentino et al., 2012]. Those large neutrino asymmetries could affect the cosmological observables [Lesgourgues & Pastor, 1999, 2006], and although the limits on such asymmetries have been

improving over the last years, current constraints are still many orders of magnitude weaker than the baryonic measurement.

On the other hand, thanks to the neutrino oscillations the initial primordial flavor asymmetries are redistributed among the active neutrinos before the onset of Big Bang Nucleosynthesis (BBN) [Dolgov et al., 2002; Wong, 2002; Abazajian et al., 2002], which makes the knowledge of the oscillation parameters important for correctly interpreting the limits on such asymmetries. Nowadays all of those parameters are accurately measured (see, *e.g.*, Fogli et al. [2011, 2012]; Schwetz et al. [2011]; Forero et al. [2012]), with the exception of the mixing angle θ_{13} that only recently started to be significantly constrained. In fact, several neutrino experiments over the last year gave indications of nonzero values for $\sin^2\theta_{13}$ [Abe et al., 2011; Adamson et al., 2011; Abe et al., 2012], and recently the Daya Bay reactor experiment claimed a measurement of $\sin^2(2\theta_{13}) = 0.092 \pm 0.016(\text{stat.}) \pm 0.005(\text{syst.})$ at 68% C.L. [An et al., 2012], excluding a zero value for θ_{13} with high significance. The same finding has been also reported by the RENO Collaboration [Ahn et al., 2012], $\sin^2(2\theta_{13}) = 0.113 \pm 0.013(\text{stat.}) \pm 0.019(\text{syst.})$ (68% C.L.).

Finally, yet another important piece of information for reconstructing the neutrino asymmetries in the Universe is the measured value of the relativistic degrees of freedom in the early universe, quantified in the so-called effective number of neutrinos, $N_{\rm eff}$, defined in eq. (3.2). In the case of the three active neutrino flavors with zero asymmetries and a standard thermal history, its value is the well-known $N_{\rm eff} \simeq 3.046$ [Mangano et al., 2005], but the presence of neutrino asymmetries can increase that number while still satisfying the BBN constraints [Pastor et al., 2009]. Interestingly enough, recent CMB data has consistently given indications of $N_{\rm eff}$ higher than the standard value: recently the Atacama Cosmology Telescope (ACT) [Dunkley et al., 2011] and the South Pole Telescope (SPT) [Benson et al., 2011; Keisler et al., 2011] have found evidence for $N_{\rm eff} > 3.046$ at 95% C. L., making the case for extra relativistic degrees of freedom stronger (see also Archidiacono et al. [2011]). It should however be kept in mind that other physical processes, like, *e.g.*, the contribution from the energy density of sterile neutrinos mixed with the active species [Giusarma et al., 2011; Hamann et al., 2011] or of gravitational waves [Sendra & Smith, 2012] could also lead to a larger value for $N_{\rm eff}$.

Some recent papers have analyzed the impact of neutrino asymmetries with

Table 3.1: Cosmological and neutrino parameters.

Type	Symbol	Meaning	Uniform Prior
Primary	$\Omega_b h^2$	Baryon density	$(0.005, 0.1)$
Cosmological	$\Omega_{dm} h^2$	Dark matter density[a]	$(0.01, 0.99)$
Parameters	τ	Optical depth to reionization	$(0.01, 0.8)$
	$100\theta_s$	Angular scale of the sound horizon at the last scattering	$(0.5, 10)$
	n_s	Scalar index of the power spectrum	$(0.5, 1.5)$
	$\log[10^{10} A_s]$	Scalar amplitude of the power spectrum [b]	$(2.7, 4)$
Neutrino	m_1(eV)	Mass of the lightest neutrino [c]	$(0, 1)$
Parameters	η_ν	Total asymmetry at $T = 10$ MeV	$(-0.8, 0.8)$
	$\eta_{\nu_e}^{\text{in}}$	Initial electron neutrino asymmetry at $T = 10$ MeV	$(-1.2, 1.2)$
Derived	h	Reduced Hubble constant[d]	-
Parameters	ΔN_{eff}	Enhancement to the standard effective number of neutrinos[e]	-

[a] Also includes neutrinos.
[b] at the pivot wavenumber $k_0 = 0.05$ Mpc^{-1}.
[c] We assume here normal mass hierarchy.
[d] $H_0 = 100h$ km s^{-1} Mpc^{-1}.
[e] $N_{\text{eff}} = 3.046$.

oscillations on BBN [Pastor et al., 2009; Mangano et al., 2011, 2012], mainly because data on light element abundances dominate the current limits on the asymmetries. Some studies using CMB data can be found in the literature (see for instance [Lattanzi et al., 2005; Popa & Vasile, 2008; Shiraishi et al., 2009] for limits on the degeneracy parameters ξ_ν using the WMAP data and [Hamann et al., 2008] for the effect of the primordial Helium fraction in a Planck forecast), but our results improve on that in two directions. First, we used for our analysis the neutrino spectra in the presence of asymmetries after taking into account the effect of flavor oscillations. Second, we checked the robustness of our results comparing the analysis of CMB and BBN data with a more complete set of cosmological data, including in particular supernovae Ia (SNIa) data [Kessler et al., 2009], the measurement of the Hubble constant from the Hubble Space Telescope (HST) [Riess et al., 2009], and the Sloan Digital Sky Survey (SDSS) data on the matter power spectrum [Reid et al., 2010]. While current CMB measurements and the other datasets are not expected to improve significantly the constraints on the asymmetries, they constrain the sum of the neutrino masses, giving a more robust and general picture of the cosmological parameters.

Our goal in this chapter is twofold: first, we constrain the neutrino asymmetries and the sum of neutrino masses for both zero and nonzero values of θ_{13} using some of the latest cosmological data to obtain an updated and clear idea of the limits on them using current data; second, we perform a forecast of the constraints that could be achievable with future CMB experiments, taking as an example the proposed mission COrE[1] [Bouchet et al., 2011]. Given that current constraints are basically dominated by the BBN constraints, we use our forecast to answer the more general question of whether future CMB experiments can be competitive with the BBN bounds.

For that, our discussion will be based on our results published in Castorina et al. [2012], and initially we briefly review in Sec. 3.1 the dynamics of the neutrino asymmetries prior to the BBN epoch. With those tools in hand, we proceed to study in Sec. 3.2 the impact on cosmological observables of the neutrino asymmetries for two values of the mixing angle θ_{13} using current cosmological data. We then step towards the future and describe in Sec. 3.3 our forecast for the experiment COrE, where we study the potential of the future data from lensing of

[1] http://www.core-mission.org

CMB anisotropies to constrain some of the cosmological parameters (in particular, neutrino asymmetries and the sum of the neutrino masses) with great precision. Finally, in Sec. 3.4 we draw some remarks on this chapter.

3.1. Evolution of cosmological neutrinos with flavor asymmetries

The dynamics of the neutrino distribution functions in the presence of flavor asymmetries and neutrino oscillations in the early Universe has been discussed in detail in the literature [Pastor et al., 2009; Mangano et al., 2011, 2012], and here we will only briefly review its main features and its consequences for the late cosmology.

We assume that flavor neutrino asymmetries, η_{ν_α}, were produced in the early Universe. As we discussed in Subsection 2.3.2, at large temperatures frequent weak interactions keep neutrinos in equilibrium thus, their energy spectrum follows a Fermi-Dirac distribution with a chemical potential μ_{ν_α} for each neutrino flavor. If $\xi_\alpha \equiv \mu_{\nu_\alpha}/T$ is the degeneracy parameter, the asymmetry is given by

$$\eta_{\nu_\alpha} \equiv \frac{n_{\nu_\alpha} - n_{\bar{\nu}_\alpha}}{n_\gamma} = \frac{1}{12\zeta(3)}\left[\pi^2\xi_\alpha + \xi_\alpha^3\right] \ . \tag{3.1}$$

Here n_{ν_α} ($n_{\bar{\nu}_\alpha}$) denotes the neutrino (antineutrino) number density.

As usual, using equation (2.39) we will write the radiation energy density of the Universe in terms of the parameter $N_{\rm eff}$, the effective number of neutrinos, as

$$\rho_r = \rho_\gamma\left[1 + \frac{7}{8}\left(\frac{4}{11}\right)^{4/3} N_{\rm eff}\right] \ , \tag{3.2}$$

with $N_{\rm eff} = 3.046$ the value in the standard case with zero asymmetries and no extra relativistic degrees of freedom [Mangano et al., 2005]. Assuming that equilibrium holds for the neutrino distribution functions, the presence of flavor asymmetries leads to an enhancement

$$\Delta N_{\rm eff} = \frac{15}{7}\sum_{\alpha=e,\mu,\tau}\left[2\left(\frac{\xi_\alpha}{\pi}\right)^2 + \left(\frac{\xi_\alpha}{\pi}\right)^4\right] \ . \tag{3.3}$$

Note that a neutrino degeneracy parameter of order $\xi_\alpha \gtrsim 0.3$ is needed in order to have a value of ΔN_{eff} at least at the same level of the effect of non-thermal distortions discussed in [Mangano et al., 2005]. This corresponds to $\eta_{\nu_\alpha} \sim \mathcal{O}(0.1)$. On the other hand, the primordial abundance of ^{4}He depends on the presence of an electron neutrino asymmetry and sets a stringent BBN bound on η_{ν_e} which does not apply to the other flavors, leaving a total neutrino asymmetry of order unity unconstrained [Kang & Steigman, 1992; Hansen et al., 2002]. However, this conclusion relies on the absence of effective neutrino oscillations that would modify the distribution of the asymmetries among the different flavors before BBN.

The evolution of the neutrino asymmetries in the epoch before BBN with three-flavor neutrino oscillations is found by solving the equations of motion for 3×3 density matrices in flavor space $\varrho_{\mathbf{p}}$ for each neutrino momentum $\mathbf{p}$ as described in Sigl & Raffelt [1993]; McKellar & Thomson [1994], where the diagonal elements are the usual flavor distribution functions (occupation numbers) and the off-diagonal ones encode phase information and vanish for zero mixing.

Oscillations in flavor space of the three active neutrinos are driven by two mass-squared differences and three mixing angles bounded by the experimental observations [Forero et al., 2012; Fogli et al., 2012]. The equations of motion (EOMs) for $\varrho_{\mathbf{p}}$ are [Pastor et al., 2009],

$$\mathrm{i}\,\frac{d\varrho_{\mathbf{p}}}{dt} = [\Omega_{\mathbf{p}}, \varrho_{\mathbf{p}}] + C[\varrho_{\mathbf{p}}, \bar{\varrho}_{\mathbf{p}}]\,, \tag{3.4}$$

and similar for the antineutrino matrices $\bar{\varrho}_{\mathbf{p}}$. The first term on the r.h.s. describes flavor oscillations,

$$\Omega_{\mathbf{p}} = \frac{\mathrm{M}^2}{2p} + \sqrt{2}\,G_{\mathrm{F}}\left(-\frac{8p}{3m_{\mathrm{w}}^2}\,\mathrm{E} + \varrho - \bar{\varrho}\right)\,, \tag{3.5}$$

where $p = |\mathbf{p}|$ and M is the neutrino mass matrix (opposite sign for antineutrinos). Matter effects are included via the term proportional to the Fermi constant G_{F}, where E is the 3×3 flavor matrix of charged-lepton energy densities [Sigl & Raffelt, 1993]. For our range of temperatures we only need to include the contribution of electrons and positrons. Finally, the last term arises from neutrino-neutrino interactions and is proportional to $\varrho - \bar{\varrho}$, where $\varrho = \int \varrho_{\mathbf{p}}\,\mathrm{d}^3\mathbf{p}/(2\pi)^3$ and similar for antineutrinos.

For the relevant values of neutrino asymmetries this matter term dominates and leads to synchronized oscillations [Dolgov et al., 2002; Wong, 2002; Abazajian et al., 2002] . The last term in eq. (3.4) corresponds to the effect of neutrino collisions, i.e. interactions with exchange of momenta. Here we follow the same considerations of Pastor et al. [2009], in particular concerning the details on the approximations made and related references. In short, the collision terms for the off-diagonal components of $\varrho_{\mathbf{p}}$ in the weak-interaction basis are momentum-dependent damping factors, while collisions and pair processes for the diagonal $\varrho_{\mathbf{p}}$ elements are implemented without approximations solving numerically the collision integrals as in Mangano et al. [2005]. These last terms are crucial for modifying the neutrino distributions to achieve equilibrium with $e^{\pm}$ and, indirectly, with photons.

Therefore, the total lepton asymmetry is redistributed among the neutrino flavors and the BBN bound on η_{ν_e} can be translated into a limit on $\eta_\nu = \eta_{\nu_e} + \eta_{\nu_\mu} + \eta_{\nu_\tau}$, unchanged by oscillations and constant until electron-positron annihilations, when it decreases due to the increase in the photon number density.

The temperature at which flavor oscillations become effective is important not only to establish η_{ν_e} at the onset of BBN, but also to determine whether weak interactions with e^+e^- can still keep neutrinos in good thermal contact with the primeval plasma. Oscillations redistribute the asymmetries among the flavors, but only if they occur early enough interactions would preserve Fermi-Dirac spectra for neutrinos, in such a way that the degeneracies ξ_α are well defined for each η_{ν_α} and the relation in Eq. (3.3) remains valid. This is the case of early conversions of muon and tau neutrinos, since oscillations and collisions rapidly equilibrate their asymmetries at $T \simeq 15$ MeV [Dolgov et al., 2002]. Therefore one can assume the initial values $\eta^{\mathsf{in}}_{\nu_\mu} = \eta^{\mathsf{in}}_{\nu_\tau} \equiv \eta^{\mathsf{in}}_{\nu_x}$, leaving as free parameters $\eta^{\mathsf{in}}_{\nu_e}$ and the total asymmetry $\eta_\nu = \eta^{\mathsf{in}}_{\nu_e} + 2\eta^{\mathsf{in}}_{\nu_x}$. The evolution of the asymmetries with temperature for a particular choice of initial values can be seen in Fig. 3.1

If the initial values of the flavor asymmetries $\eta^{\mathsf{in}}_{\nu_e}$ and $\eta^{\mathsf{in}}_{\nu_x}$ have opposite signs, neutrino conversions will tend to reduce the asymmetries which in turn will decrease N_{eff}. But if flavor oscillations take place at temperatures close to neutrino decoupling this would not hold and an extra contribution of neutrinos to radiation is expected with respect to the value in Eq. (3.3), as emphasized in Pastor et al. [2009] and shown in Fig. 3.2, where the N_{eff} isocontours for non-zero mixing are

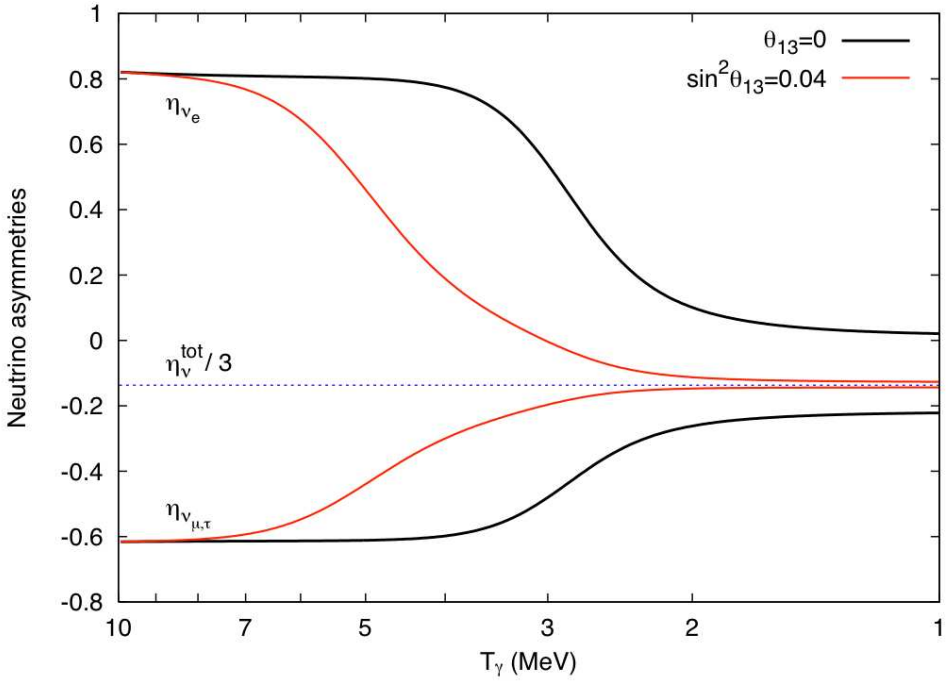

Figure 3.1: Example of evolution of the flavor asymmetries for two different values of $sin^2\theta_{13}$ (in this example $\eta_\nu = -0.41$ and $\eta^{\rm in}_{\nu_e} = 0.82$). The total neutrino asymmetry is constant and equal to three times the value shown by the blue dotted line. From Mangano et al. [2011].

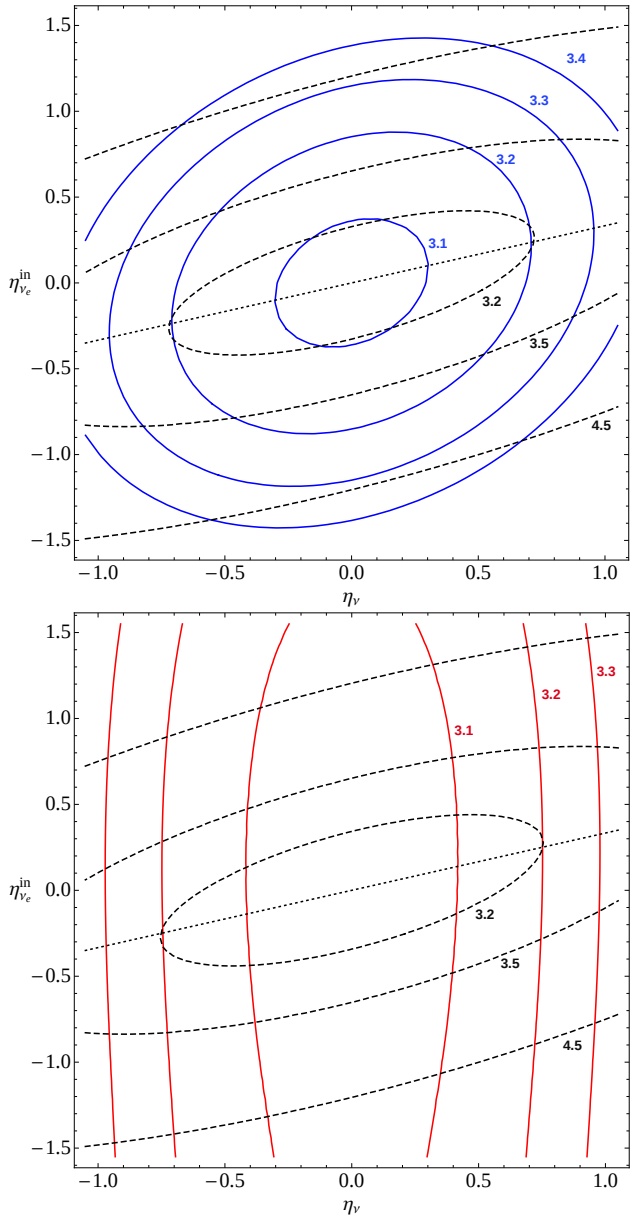

Figure 3.2: Final contribution of neutrinos with primordial asymmetries to the radiation energy density. The isocontours of $N_{\rm eff}$ on the plane $\eta^{\rm in}_{\nu_e}$ vs. η_ν, including flavor oscillations, are shown for two values of $\sin^2\theta_{13}$: 0 (blue solid curves, top panel) and 0.04 (red solid curves, bottom panel) and compared to the case with zero mixing (dashed curves). The dotted line corresponds to $\eta_\nu = \eta_{\nu_x}$ $(x = \mu, \tau)$, where one expects oscillations to have negligible effects.

compared with those obtained from the frozen neutrino distributions taking into account the effect of flavor oscillations [Mangano et al., 2011]. One can see that oscillations efficiently reduce $N_{\rm eff}$ for neutrino asymmetries with respect to the initial values from Eq. (3.3).

The evolution of the neutrino and antineutrino distribution functions with non-zero initial asymmetries, from $T = 10$ MeV until BBN, has been calculated by Pastor et al. [2009] and Mangano et al. [2011]. Here we use the final numerical results for these spectra in a range of values for $\eta_{\nu_e}^{\rm in}$ and η_ν as an input for our analysis, described in the next Section. Note that an analysis in terms of the degeneracy parameters ξ_α as done for instance in Shiraishi et al. [2009] is no longer possible. We adopt the best fit values for the neutrino oscillation parameters quoted in Schwetz et al. [2011], assuming a normal hierarchy of the neutrino masses, except for the mixing angle θ_{13}, for which we will adopt two distinct values: $\theta_{13} = 0$ and $\sin^2\theta_{13} = 0.04$. The latter is close to the upper limit placed by the Daya Bay [An et al., 2012] and RENO [Ahn et al., 2012] experiments on this mixing angle (with a best-fit value of $\sin^2\theta_{13} = 0.024$ and $\sin^2\theta_{13} = 0.029$, respectively), and is used as an example to understand the cosmological implications of a nonzero θ_{13}. Moreover, since the flavor asymmetries equilibrate for large values of this mixing angle, the cosmological effects are similar for $\sin^2\theta_{13} \gtrsim 0.02$, as in the case of an inverted hierarchy for a broad range of θ_{13} values (see, for instance, Fig. 3.3). As for the case $\theta_{13} = 0$, though it seems presently disfavoured with a high statistical significance after the Daya Bay and RENO results, we have decided to include it for comparison.

3.2. Cosmological constraints on neutrino parameters

Having set the basic framework for the calculation of the neutrino distribution functions in the presence of asymmetries and for different θ_{13}, we can now proceed to investigate its cosmological effects.

In order to constrain the values of the cosmological neutrino asymmetries, we compare our results to the observational data. In particular, we use a modified

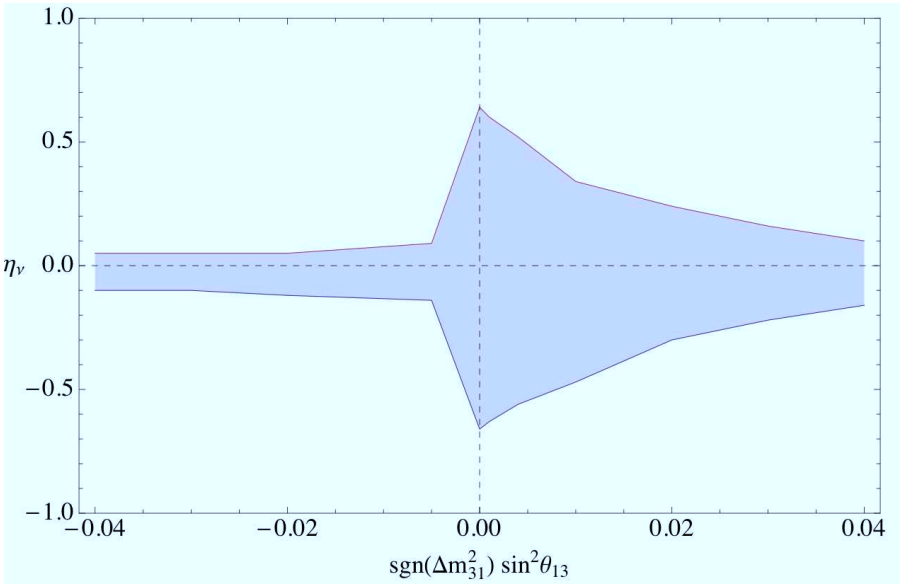

Figure 3.3: The shadowed region corresponds to the values of the total neutrino asymmetry compatible with BBN at 95% C.L., as a function of θ_{13} and the neutrino mass hierarchy. From Mangano et al. [2012].

version of the CAMB code[2] [Lewis et al., 2000] to evolve the cosmological perturbations and obtain the CMB and matter power spectra in the presence of non-zero neutrino asymmetries in the neutrino distribution functions. We checked that the spectra computed by our modified CAMB version are consistent up to high accuracy with those obtained with CLASS [Blas et al., 2011], that incorporates the models considered here in its public version. This version of CAMB is interfaced with the Markov chain Monte Carlo package CosmoMC[3] [Lewis & Bridle, 2002] that we use to sample the parameter space and obtain the posterior distributions for the parameters of interest.

We derive our constraints in the framework of a flat ΛCDM model with the three standard model neutrinos and purely adiabatic initial conditions. The parameters we use are described in Table 3.1 as well as the range of the flat priors used. As can be seen, six of them are the standard ΛCDM cosmological parameters, and we add to those three new parameters, namely the mass of the lightest neutrino

[2] `http://camb.info/`
[3] `http://cosmologist.info/cosmomc/`

mass eigenstate m_1 (the other two masses are calculated using the best fit for Δm^2_{21} and Δm^2_{31} obtained in [Schwetz et al., 2011], assuming normal hierarchy) and the two neutrino asymmetries we mentioned earlier, $\eta^{\rm in}_{\nu_e}$ and η_ν. The values of the effective degeneracy parameters ξ_α after BBN[4], needed by CAMB, are pre-calculated as a function of the asymmetries (following the method described in the previous section) over a grid in ($\eta^{\rm in}_{\nu_e}$, η_ν) and stored on a table, used for interpolation during the Monte Carlo run.

A comment on the parameterization is in order. It is a standard practice in cosmological analyses to parameterize the neutrino masses via $\Omega_\nu h^2$ or equivalently $f_\nu \equiv \Omega_\nu/\Omega_{dm}$, and from that (assuming that neutrinos decoupled at equilibrium) derive the sum of neutrino masses, which are taken to be degenerate. The presence of lepton asymmetries dramatically changes this simple scheme. Now the neutrino number density is a complicated function of the η's obtained from a non-equilibrium distribution function. When f_ν is used, any effect related to the way in which the total neutrino density is shared among the different mass eigenstates is completely lost. In that sense, the parameterization used in this paper looks more physically motivated since energy densities of neutrinos are constructed from two fundamental quantities, namely their phase space distributions and their masses.

The most basic dataset that we consider only consists of the WMAP 7-year CMB temperature and polarization anisotropy data. We will refer to it simply as "WMAP". The likelihood is computed using the the WMAP likelihood code publicly available at the LAMBDA website[5]. We marginalize over the amplitude of the Sunyaev-Zel'dovich signal.

In addition to the WMAP data, we also include the BBN measurement of the ^{4}He mass fraction Y_p from the data collection analysis done in [Iocco et al., 2009], in the form of a Gaussian prior

$$Y_p = 0.250 \pm 0.003 \quad (1\sigma)\,. \tag{3.6}$$

Indeed, some authors have recently reported a larger central value, $Y_p \sim 0.257$ [Izotov & Thuan, 2010; Aver et al., 2010, 2011], with quite different uncertainty

[4]The neutrino distribution functions can be parameterized by Fermi-Dirac-like functions with an effective ξ_α and temperature T_α [Mangano et al., 2011], which are related to the first two moments of the distribution, the number density and energy density.

[5]`http://lambda.gsfc.nasa.gov/`

determinations. In [Aver et al., 2012] using a Markov chain Monte Carlo technique already exploited in [Aver et al., 2011], the primordial value of ^{4}He decreased again to $Y_p = 0.2534 \pm 0.0083$, which is compatible at 1σ with the measurement quoted in eq. (3.6). We will not use these results in our analysis, but we will comment on their possible impact in the following. We also note that in [Mangano & Serpico, 2011] a robust upper bound $Y_p < 0.2631$ (95 % C.L.) has been derived based on very weak assumptions on the astrophysical determination of ^{4}He abundance, namely that the minimum effect of star processing is to keep constant the helium content of a low-metallicity gas, rather than increase it, as expected. As we will show, the measurement of Y_p currently dominates the constraints on the asymmetries: if we were to conservatively allow for larger uncertainties on that measurement, like for example those reported in [Aver et al., 2012], our constraints from present data would correspondingly be weakened. Moreover, we decided not to use the Deuterium measurements since at the moment they are not competitive with Helium for constraining the asymmetries (see Fig. 3.4), although there are recent claims that they could place strong constraints on $N_{\rm eff}$ at the level of $\Delta N_{\rm eff} \simeq \pm 0.5$ [Pettini & Cooke, 2012]. This is a very interesting perspective but at the moment, Deuterium measurements in different QSO absorption line systems show a significant dispersion, much larger than the quoted errors.

The dataset that uses both WMAP 7-year data and the determination of the primordial abundance of Helium as in (3.6) will be referred to as "WMAP+He". Measurements of Y_p represent the best "leptometer" currently available, in the sense that they place the most stringent constraints on lepton asymmetries for a given baryonic density [Serpico & Raffelt, 2005]. The ^{4}He mass fraction depends on the baryonic density, the electron neutrino degeneracy parameter and the effective number of neutrino families. Thus, in order to consistently implement the above determination of Y_p in our Monte Carlo analysis, we compute $\Delta N_{\rm eff}$ and ξ_e coming from the distribution functions calculated with the asymmetries (as explained in the previous section) and store them on a table. During the CosmoMC run, we use this table to obtain by interpolation the values $\Delta N_{\rm eff}$ and ξ_e corresponding to given values of the asymmetries (which are the parameters actually used in the Monte Carlo), and finally to obtain Y_p as a function of $\Delta N_{\rm eff}$, ξ_e and $\Omega_b h^2$. Notice that this approach is slightly less precise than the one used in Mangano et al. [2011, 2012], where a full BBN analysis was performed, but this approximation should

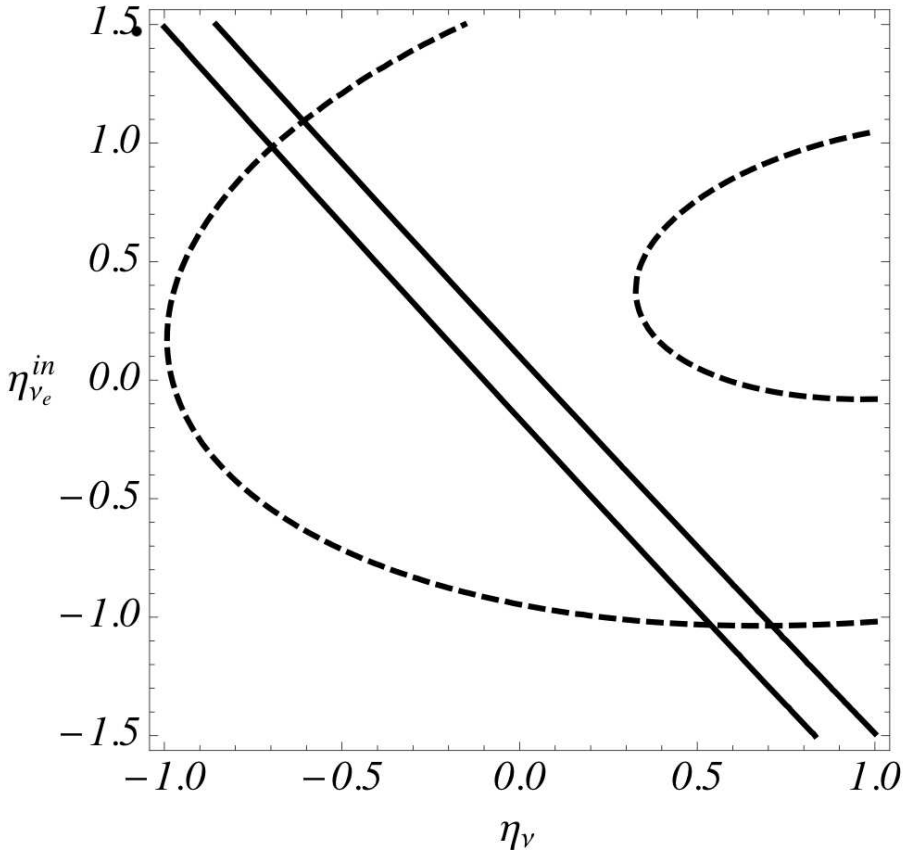

Figure 3.4: Bounds in the η_ν vs. $\eta^{\rm in}_{\nu_e}$ plane for each nuclear yield. Areas between the lines correspond to 95% C.L. regions singled out by the ^{4}He mass fraction (solid lines) and Deuterium (dashed lines). From Mangano et al. [2011].

suffice for our purposes, especially taking into account that we will be comparing BBN limits on the asymmetries with the ones placed by other cosmological data, that as we shall see are far less constraining. In any case, we have checked that the agreement between the interpolation scheme and the full BBN analysis is at the percent level.

We derive our constraints from parallel chains generated using the Metropolis-Hastings algorithm [Gilks et al., 1996]. For a subset of the models, we have also generated chains using the slice sampling method, in order to test the robustness of our results against a change in the algorithm. We use the Gelman and Rubin R parameter to evaluate the convergence of the chains, demanding that $R-1 < 0.03$. The one- and two-dimensional posteriors are derived by marginalizing over the other parameters.

Our results for the cosmological and neutrino parameters from the analysis are shown in Table 3.2, while Fig. 3.5 shows the marginalized one-dimensional probability distributions for the lightest neutrino mass, the initial electron-neutrino asymmetry, and the total asymmetry, for the different values of θ_{13}. Notice that the posterior for $\eta^{\rm in}_{\nu_e}$ (middle panel) is still quite large at the edges of the prior range. This happens also for both the $\eta^{\rm in}_{\nu_e}$ and η_ν posteriors obtained using only the WMAP data (not shown in the figure). Since the priors on these parameters do not represent a real physical constraint (as in the case $m_\nu > 0$), but just a choice of the range to explore, we refrain from quoting 95% credible intervals in these cases, as in order to do this one would need knowledge of the posterior in all the region where it significantly differs from zero. However, it is certain that the *actual* 95% C.L. includes the one that one would obtain using just part of the posterior (as long as this contains the peak of the distribution). If we do this, we obtain constraints that are anyway much worse than those from BBN. Finally, we also stress that if a larger experimental determination of Y_p or measurements with larger uncertainities were used, as those reported in [Izotov & Thuan, 2010; Aver et al., 2010, 2011], BBN would show a preference for larger values of $N_{\rm eff}$ as well.

Concerning the neutrino asymmetries, shown in the middle and bottom panels of Fig. 3.5, we notice that while the initial flavor asymmetries remain highly unconstrained by current data, the total asymmetry constraint improves significantly for $\theta_{13} \neq 0$. This result agrees with previous results from BBN-only studies [Mangano et al., 2011, 2012], and it is a result of the equilibration of flavor asymmetries

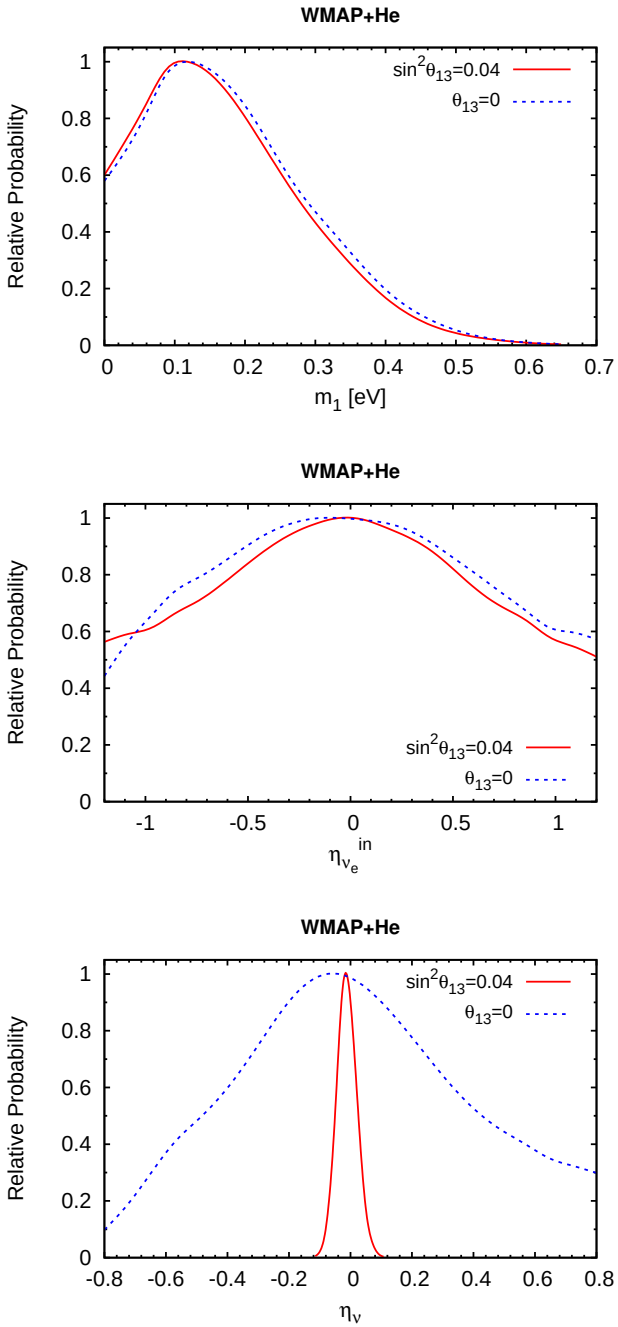

Figure 3.5: One-dimensional posterior probability density for m_1, $\eta_{\nu_e}^{\rm in}$, and η_ν for the WMAP+He dataset.

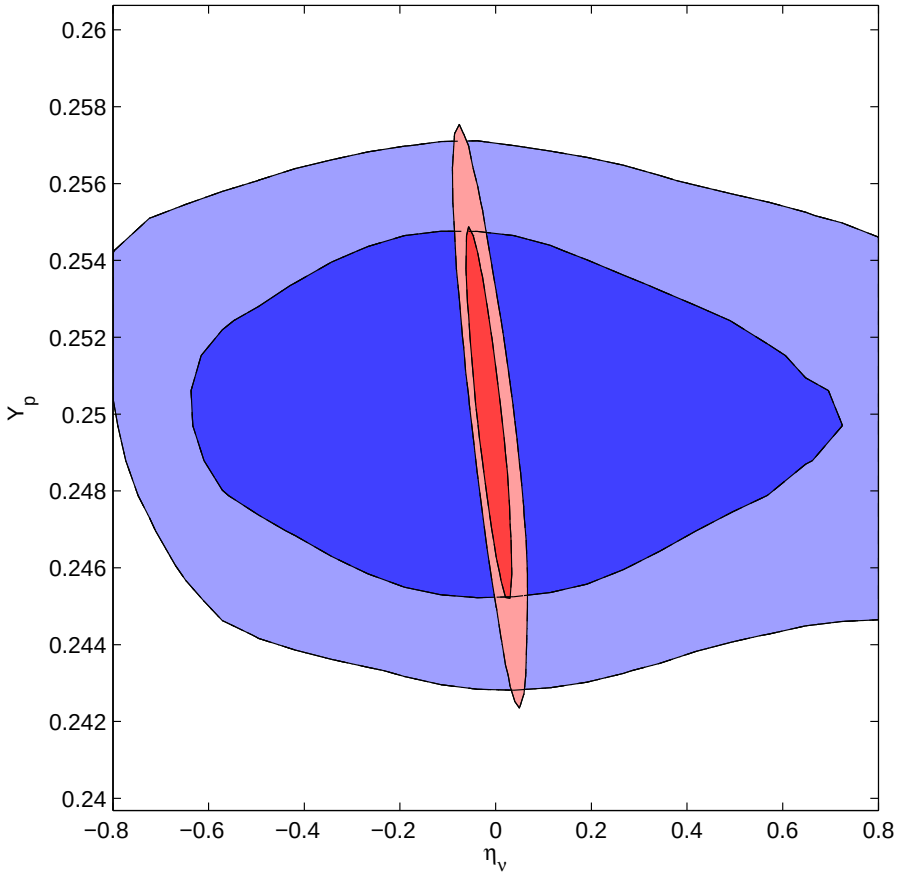

Figure 3.6: 68% and 95% confidence regions in total neutrino asymmetry η_ν vs. the primordial abundance of Helium Y_p plane for $\theta_{13} = 0$ (blue) and $\sin^2\theta_{13} = 0.04$ (red), from the analysis of the WMAP+He dataset. Notice the much stronger constraint for the nonzero mixing angle due to the faster equilibration of flavor asymmetries.

Table 3.2: 95% C.L. constraints on cosmological parameters for the WMAP and WMAP+He datasets.

Parameter	WMAP		WMAP+He	
	$\sin^2\theta_{13}=0$	$\sin^2\theta_{13}=0.04$	$\sin^2\theta_{13}=0$	$\sin^2\theta_{13}=0.04$
$100\ \Omega_b h^2$	$2.20^{+0.14}_{-0.12}$	$2.20^{+0.13}_{-0.12}$	2.20 ± 0.12	2.20 ± 0.12
$\Omega_{dm}h^2$	0.118 ± 0.016	$0.117^{+0.017}_{-0.016}$	0.119 ± 0.017	0.117 ± 0.016
τ	$0.085^{+0.029}_{-0.026}$	$0.085^{+0.030}_{-0.027}$	$0.085^{+0.030}_{-0.027}$	$0.085^{+0.029}_{-0.027}$
$100\theta_s$	1.0387 ± 0.0063	$1.0389^{+0.0069}_{-0.0063}$	$1.0381^{+0.054}_{-0.053}$	$1.0387^{+0.0053}_{-0.0054}$
n_s	0.953 ± 0.032	$0.953^{+0.032}_{-0.033}$	$0.955^{+0.034}_{-0.035}$	$0.952^{+0.031}_{-0.032}$
$\log\left[10^{10}A_s\right]$	$3.064^{+0.080}_{-0.082}$	$3.062^{+0.080}_{-0.079}$	$3.068^{+0.081}_{-0.078}$	$3.062^{+0.073}_{-0.075}$
m_1 (eV)	≤ 0.39	≤ 0.38	≤ 0.38	≤ 0.38
$\eta^{\rm in}_{\nu_e}$	– [6]	– [a]	– [a]	– [a]
η_ν	– [a]	– [a]	$[-0.64; 0.72]$	$[-0.071; 0.054]$
h	$0.652^{+0.084}_{-0.083}$	$0.653^{+0.081}_{-0.082}$	$0.656^{+0.084}_{-0.081}$	$0.650^{+0.078}_{-0.081}$
$\Delta N_{\rm eff}$	≤ 0.32	≤ 0.16	≤ 0.43	≤ 0.03

when θ_{13} is large (see Fig. 3.7).

When the flavors equilibrate in the presence of a nonzero mixing angle ($\sin^2\theta_{13}=0.04$ in our example) the total asymmetry is distributed almost equally among the different flavors, leading to a final asymmetry $\eta^{\rm fin}_{\nu_e}\approx\eta^{\rm fin}_{\nu_x}\approx\eta_\nu/3$ (where $x=\mu,\tau$). Hence, the fact that the BBN prior requires $\eta^{\rm fin}_{\nu_e}\approx 0$ for the correct abundance of primordial Helium (see Fig. 3.6) leads to a strong constraint on the constant total asymmetry, $-0.071\leq\eta_\nu\leq 0.054$ (95% C.L.).

On the other hand, since the constraints come most from the distortion in the electron neutrino distribution function, when $\theta_{13}=0$ (and therefore there is less mixing) the direct relation between $\eta^{\rm fin}_{\nu_e}$ and η_ν is lost. In this case, the total asymmetry could still be large, even if the final electron neutrino asymmetry is small, as asymmetries can still be stored on the other two flavors, leading to a constraint an order of magnitude weaker than the previous case, $-0.64\leq\eta_\nu\leq 0.72$ (95% C.L.). As expected, this is reflected on the allowed ranges for $\Delta N_{\rm eff}$, as shown in Fig. 3.8: while for $\theta_{13}=0$ the $\Delta N_{\rm eff}\simeq 0.5$ are still allowed by the data, nonzero values of this mixing angle reduce the allowed region in the parameter space by approximately an order of magnitude in both $\Delta N_{\rm eff}$ and η_ν.

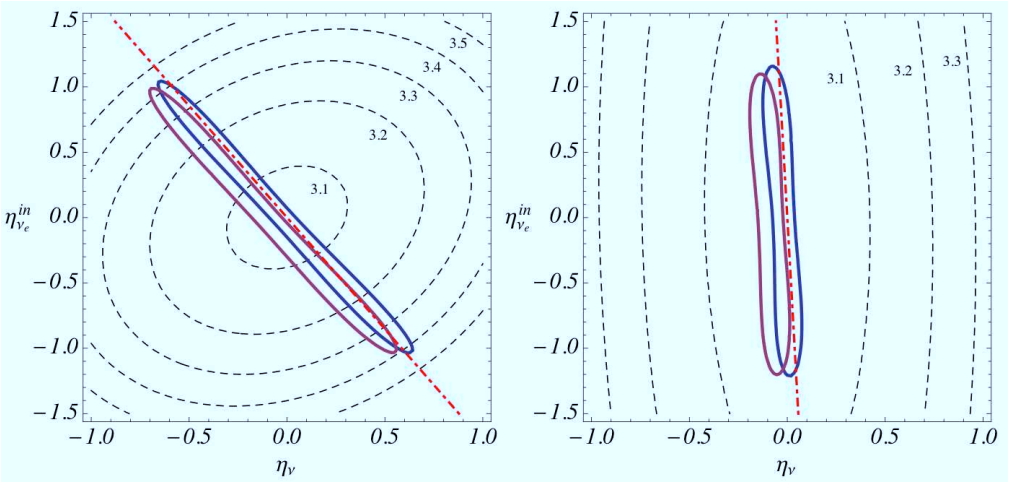

Figure 3.7: The 95% C.L. contours from the BBN analysis [Mangano et al., 2011] in the plane η_ν vs. $\eta_{\nu_e}^{\rm in}$ for $\theta_{13} = 0$ (left) and $\sin^2\theta_{13} = 0.04$ (right) for different choices of the abundance of ^{4}He. From Mangano et al. [2011].

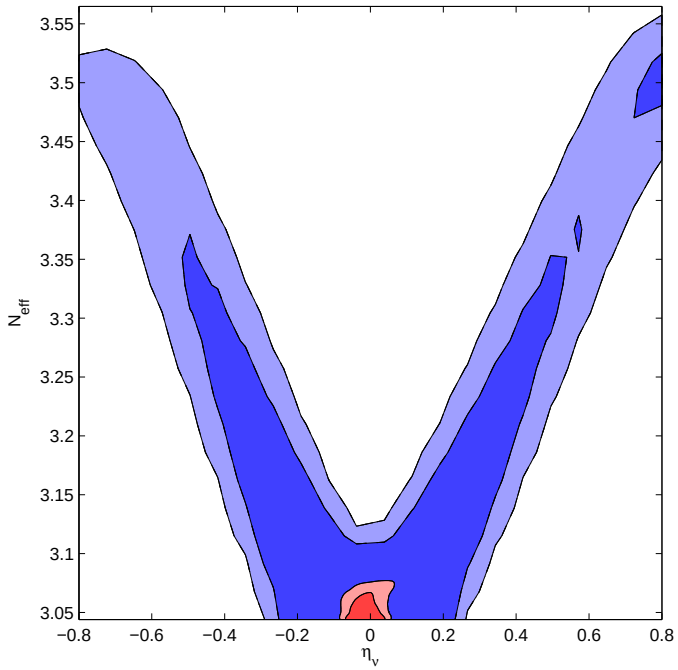

Figure 3.8: Two-dimensional 68% and 95% confidence regions in the (η_ν, $N_{\rm eff}$) plane from the analysis of the WMAP+He dataset, for $\theta_{13} = 0$ (blue) and $\sin^2\theta_{13} = 0.04$ (red). Even for zero θ_{13} the data seem to favor $N_{\rm eff}$ around the standard value $N_{\rm eff} = 3.046$.

We confirmed in our analysis that the constraints on the asymmetry are largely dominated by the BBN prior at present. This is shown in Fig. 3.9, where we compare the results of our analysis with a more complete dataset (which we refer to as ALL) that includes distance measurements of SNIa from the SDSS compilation [Kessler et al., 2009] and the HST determination of the Hubble constant H_0 [Riess et al., 2009], as well as data on the power spectrum of the matter density field, as reconstructed from a sample of Luminous Red Galaxies of the SDSS Seventh Data Release [Reid et al., 2010]. This is due to the fact that other cosmological data constrain the asymmetries via their effect on increasing $N_{\rm eff}$, and currently the errors on the measurement of the effective number of neutrinos [Komatsu et al., 2011; Dunkley et al., 2011; Keisler et al., 2011; Benson et al., 2011] are significantly weaker than our prior on Y_p, eq. (3.6)[7]. The fact that bounds on leptonic asymmetries are dominated by the BBN prior (i.e. by ^{4}He data) is also confirmed by the similarity of our bounds on (η_ν, $\eta^{\rm in}_{\nu_e}$) with those of [Mangano et al., 2012]. Note that the limits reported in Mangano et al. [2012] sound weaker, because they are frequentist bounds obtained by cutting the parameter probability at $\Delta\chi^2 = 6.18$, i.e. they represent 95% bounds on joint two-dimensional parameter probabilities (in the Gaussian approximation). The one-dimensional 95% confidence limits, corresponding to $\Delta\chi^2 = 4$, are smaller and very close to the results of the present paper. We also checked that using our codes and data sets, we obtain very similar results when switching from Bayesian to frequentist confidence limits.

We conclude this section noting that the current constraints on the sum of neutrino masses are robust under a scenario with lepton asymmetries, as those extra degrees-of-freedom do not correlate with the neutrino mass. On the other hand, to go beyond the BBN limits on the asymmetries more precise measurements of $N_{\rm eff}$ are clearly needed, and in the next section we forecast the results that could be achievable with such an improvement using COrE as an example of future CMB experiments.

[7] On the other hand, these other cosmological data sets have an impact on other parameters like e.g. the neutrino mass. But since in this work we are primarily interested in bounding the asymmetries, we prefer to stick to the robust WMAP+He data set. In that way, our results are not contaminated by possible systematic uncertainties in the other data. Actually, the inclusion of all external datasets (in particular, of SNIa together with H_0) reveals a conflict between them, leading to a bimodal posterior probability for $\Omega_{dm}h^2$ and to a preference for $m_1 > 0$ at 95% C.L.

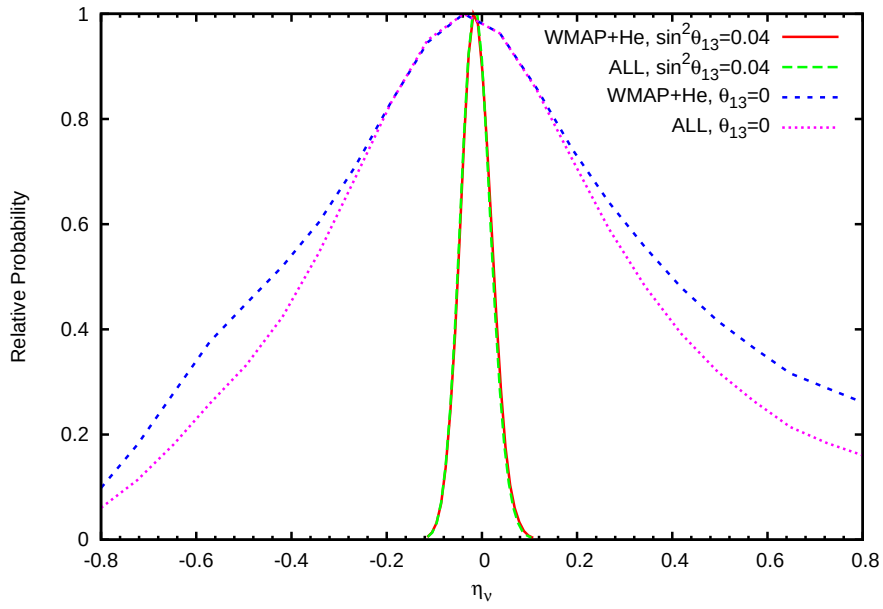

Figure 3.9: One-dimensional posterior probability density for η_ν comparing the WMAP+He and the ALL datasets. As mentioned in the text, the constraints on the total asymmetry do not improve significantly with the inclusion of other cosmological datasets, as they are mainly driven by the determination of the primordial Helium abundance.

3.3. Forecast

Given that the current constraints on the lepton asymmetries are dominated by their effect on the primordial production of light elements, one can ask whether future cosmological experiments can improve over the current limits imposed by BBN. With that goal in mind, we take as an example a proposed CMB experiment, COrE (Cosmic Origins Explorer) [Bouchet et al., 2011], designed to detect the primordial gravitational waves and measure the CMB gravitational lensing deflection power spectrum on all linear scales to the cosmic variance limit. The latter is of special interest for this work, as the CMB lensing is expected to probe with high sensitivity the absolute neutrino masses and $N_{\rm eff}$ [Lesgourgues et al., 2006].

We used the package FuturCMB[8] in combination with CAMB and CosmoMC for producing mock CMB data, and fit it with a likelihood based on the potential sensitivity of COrE. We include, also in this case, the information coming from present measurements of the Helium fraction, encoded in the Gaussian prior (3.6). We consider five of COrE's frequency channels, ranging from 105 to 225 GHz, with the specifications given in [Bouchet et al., 2011] and reported for convenience in Table 3.3, and assume an observed fraction $f_{\rm sky} = 0.65$. We do not consider other channels as they are likely to be foreground dominated. We take a maximum multipole $\ell_{\rm max} = 2500$. In our analysis, we have assumed that the uncertainties associated to the beam and foregrounds have been properly modeled and removed, so that we can only consider the statistical uncertainties. Those are optimistic assumptions, as under realistic conditions systematic uncertainties will certainly play an important role. In that sense, our results represent an illustration of what future CMB experiments could ideally achieve.

We use CMB lensing information in the way described in [Perotto et al., 2006], assuming that the CMB lensing potential spectrum will be extracted from COrE maps with a quadratic estimator technique.

For the forecast we adopt the fiducial values for the cosmological parameters shown in Table 3.4 for both cases of θ_{13} discussed previously. The two sets of fiducial values correspond to the best-fit models of the WMAP+He dataset for the two values of θ_{13}. In the case of the neutrino mass, since the likelihood is essentially flat between 0 and 0.2 eV, we have chosen to take $m_1 = 0.02$ eV. This

[8] `http://lpsc.in2p3.fr/perotto/`

Frequency [GHz]	$\theta_{\rm fwhm}$ [arcmin]	σ_T [μK]	σ_P [μK]
105	10.0	0.268	0.463
135	7.8	0.337	0.583
165	6.4	0.417	0.720
195	5.4	0.487	0.841
225	4.7	0.562	0.972

Table 3.3: Experimental specifications for COrE [Bouchet et al., 2011]. For each channel, we list the channel frequency in GHz, the FWHM in arcminutes, the temperature (σ_T) and polarization (σ_P) noise per pixel in μK.

is below the expected sensitivity of COrE and should thus be essentialy equivalent to the case where the lightest neutrino is massless.

Table 3.4: Fiducial values for the cosmological parameters for the COrE forecast.

Parameter	Fiducial Value ($\sin^2\theta_{13}=0$)	Fiducial Value ($\sin^2\theta_{13}=0.04$)
$\Omega_b h^2$	0.0218	0.0224
$\Omega_{dm} h^2$	0.121	0.118
τ	0.0873	0.0865
h	0.709	0.705
n_s	0.978	0.968
$\log[10^{10} A_s]$	3.12	3.08
m_1 (eV)	0.02	0.02
$\eta^{\rm in}_{\nu_e}$	0	0
η_ν	0	0

The sensitivities on the neutrino parameters for COrE are shown in Fig. 3.10 for the two values of θ_{13}. As expected for the sum of the neutrino masses, the constraints are significantly better than the current ones, and could in principle start probing the minimal values guaranteed by flavor oscillations [Lesgourgues et al., 2006]. Note that our forecast error for m_1 differs slightly from the one presented in [Bouchet et al., 2011], most probably because the forecasts in this reference are based on the Fisher matrix approximation. But our main goal in this section is to discuss how COrE observations will help improving the limits on the asymmetries discussed previously, that are basically dominated by the available measurements of the ^{4}He abudance. The bottom panel of Fig. 3.10 shows the

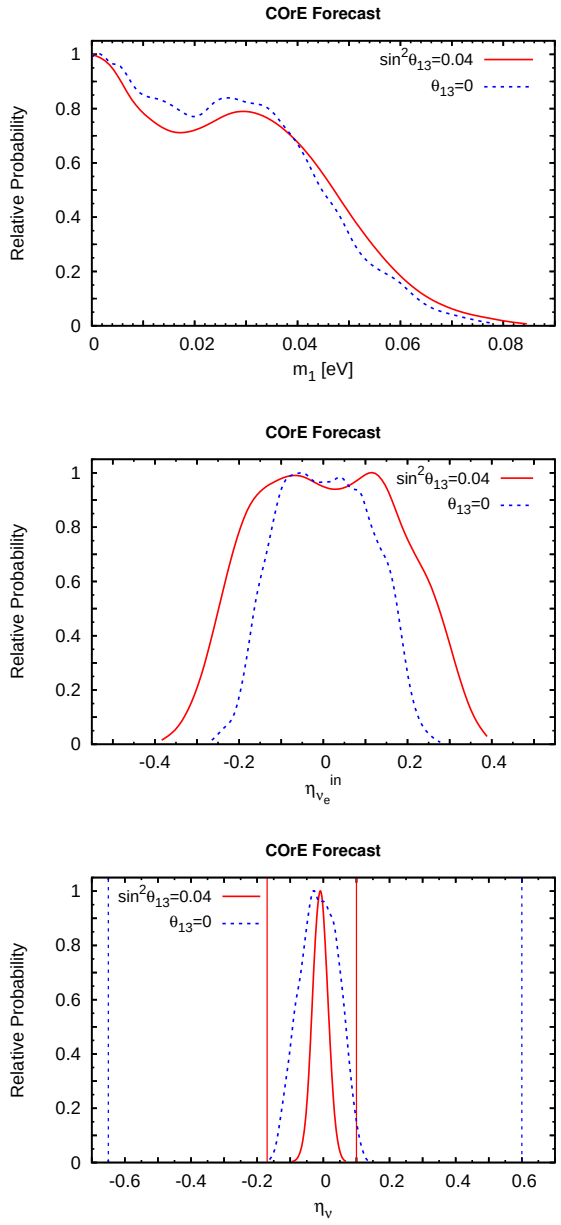

Figure 3.10: One-dimensional probability distribution function for m_1 and η_ν for COrE forecast. The middle panel shows that an experiment like COrE could start constrain the initial electron neutrino asymmetry. The vertical lines on the bottom panel show the current 95% C.L. limits obtained in the previous section. The errors on the asymmetries are improved by approximately a factor 6.6 or 1.6 for $\theta_{13} = 0$ and $\sin^2\theta_{13} = 0.04$, respectively, compared to the results shown in Fig. 3.5.

Table 3.5: 95% confidence intervals for the neutrino parameters with COrE.

Parameter	$\sin^2\theta_{13}=0$	$\sin^2\theta_{13}=0.04$
m_1 (eV)	<0.049	<0.048
$\eta^{\rm in}_{\nu_e}$	$[-0.20;0.20]$	$[-0.25;0.24]$
η_ν	$[-0.12;0.09]$	$[-0.048;0.030]$

forecasted posterior probability distribution for η_ν, and the marginalized constraints for it are listed in Table 3.5 for both values of θ_{13}; in particular, the vertical lines of the bottom panel show the 95% C.L. limits obtained from the full BBN analysis of Mangano et al. [2012]. Comparing the values from Tables 3.2 and 3.5 one can see that an experiment like COrE would improve current 95% limits on the total leptonic asymmetry by nearly a factor 6.6 ($\theta_{13}=0$) and 1.6 ($\sin^2\theta_{13}=0.04$), competitive over the constraints from ^{4}He abundance only. It should be noted that the error bars on the primordial abundances are very difficult to be reduced due to systematic errors on astrophysical measurements [Iocco et al., 2009], and therefore it is feasible that CMB experiments will be an important tool in the future to improve the constraints on the asymmetries. Notice however that, since the CMB is insensitive to the sign of the η's, BBN measurements will still be needed in order to break this degeneracy.

Finally, in Fig. 3.11 we show the COrE sensitivity on the asymmetries in the plane η_ν vs. $\eta^{\rm in}_{\nu_e}$ compared to the constraints of Sec. 3.2 obtained using current data and to the full BBN analysis of Mangano et al. [2012]. Notice that in the case $\theta_{13}=0$ the constraints of the previous section are quite less constraining than the ones coming from the full BBN analysis because we are not using deuterium data, known to be important to close the contours on the asymmetries plane, especially for small values of θ_{13} [Mangano et al., 2011]. Moreover, future CMB experiments have the potential to reduce the allowed region, dominating the errors in this analysis.

In summary, a future CMB experiment like COrE is capable of improving the constraints on the lepton asymmetries by up to a factor 6.6 on the total and/or flavor asymmetries depending on the value of the mixing angle θ_{13}. In addition to that, such an experiment would also constrain other cosmological parameters (in particular the sum of the neutrino masses) with significant precision, providing

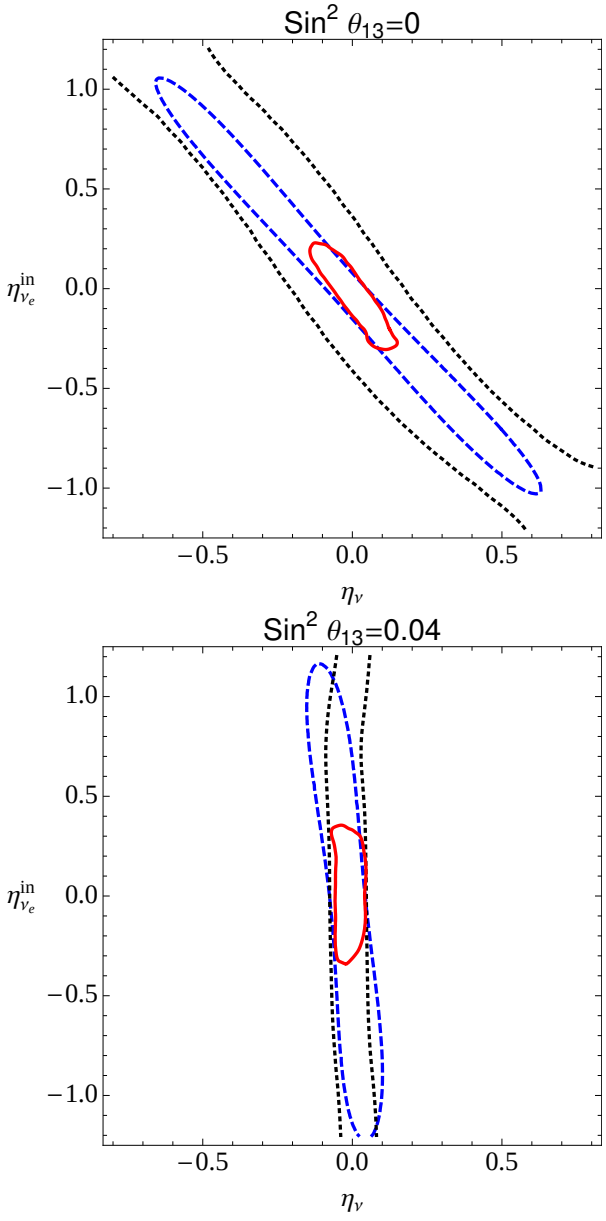

Figure 3.11: The 95% C.L. contours on the η_ν vs. $\eta^{\rm in}_{\nu_e}$ plane from our analysis with current data (WMAP+He dataset, black dotted) compared to the results of the BBN analysis of Mangano et al. [2012] (blue dashed) and with the COrE forecast (red solid).

yet another step towards the goal of accurately measuring the properties of the Universe.

3.4. Concluding remarks

Understanding the physical processes that took place in the early Universe is a crucial ingredient for deciphering the physics at energies that cannot be currently probed in terrestrial laboratories. In particular, since the origin of the matter-antimatter is still an open question in cosmology, it is important to keep an open mind for theories that predict large lepton asymmetries. In that case, constraining total and flavor neutrino asymmetries using cosmological data is a way to test and constrain some of the possible particle physics scenarios at epochs earlier than the BBN.

For that, in this chapter we initially used current cosmological data to constrain not only the asymmetries, but also to understand the robustness of the cosmological parameters (and the limits on the sum of the neutrino masses) for two different values of the mixing angle θ_{13} to account for the evidences of a nonzero value for this angle. Our results confirm the fact that at present the limits on the cosmological lepton asymmetries are dominated by the abundance of primordial elements generated during the BBN, in particular the abundance of ^{4}He, currently the most sensitive "leptometer" available.

However, future CMB experiments might be able to compete with BBN data in what concerns constraining lepton asymmetries, although BBN will always be needed in order to get information on the sign of the η's. We took as an example the future CMB mission COrE, proposed to measure with unprecedent precision the lensing of CMB anisotropies, and our results indicate that it has the potential to significantly improve over current constraints while, at the same time placing limits on the sum of the neutrino masses that are of the order of the neutrino mass differences.

Finally, we notice that for the values of θ_{13} measured by the Daya Bay and RENO experiments the limits on the cosmological lepton asymmetries and on its associated effective number of neutrinos are quite strong, so that lepton asymmetries cannot increase $N_{\rm eff}$ significantly above 3.1. Under those circumstances, if the cosmological data (other than BBN) continues to push for large values of $N_{\rm eff}$,

new pieces of physics such as sterile neutrinos will be necessary to explain that excess.

4

Mass-Varying Neutrino Models

As we have discussed earlier in this thesis, the Universe seems to be dominated by a component of energy with negative pressure that is causing its expansion to accelerate at least since $z \approx 1$.

Several candidates for this so-called dark energy have been proposed (see Section 2.5), but understanding them theoretically and observationally has proven to be challenging. On the theoretical side, explaining the small value of the observed dark energy density component, $\rho_\phi \sim (10^{-3}\ \text{eV})^4$, as well as the fact that both dark energy and matter densities contribute significantly to the energy budget of the present universe requires in general a strong fine tuning on the overall scale of the dark energy models. In the case in which the dark energy is assumed to be a scalar field ϕ slowly rolling down its flat potential $V(\phi)$, the quintessence models, the effective mass of the field has to be taken of the order $m_\phi = |d^2V(\phi)/d\phi^2|^{1/2} \sim 10^{-33}$ eV for fields with vacuum expectation values of the order of the Planck mass.

On the observational side, choosing among the dark energy models is a complicated task [Linder, 2008a]. Most of them can mimic a cosmological constant at late times (that is, an equation of state $w_\phi \equiv p_\phi/\rho_\phi = -1$) [Albrecht et al., 2006], and all data until now are perfectly consistent with this limit. In this sense, looking for different imprints that could favor the existence of a particular model of dark energy is a path worth taking.

Our goal in this chapter, which follows closely one of our works [França et al., 2009], consists in understanding whether a class of dark energy models, the so-called Mass-Varying Neutrinos (MaVaNs) scenario [Gu et al., 2003; Fardon et al.,

2004; Peccei, 2005; Amendola et al., 2008; Wetterich, 2007] could be constrained not only via the dark energy effects, but also by indirect signs of the neutrino mass variation during cosmological evolution, since neutrinos play a key role in several epochs [Hannestad, 2006; Lesgourgues & Pastor, 2006]. An indication of the variation of the neutrino mass would certainly tend to favor this models (at least on a theoretical basis) with respect to most DE models. Notice that although MaVaNs scenarios can suffer from stability issues for the neutrino perturbations [Afshordi et al., 2005], there is a wide class of models and couplings that avoid this problem [Eggers Bjælde et al., 2008; Bean et al., 2008a,b,c; Bernardini & Bertolami, 2008].

Similar analyses have been made in the past, but they have either assumed particular models for the interaction between the neutrinos and the DE field [Brookfield et al., 2006b,a; Ichiki & Keum, 2008], or chosen a parameterization that does not reflect the richness of the possible behavior of the neutrino mass variations [Zhao et al., 2007].

In order to be able to deal with a large number of models, instead of focusing on a particular model for the coupling between the DE field and the neutrino sector, we choose to parameterize the neutrino mass variation to place general and robust constraints on the MaVaNs scenario. In this sense, our work complements previous analyses by assuming a realistic and generic parameterization for the neutrino mass, designed in such a way to probe almost all the different regimes and models within the same framework. In particular, our parameterization allows for fast and slow mass transitions between two values of the neutrino mass, and it takes into account that the neutrino mass variation should start when the coupled neutrinos change their behavior from relativistic to nonrelativistic species. We can mimic different neutrino-dark energy couplings and allow for almost any monotonic behavior in the neutrino mass, placing reliable constraints on this scenario in a model independent way.

For that, we start this chapter, based on França et al. [2009], by reviewing briefly the MaVaNs scenario and its main equations. In Section 4.2 we present our parameterization with the results for the background and the perturbation equations obtained within this context. The results of our comparison of the numerical results with the data and the discussion of its main implications are shown in section 4.3. Finally, in section 4.4 the main conclusions, and some recent

results are discussed in section 4.5.

4.1. Mass-varying neutrinos

For simplicity, instead of using the standard Friedmann equations, eqs. (2.12) and (2.13), we will write them using the *conformal time*[1] τ that can be written in terms of the cosmic time and scale factor by $d\tau = dt/a$, in natural units. In this case, the Friedmann equations read

$$\mathcal{H}^2 = \left(\frac{\dot{a}}{a}\right)^2 = \frac{a^2}{3m_p^2}\rho, \tag{4.1}$$

$$\dot{\mathcal{H}} = -\frac{a^2}{6m_p^2}(\rho + 3p), \tag{4.2}$$

where the dot (in this chapter) denotes a derivative with respect to conformal time, and the reduced Planck mass is $m_p = 1/\sqrt{8\pi G} = 2.436 \times 10^{18}$ GeV. The neutrino mass in the models we are interested in is a function of the scalar field ϕ that plays the role of the dark energy, and can be written as

$$m_\nu(\phi) = M_\nu f(\phi)\ , \tag{4.3}$$

where M_ν is a constant and different models are represented by distinct $f(\phi)$ as discussed in Subsection 2.5.5.

The fluid equation of the neutrino species can be directly obtained from the Boltzmann equation for its distribution function [Brookfield et al., 2006a],

$$\dot{\rho}_\nu + 3\mathcal{H}\rho_\nu(1 + w_\nu) = \alpha(\phi)\dot{\phi}(\rho_\nu - 3p_\nu)\ , \tag{4.4}$$

where $\alpha(\phi) = d\ln[m_\nu(\phi)]/d\phi$ takes into account the variation of the neutrino mass, and $w_x = p_x/\rho_x$ is the equation of state of the species x. Moreover, since the total energy momentum tensor is conserved, the dark energy fluid equation also presents an extra right-hand side term proportional to the neutrino energy

[1] Not to be confused with the optical depth of the Universe, also denoted by τ in other chapters.

momentum tensor trace, $T^{\alpha}_{(\nu)\alpha} = (\rho_\nu - 3p_\nu)$, and can be written as

$$\dot{\rho}_\phi + 3\mathcal{H}\rho_\phi\,(1 + w_\phi) = -\alpha(\phi)\dot{\phi}\,(\rho_\nu - 3p_\nu) \ . \tag{4.5}$$

For a homogeneous and isotropic scalar field, the energy density and pressure are given by

$$\rho_\phi = \frac{\dot{\phi}^2}{2a^2} + V(\phi) \ , \qquad p_\phi = \frac{\dot{\phi}^2}{2a^2} - V(\phi) \ , \tag{4.6}$$

and both equations lead to the standard cosmological Klein-Gordon equation (in conformal time) for an interacting scalar field, namely,

$$\ddot{\phi} + 2\mathcal{H}\dot{\phi} + a^2\frac{dV(\phi)}{d\phi} = -a^2\alpha(\phi)\,(\rho_\nu - 3p_\nu) \ . \tag{4.7}$$

From the above equations one sees that, given a potential $V(\phi)$ for the scalar field and a field-dependent mass term $m_\nu(\phi)$ for the neutrino mass, the coupled system given by equations (4.1), (4.4), and (4.7), together with the fluid equations for the baryonic matter, cold dark matter and radiation (photons and other massless species) can be numerically solved [Brookfield et al., 2006a]. Notice that a similar approach is basically the same discussed in Subsection 2.5.5 for a possible variation of the dark matter mass [Anderson & Carroll, 1998] and its possible interaction with the dark energy [Amendola, 2000; Amendola & Tocchini-Valentini, 2001], with several interesting phenomenological ramifications [Farrar & Peebles, 2004; França & Rosenfeld, 2004; Huey & Wandelt, 2006; Das et al., 2006; Quartin et al., 2008; La Vacca et al., 2009].

Following the equations given in (2.134), equations (4.4) and (4.5) can be rewritten in the standard form,

$$\begin{aligned} \dot{\rho}_\nu &+ 3\mathcal{H}\rho_\nu\left(1 + w_\nu^{(\mathrm{eff})}\right) = 0 \ , \\ \dot{\rho}_\phi &+ 3\mathcal{H}\rho_\phi\left(1 + w_\phi^{(\mathrm{eff})}\right) = 0 \ , \end{aligned} \tag{4.8}$$

if one defines the *effective* equation of state of neutrinos and DE as

$$\begin{aligned} w_\nu^{(\mathrm{eff})} &= \frac{p_\nu}{\rho_\nu} - \frac{\alpha(\phi)\dot{\phi}\,(\rho_\nu - 3p_\nu)}{3\mathcal{H}\rho_\nu}\ , \\ w_\phi^{(\mathrm{eff})} &= \frac{p_\phi}{\rho_\phi} + \frac{\alpha(\phi)\dot{\phi}\,(\rho_\nu - 3p_\nu)}{3\mathcal{H}\rho_\phi}\ . \end{aligned} \tag{4.9}$$

The effective equation of state can be understood in terms of the dilution of the energy density of the species. In the standard noncoupled case, the energy density of a fluid with a given constant equation of state w scales as $\rho \propto a^{-3(1+w)}$, eq. (2.20). However, in the case of interacting fluids, one should also take into account the energy transfer between them, and the energy density in this case will be given by

$$\rho(z) = \rho_0 \exp\left[3\int_0^z \left(1 + w^{(\mathrm{eff})}(z')\right) d\ln(1+z')\right]\ . \tag{4.10}$$

For a constant effective equation of state one obtains the standard result, $\rho \propto a^{-3(1+w^{(\mathrm{eff})})}$, as expected.

Notice that this mismatch between the effective and standard DE equations of state could be responsible for the "phantom behavior" suggested by supernovae data when fitting it using a cosmological model with noninteracting components [Das et al., 2006]. This effect could be observable if dark energy was coupled to the dominant dark matter component. For the models discussed here, however, it cannot be significant: the neutrino fraction today ($\Omega_{\nu 0}/\Omega_{\phi 0} \sim 10^{-2}$) is too small to induce an "effective phantom-like" behavior.

As we commented before, the analysis until now dealt mainly with particular models, that is, with particular functional forms of the dark energy potential $V(\phi)$ and field dependence of the neutrino mass $\alpha(\phi)$. A noticeable exception is the analysis of Zhao et al. [2007], in which the authors use a parameterization for the neutrino mass *a là* Chevallier-Polarski-Linder (CPL) [Albrecht et al., 2006; Chevallier & Polarski, 2001; Linder, 2003]: $m_\nu(a) = m_{\nu 0} + m_{\nu 1}(1-a)$. However, although the CPL parameterization works well for the dark energy equation of state, it cannot reproduce the main features of the mass variation in the case of variable mass particle models. In the case of the models discussed here, for instance, the mass variation is related to the relativistic/nonrelativistic nature of the coupled neutrino species. With a CPL mass parameterization, the transition

from m_1 to m_0 always takes place around $z \sim 1$, which is in fact only compatible with masses as small as 10^{-3} eV. Hence, the CPL mass parameterization is not suited for a self-consistent exploration of all interesting possibilites.

One of the goals in this chapter is to discuss and test a parameterization suggested in França et al. [2009] that allows for a realistic simulation of mass-varying scenarios in a model independent way, with the minimum possible number of parameters, as explained in the next section.

4.2. Model independent approach

4.2.1. Background equations

As usual, the neutrino energy density and pressure are given in terms of the zero order Fermi-Dirac distribution function by eq. (2.29)

$$f^0(q) = \frac{g_\nu}{e^{q/T_{\nu 0}} + 1} \ , \tag{4.11}$$

where $q = ap$ denotes the modulus of the comoving momentum $q_i = qn_i$ ($\delta^{ij} n_i n_j = 1$), g_ν corresponds to the number of neutrino degrees of freedom, and $T_{\nu 0}$ is the present neutrino background temperature. Notice that in the neutrino distribution function we have used the fact that the neutrinos decouple very early in the history of the universe while they are relativistic, and therefore their equilibrium distribution depends on the comoving momentum, but not on the mass. In what follows we have neglected the small spectral distortions arising from non-instantaneous neutrino decoupling [Mangano et al., 2005]. Thus, the neutrino energy density and pressure are given by

$$\rho_\nu = \frac{1}{a^4} \int \frac{dq}{(2\pi)^3} \, d\Omega \, q^2 \epsilon f^0(q) \ , \tag{4.12}$$

$$p_\nu = \frac{1}{3a^4} \int \frac{dq}{(2\pi)^3} \, d\Omega \, q^2 f^0(q) \frac{q^2}{\epsilon} \ , \tag{4.13}$$

where $\epsilon^2 = q^2 + m_\nu^2(a) a^2$ (assuming that m_ν depends only on the scale factor). Taking the time-derivative of the energy density, one can then obtain the fluid

equation for the neutrinos,

$$\dot{\rho}_\nu + 3\mathcal{H}\left(\rho_\nu + p_\nu\right) = \frac{d\ln m_\nu(u)}{du}\mathcal{H}\left(\rho_\nu - 3p_\nu\right) \ , \tag{4.14}$$

where $u \equiv \ln a = -\ln(1+z)$, already defined in Subsection 2.5.5, is the number of e-folds counted back from today. Due to the conservation of the total energy momentum tensor, the dark energy fluid equation is then given by

$$\dot{\rho}_\phi \ + 3\mathcal{H}\rho_\phi\left(1 + w_\phi\right) = -\frac{d\ln m_\nu(u)}{du}\mathcal{H}\left(\rho_\nu - 3p_\nu\right) \ . \tag{4.15}$$

We can write the effective equations of state, defined in eqs. (4.8), as

$$\begin{aligned} w_\nu^{\text{eff}} &= \frac{p_\nu}{\rho_\nu} - \frac{d\ln m_\nu(u)}{du}\left(\frac{1}{3} - \frac{p_\nu}{\rho_\nu}\right) \ , \\ w_\phi^{\text{eff}} &= \frac{p_\phi}{\rho_\phi} + \left(\frac{\Omega_\nu}{\Omega_\phi}\right)\frac{d\ln m_\nu(u)}{du}\left(\frac{1}{3} - \frac{p_\nu}{\rho_\nu}\right) \ . \end{aligned} \tag{4.16}$$

The above results only assume that the neutrino mass depends on the scale factor a, and up to this point, we have not chosen any particular parameterization. Concerning the particle physics models, it is important to notice that starting from a value of w_ϕ and a function $m_\nu(a)$ one could, at least in principle, reconstruct the scalar potential and the scalar interaction with neutrinos following an approach similar to the one discussed in Rosenfeld [2007].

4.2.2. Mass variation parameters

Some of the main features of the MaVaNs scenario are:

(i) that the dark energy field gets kicked and moves away from its minimum (if $m_\phi > H$) or from its previous slow-rolling trajectory (if $m_\phi < H$) when the neutrinos become non-relativistic, very much like the case when it is coupled to the full matter content of the universe in the so-called *chameleon* scenarios [Brax et al., 2004];

(ii) that as a consequence, the coupling with the scalar field generates a neutrino mass variation at that time.

Any parameterization that intends to mimic scalar field models interacting with a mass-varying particle (neutrinos, in our case) for the large redshift range to which the data is sensitive should at least take into account those characteristics. Moreover, the variation of the mass in most models (see Brookfield et al. [2006b], for instance) can be well approximated by a transition between two periods: an earlier one, in which the mass is given by m_1, and the present epoch, in which the mass is given by m_0 (we will not consider here models in which the neutrino mass behavior is nonmonotonic). The transition for this parameterization, as mentioned before, starts when neutrinos become nonrelativistic, which corresponds approximately to

$$z_{\rm NR} \approx 1.40 \left(\frac{1\ {\rm eV}}{3\ T_{\gamma 0}}\right) \left(\frac{m_1}{1\ {\rm eV}}\right) \approx 2 \times 10^3 \left(\frac{m_1}{1\ {\rm eV}}\right) \tag{4.17}$$

where m_1 corresponds to the mass of the neutrino during the period in which it is a relativistic species. Before $z_{\rm NR}$ we can treat the neutrino mass as essentially constant, since the right-hand side of the fluid equation is negligible compared to the left-hand side, and therefore there is no observable signature of a possible mass variation.

When the neutrinos become nonrelativistic, the r.h.s. of the DE and neutrino fluid equations becomes important, and the neutrino mass starts varying. In order to model this variation, we use two parameters, namely the current neutrino mass, m_0, and Δ, a quantity related to the amount of time that it takes to complete the transition from m_1 to m_0 (see Fig. 4.1). That behavior resembles very much the parameterization of the dark energy equation of state discussed in Corasaniti & Copeland [2003], except for the fact that in our case the transition for the mass can be very slow, taking several e-folds to complete, and must be triggered by the time of the nonrelativistic transition, given by equation (4.17).

Defining $f = [1 + e^{-[u\ (1+\Delta) - u_{\rm NR}]/\Delta}]^{-1}$ and $f_* = [1 + e^{u_{\rm NR}/\Delta}]^{-1}$ we can use the form

$$m_\nu = m_0 + (m_1 - m_0) \times \Gamma(u, u_{\rm NR}, \Delta)\ , \tag{4.18}$$

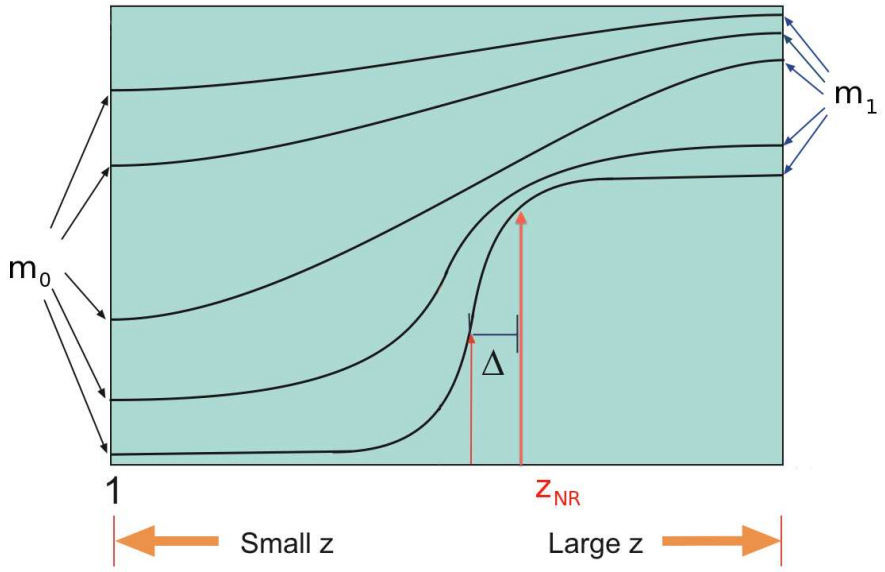

Figure 4.1: Schematic plot of the mass variation. Based on Fig. 1 of Corasaniti et al. [2004].

where

$$\begin{aligned} \Gamma(u, u_{\rm NR}, \Delta) &= 1 - \frac{f}{f_*} \\ &= \left[1 - \frac{1 + e^{u_{\rm NR}/\Delta}}{1 + e^{-[u\ (1+\Delta) - u_{\rm NR}]/\Delta}}\right] . \end{aligned} \tag{4.19}$$

Starting at $u_{\rm NR} = -\ln(1 + z_{\rm NR})$, the function $\Gamma(u, u_{\rm NR}, \Delta)$ decreases from 1 to 0, with a velocity that depends on Δ. The top panel in Figure 4.2 gives the behavior of eq. (4.18) with different parameters; the bottom panels shows that in this parametrization, the derivative of the mass with respect to e-fold number resembles a Gaussian function. The peak of the quantity dm/du occurs at the value $\bar{u} = u_{\rm NR}/(1 + \Delta)$; hence, for $\Delta \ll 1$, the mass variation takes place immediately after the non-relativistic transition ($\bar{u} \simeq u_{\rm NR}$) and lasts a fraction of e-folds (roughly, 3Δ e-folds); for $1 \leq \Delta \leq |u_{\rm NR}|$ the variation is smooth and centered on some intermediate redshift between z_{NR} and 0; while for $\Delta \gg |u_{NR}|$, the transition is still on-going today, and the present epoch roughly coincides with the maximum variation.

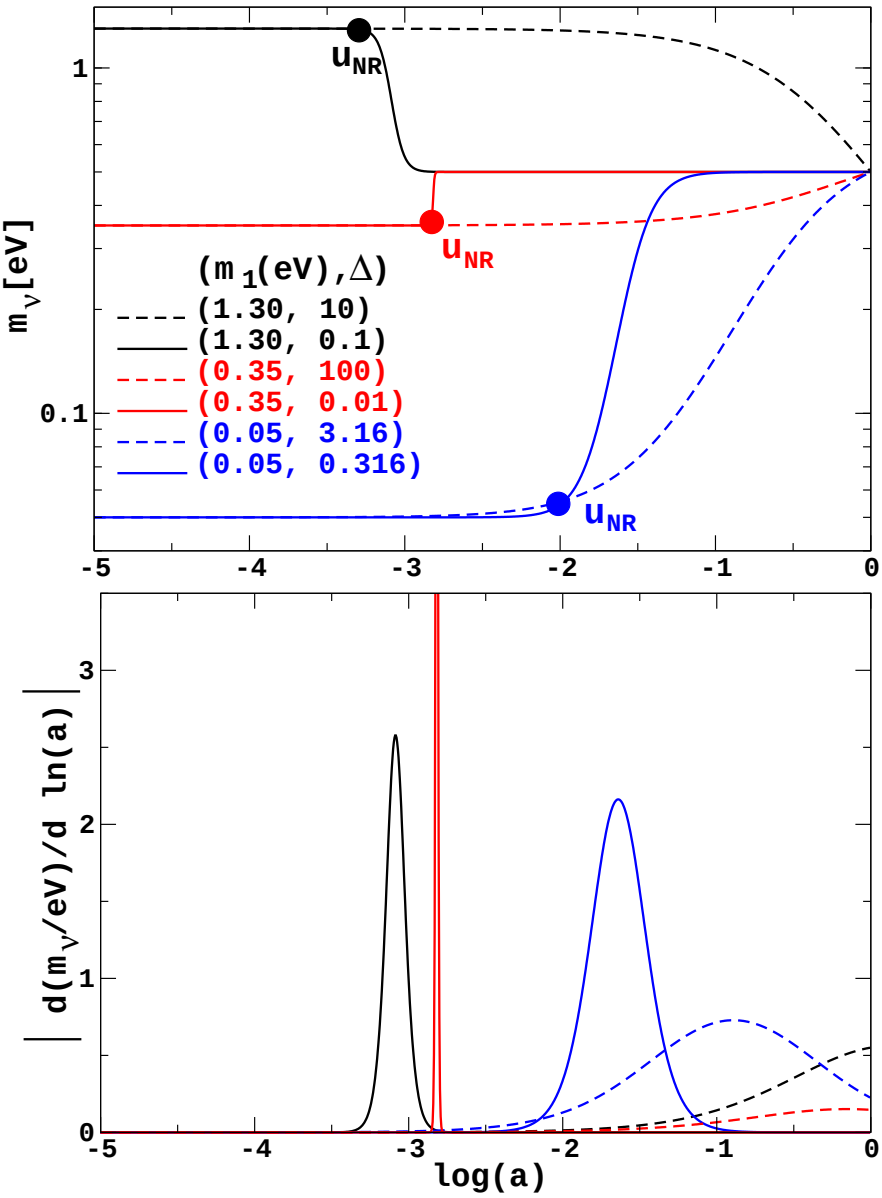

Figure 4.2: Neutrino mass behavior for the parameterization given by equation (4.18). *Top panel*: Neutrino mass as a function of $\log(a) = u/\ln(10)$ for models with $m_0 = 0.5$ eV and different values of m_1 and Δ. *Bottom panel:* Neutrino mass variation for the same parameters as in the top panel.

Although the functional form of Γ, eq. (4.19), seems complicated, one should note that it is one of the simplest forms satisfying our requirements with a minimal number of parameters. An example that could look simpler, but that for practical purposes is not, would be to assume that the two plateaus are linked together by a straight line. In this case, we would need a parameterization of the form

$$m_\nu = \begin{cases} m_1 & , \quad u < u_{\rm NR} \ , \\ m_0 + (m_1 - m_0)\left[\frac{u-u_{\rm end}}{u_{\rm NR}-u_{\rm end}}\right] & , \quad u_{\rm NR} \leq u \leq u_{\rm end} \ , \\ m_0 & , \quad u > u_{\rm end} \end{cases}$$

where $u_{\rm end}$ corresponds to the chosen redshift in which the transition stops. Notice that in this case not only we still have three parameters to describe the mass variation, but also the function is not smooth. Moreover, the derivative of the mass with respect to u gives a top-hat-like function which is discontinuous at both $u_{\rm NR}$ and $u_{\rm end}$. In this sense, it seemed to us that equation (4.18) would give us the best "price-to-earnings ratio" among the possibilities to use phenomenologically motivated parameterizations for the mass-varying neutrinos, although certainly there could be similar proposals equally viable, such as for instance the possibility of adapting for the mass variation the parameterization used for the dark energy equation of state in Douspis et al. [2008] and Linden & Virey [2008]. There, the transition between two constant values of the equation of state exhibits a $\tanh\left[\Gamma_t(u-u_t)\right]$ dependence, where Γ_t is responsible for the duration of the transition and u_t is related to its half-way point.

In the rest of our analysis, we will use a couple of extra assumptions that need to be taken into account when going through our results. First, we will consider that only one of the three neutrino species is interacting with the dark energy field, that is, only one of the mass eigenstates has a variable mass. The reason for this approximation is twofold: it is a simpler case (compared to the case with 3 varying-mass neutrinos), since instead of 6 extra parameters with respect to the case of constant mass, we have only 2, namely the early mass of the neutrino whose mass is varying, m_1, and the velocity of the transition, related to Δ.

Besides simplicity, the current choice is the only one allowed presently in the case in which neutrinos were heavier in the past. Indeed, we expect our stronger constraints to come from those scenarios, especially if the neutrino species behaves

as a nonrelativistic component at the time of radiation-matter equality, given by $1 + z_{\rm eq} \sim 4.05 \times 10^4 (\Omega_{c0} h^2 + \Omega_{b0} h^2)/(1 + 0.23 N_{\rm eff})$ (here the indexes c stands for cold dark matter). Taking the three neutrino species to be nonrelativistic at equality would change significantly the value of $z_{\rm eq}$, contradicting CMB data (according to WMAP5, $1 + z_{\rm eq} = 3141^{+154}_{-157}$ (68% C.L.) [Komatsu et al., 2009]). Instead, a single neutrino species is still marginally allowed to be non-relativistic at that time.

To simplify the analysis, we also assumed that the dark energy field, when not interacting with the neutrinos, reached already the so-called scaling solution (see discussion in Subsection 2.5.3), i.e., the dark energy equation of state w_ϕ in eq. (4.15) is constant in the absence of interaction. Notice however that when the neutrinos become non-relativistic the dark energy fluid receives the analogous of the chameleon kicks we mentioned before, and the dark energy effective equation of state, eq. (4.16), does vary for this period in a consistent way.

The upper panel of Figure 4.3 shows how the density parameters of the different components of the universe evolve in time, in a typical MaVaNs model. The lower panel displays a comparison between mass-varying and constant mass models, in particular during the transition from m_1 to m_0. As one would expect, far from the time of the transition, the densities evolve as they would do in the constant mass case.

4.2.3. Perturbation equations

The next step is to calculate the cosmological perturbation equations and their evolution using this parameterization. We chose to work in the synchronous gauge, and our conventions follow the ones by Ma and Bertschinger [Ma & Bertschinger, 1995]. In this case, the perturbed metric is given by

$$ds^2 = -a^2 d\tau^2 + a^2 \left(\delta_{ij} + h_{ij}\right) dx^i dx^j \ . \tag{4.20}$$

In this gauge, the equation for the three-momentum of the neutrinos reads [Ichiki & Keum, 2008]

$$\frac{dq}{d\tau} = -\frac{1}{2} q \dot{h}_{ij} n_i n_j - a^2 \frac{m_\nu^2}{q} \beta \frac{\partial \rho_\phi}{\partial x^i} \frac{\partial x^i}{d\tau} \ , \tag{4.21}$$

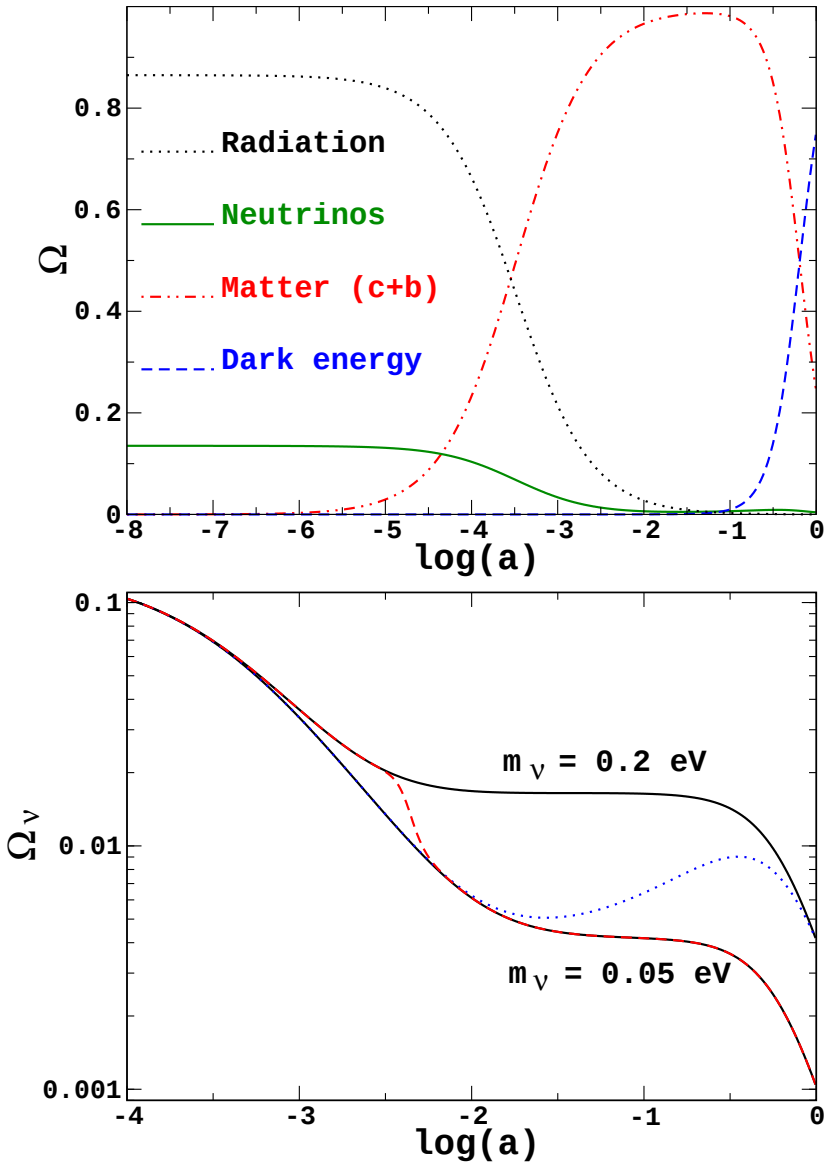

Figure 4.3: *Top panel*: Density parameters for the different components of the universe versus $\log(a) = u/\ln(10)$ in a model with $m_1 = 0.05$ eV, $m_0 = 0.2$ eV, $\Delta = 10$, and all the other parameters consistent with present data. The radiation curve include photons and two massless neutrino species, and matter stands for cold dark matter and baryons. The bump in the neutrino density close to $\log(a) = -0.5$ is due to the increasing neutrino mass. *Bottom panel:* Density parameters for two different mass-varying neutrino models. The solid black curves show the density parameter variation for two distinct constant mass models, with masses $m_\nu = 0.05$ eV and $m_\nu = 0.2$ eV. The dashed (red) curve shows a model in which the mass varies from $m_1 = 0.2$ eV to $m_0 = 0.05$ eV, with $\Delta = 0.1$, and the dotted (blue) line corresponds a model with $m_1 = 0.05$ eV to $m_0 = 0.2$ eV, with $\Delta = 10$.

where, as in equation (4.4), we define

$$\beta(a) \equiv \frac{d\ln m_\nu}{d\rho_\phi} = \frac{d\ln m_\nu}{d\ln a}\left(\frac{d\rho_\phi}{d\ln a}\right)^{-1} . \tag{4.22}$$

Since the neutrino phase space distribution [Ma & Bertschinger, 1995] can be written as $f\left(x^i, q, n_j, \tau\right) = f^0(q)\left[1+\Psi\left(x^i, q, n_j, \tau\right)\right]$, one can show that the first order Boltzmann equation for a massive neutrino species, after Fourier transformation, is given by [Brookfield et al., 2006a; Ichiki & Keum, 2008]

$$\begin{aligned} \frac{\partial\Psi}{\partial\tau} &+ i\frac{q}{\epsilon}(\hat{\mathbf{n}}\cdot\mathbf{k})\Psi + \left(\dot\eta - (\hat{\mathbf{k}}\cdot\hat{\mathbf{n}})^2\frac{\dot h+6\dot\eta}{2}\right)\frac{d\ln f^0}{d\ln q} \\ &= -i\beta\frac{qk}{\epsilon}(\hat{\mathbf{n}}\cdot\mathbf{k})\frac{a^2m_\nu^2}{q^2}\frac{d\ln f^0}{d\ln q}\delta\rho_\phi , \end{aligned} \tag{4.23}$$

where η and h are the synchronous potentials in the Fourier space. Notice that the perturbed neutrino energy density and pressure are also going to be modified due to the interaction, and are written as

$$\delta\rho_\nu = \frac{1}{a^4}\int\frac{d^3q}{(2\pi)^3}f^0\left(\epsilon\Psi + \beta\frac{m_\nu^2a^2}{\epsilon}\delta\rho_\phi\right) , \tag{4.24}$$

$$3\delta p_\nu = \frac{1}{a^4}\int\frac{d^3q}{(2\pi)^3}f^0\left(\frac{q^2}{\epsilon}\Psi - \beta\frac{q^2m_\nu^2a^2}{\epsilon^3}\delta\rho_\phi\right) . \tag{4.25}$$

This extra term comes from the fact that the comoving energy ϵ depends on the dark energy density, leading to an extra-term which is proportional to β.

Moreover, if we expand the perturbation $\Psi\left(\mathbf{k}, q, \mathbf{n}, \tau\right)$ in a Legendre series [Ma & Bertschinger, 1995], the neutrino hierarchy equations will read,

$$\begin{aligned} \dot\Psi_0 &= -\frac{qk}{\epsilon}\Psi_1 + \frac{\dot h}{6}\frac{d\ln f^0}{d\ln q} , \\ \dot\Psi_1 &= \frac{qk}{3\epsilon}\left(\Psi_0 - 2\Psi_2\right) + \kappa , \\ \dot\Psi_2 &= \frac{qk}{5\epsilon}(2\Psi_1 - 3\Psi_3) - \left(\frac{1}{15}\dot h + \frac{2}{5}\dot\eta\right)\frac{d\ln f^0}{d\ln q}, \\ \dot\Psi_\ell &= \frac{qk}{(2\ell+1)\epsilon}\left[\ell\Psi_{\ell-1} - (\ell+1)\Psi_{\ell+1}\right] . \end{aligned} \tag{4.26}$$

where

$$\kappa = -\frac{1}{3}\beta\ \frac{qk}{\epsilon}\frac{a^2 m_\nu^2}{q^2}\frac{d\ln f^0}{d\ln q}\delta\rho_\phi\ . \tag{4.27}$$

For the dark energy, we use the "fluid approach" [Hu, 1998] (see also Bean & Doré [2004]; Hannestad [2005]; Koivisto & Mota [2006]), so that the density and velocity perturbations are given by,

$$\begin{aligned}\dot{\delta}_\phi = &+ \frac{3\mathcal{H}(w_\phi - \hat{c}_\phi^2)\left(\delta_\phi + \frac{3\mathcal{H}(1+w_\phi)}{1+\beta\rho_\nu(1-3w_\nu)}\frac{\theta_\phi}{k^2}\right) - (1+w_\phi)\left(\theta_\phi + \frac{\dot{h}}{2}\right)}{1+\beta\rho_\nu(1-3w_\nu)} \\ &- \frac{\left(\frac{\rho_\nu}{\rho_\phi}\right)\left[\beta\dot{\rho}_\phi(1-3c_\nu^2)\delta_\nu + \dot{\beta}\rho_\phi(1-3w_\nu)\delta_\phi\right]}{1+\beta\rho_\nu(1-3w_\nu)}\ ,\end{aligned} \tag{4.28}$$

$$\begin{aligned}\dot{\theta}_\phi = &- \left[\frac{\mathcal{H}(1-3\hat{c}_\phi^2)+\beta\rho_\nu(1-3w_\nu)\mathcal{H}(1-3w_\phi)}{1+\beta\rho_\nu(1-3w_\nu)}\right]\theta_\phi + \frac{k^2}{1+w_\phi}\hat{c}_\phi^2\delta_\phi \\ &- \beta(1-3w_\nu)\left(\frac{\rho_\nu}{\rho_\phi}\right)\left[\frac{k^2}{1+w_\phi}\rho_\phi\delta_\phi - \dot{\rho}_\phi\theta_\phi\right]\ ,\end{aligned} \tag{4.29}$$

where the dark energy anisotropic stress is assumed to be zero [Mota et al., 2007], and the sound speed $\hat{c}_\phi^2$ is defined in the frame comoving with the dark energy fluid [Weller & Lewis, 2003]. So, in the synchronous gauge, the quantity $c_\phi^2 \equiv \delta p_\phi/\delta\rho_\phi$ is related to $\hat{c}_\phi^2$ through

$$c_\phi^2\delta_\phi = \hat{c}_\phi^2\left(\delta_\phi - \frac{\dot{\rho}_\phi}{\rho_\phi}\frac{\theta_\phi}{k^2}\right) + w_\phi\frac{\dot{\rho}_\phi}{\rho_\phi}\frac{\theta_\phi}{k^2}\ . \tag{4.30}$$

In addition, from eqs. (4.15) and (4.22), we have that

$$\frac{\dot{\rho}_\phi}{\rho_\phi} = \frac{-3\mathcal{H}(1+w_\phi)}{1+\beta\rho_\nu(1-3w_\nu)}\ . \tag{4.31}$$

4.3. Results and Discussion

4.3.1. Numerical approach

Equipped with the background and perturbation equations, we can study this scenario by modifying the numerical packages that evaluate the CMB anisotropies and the matter power spectrum. In particular, we modified the CAMB code [Lewis et al., 2000], based on CMBFast[2] [Seljak & Zaldarriaga, 1996] routines. We use CosmoMC [Lewis & Bridle, 2002] in order to sample the parameter space of our model with a Markov Chain Monte Carlo (MCMC) technique.

We assume a flat universe, with a constant equation of state dark energy fluid, cold dark matter, 2 species of massless neutrinos plus a massive one, and ten free parameters. Six of them are the standard ΛCDM parameters, namely, the physical baryon density $\Omega_{b0}h^2$, the physical cold dark matter density $\Omega_{c0}h^2$, the dimensionless Hubble constant h, the optical depth to reionization $\tau_{\rm reion}$, the amplitude (A_s) and spectral index (n_s) of primordial density fluctuations. In addition, we vary the constant dark energy equation of state parameter w_ϕ and the three parameters accounting for the neutrino mass: the present mass m_0, the logarithm of the parameter Δ related to the duration of the transition, and the logarithm of the ratio of the modulus of the mass difference over the current mass, $\log\mu$, where we define

$$\mu \equiv \frac{|m_1 - m_0|}{m_0} \begin{cases} \mu_+ \equiv \frac{m_1}{m_0} - 1 \quad , \quad m_1 > m_0 \ , \\ \mu_- \equiv 1 - \frac{m_1}{m_0} \quad , \quad m_1 < m_0 \ . \end{cases}$$

All these parameters take implicit flat priors in the regions in which they are allowed to vary (see Table 4.1).

Table 4.1: Assumed ranges for the MaVaNs parameters

Parameter	Range
w_ϕ	$-1 < w_\phi < -0.5$
m_0	$0 < m_0/\mathrm{eV} < 5$
Δ	$-4 < \log\Delta < 2$
μ	$-6 < \log(\mu_+) < 0$
	$-6 < \log(\mu_-) < 0$

[2] http://cfa-www.harvard.edu/∼mzaldarr/CMBFAST/cmbfast.html

Concerning the last parameter, notice that we choose to divide the parameter space between two regions: one in which the mass is decreasing over time (μ_+) and one in which it is increasing (μ_-). We chose to make this separation because the impact on cosmological observables is different in each regime, as we will discuss later, and by analyzing this regions separately we can gain a better insight of the physics driving the constraints in each one of them. Moreover, we do not allow for models with $w_\phi < -1$, since we are only considering scalar field models with standard kinetic terms.

For given values of all these parameters, our modified version of CAMB first integrates the background equations backward in time, in order to find the initial value of ρ_ϕ leading to the correct dark energy density today. This problem does not always admit a solution leading to well-behaved perturbations: the dark energy perturbation equations (4.28), (4.29) become singular whenever one of the two quantities appearing in the denominators, ρ_ϕ or $[1 + \beta\rho_\nu(1 - 3w_\nu)]$, vanishes. As we shall see later, in the case in which the neutrino mass decreases, the background evolution is compatible with cases in which the dark energy density crosses zero, while the second term can never vanish. We exclude singular models by stopping the execution of CAMB whenever $\rho_\phi < 0$, and giving a negligible probability to these models in CosmoMC. The physical interpretation of these pathological models will be explained in the next sections. For other models, CAMB integrates the full perturbation equations, and passes the CMB and matter power spectra to CosmoMC for comparison with the data.

Table 4.2: Results for increasing and decreasing neutrino mass, using WMAP 5yr + small scale CMB + LSS + SN + HST data.

	(+)Region 95% (68%) C.L.	(−)Region 95% (68%) C.L.
w_ϕ	< -0.85 (< -0.91)	< -0.87 (< -0.93)
m_0 (eV)	< 0.28 (< 0.10)	< 0.43 (< 0.21)
$\log \mu_+$	< -2.7 (< -4.5)	—
$\log \mu_-$	—	< -1.3 (< -3.1)
$\log \Delta$	$[-3.84; 0.53]$ $([-2.20; 0.05])$	$[-0.13; 4]$ $([0.56; 4])$

We constrain this scenario using CMB data (from WMAP 5yr [Komatsu et al., 2009; Dunkley et al., 2009], VSA [Scott et al., 2003], CBI [Pearson et al., 2003] and ACBAR [Kuo et al., 2004]); matter power spectrum from large scale struc-

ture (LSS) data (2dFGRS [Cole et al., 2005] and SDSS [Tegmark et al., 2006]); supernovae Ia (SN) data from Kowalski et al. [2008], and the HST Key project measurements of the Hubble constant [Freedman et al., 2001][3].

Once the posterior probability of all ten parameters has been obtained, we can marginalize over all but one or two of them, to obtain one- or two-dimensional probability distributions. We verified that the confidence limits on the usual six parameters do not differ significantly from what is obtained in the "vanilla model" [Komatsu et al., 2009], and therefore we only provide the results for the extra neutrino and dark energy parameters (Figures 4.4, 4.5, 4.7, 4.8, and Table 4.2).

4.3.2. Increasing neutrino mass

In this model, the background evolution of the dark energy component obeys to equation (4.15), which reads after division by ρ_ϕ:

$$\begin{aligned} \frac{\dot{\rho}_\phi}{\rho_\phi} &= -3\mathcal{H}(1+w_\phi) - \frac{d\ln m_\nu}{du}\frac{\rho_\nu}{\rho_\phi}\mathcal{H}(1-3w_\nu) \\ &\equiv -\Gamma_d - \Gamma_i \end{aligned} \tag{4.32}$$

where the two positive quantities Γ_d and Γ_i represent respectively the dilution rate and interaction rate of the dark energy density. For any parameter choice, ρ_ϕ can only decrease with time, so that the integration of the dark energy background equation backward in time always find well-behaved solutions with positive values of ρ_ϕ. Moreover, the quantity $[1+\beta\rho_\nu(1-3w_\nu)]$ appearing in the denominator of the dark energy perturbation equations is equal to the contribution of the dilution rate to the total energy loss rate, $\Gamma_d/(\Gamma_d+\Gamma_i)$. This quantity is by construction greater than zero, and the dark energy equations cannot become singular. However, when the the interaction rate becomes very large with respect to the dilution rate, this denominator can become arbitrarily close to zero. Then, the dark energy perturbations can be enhanced considerably, distorting the observable spectra and conflicting the data. Actually, this amplification mechanism is well-known and was

[3]While this work was being finished, the SHOES (Supernova, HO, for the Equation of State) Team [Riess et al., 2009] reduced the uncertainty on the Hubble constant by more than a factor 2 with respect to the value obtained by the HST Key Project, finding $H_0 = 74.2 \pm 3.6$ km s^{-1} Mpc^{-1}. However, since we are taking a flat prior on H_0, and our best fit value for H_0 is contained in their 1σ region, we do not expect our results to be strongly affected by their results.

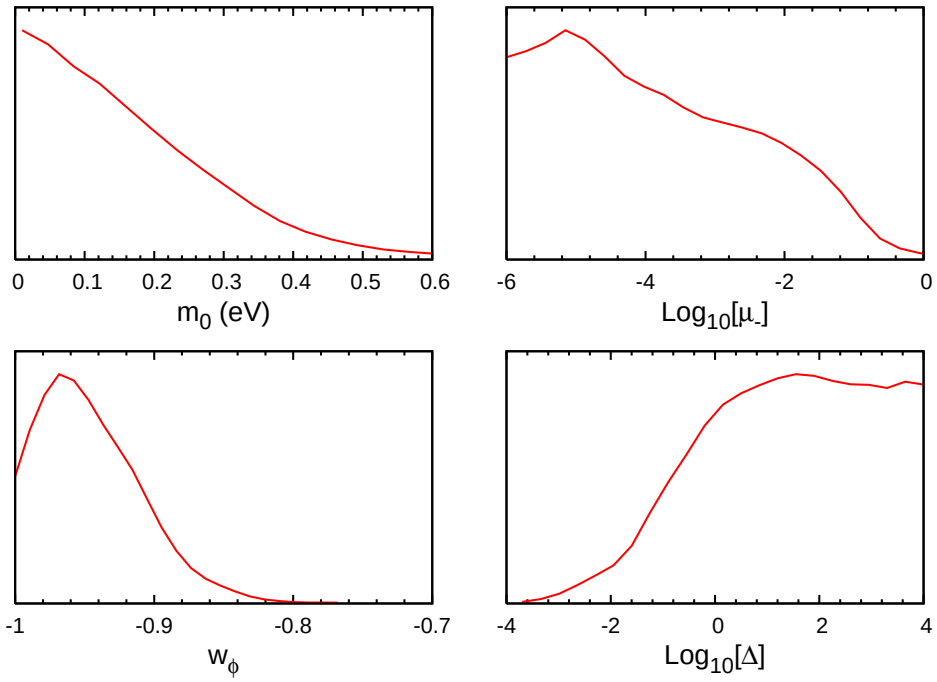

Figure 4.4: Marginalized 1D probability distribution in the increasing mass case $m_1 < m_0$, in arbitrary scale, for the neutrino / dark energy parameters: m_0, $\log_{10}[\mu_-]$ (top panels), w_ϕ, and $\log \Delta$ (bottom panels).

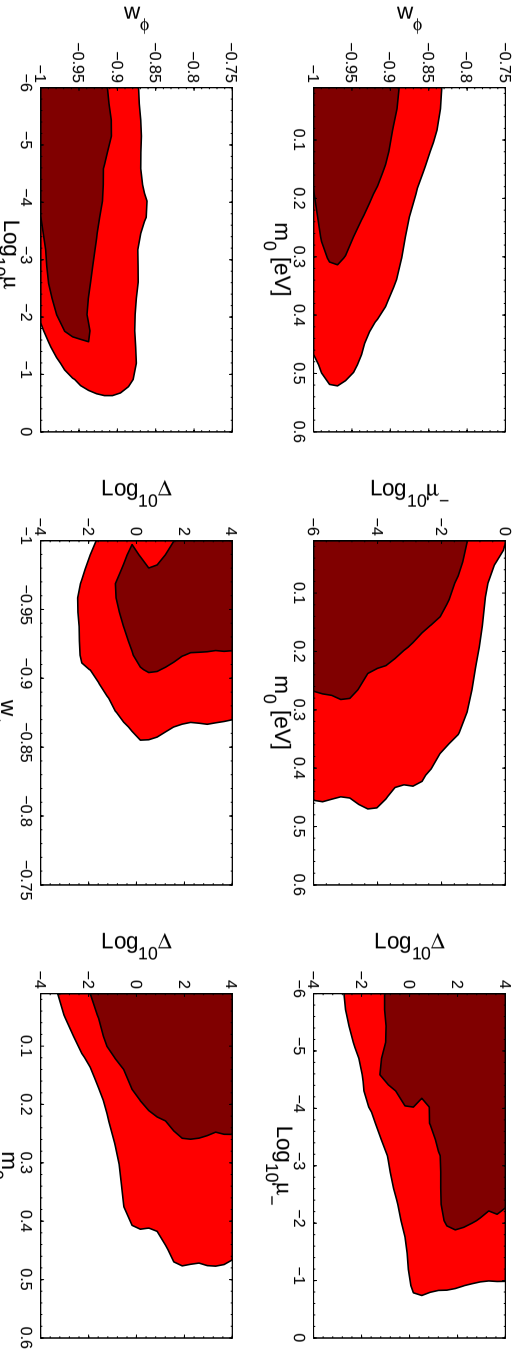

Figure 4.5: Marginalized 2D probability distribution in the increasing mass case $m_1 < m_0$.

studied by various authors [Bean et al., 2008b; Väliviita et al., 2008; Gavela et al., 2009]. It was found to affect the largest wavelengths first, and is usually refered as the large-scale instability of coupled dark energy models. The condition for avoiding this instability can be thought to be roughly of the form

$$\Gamma_i < A\Gamma_d \ , \tag{4.33}$$

where A is some number depending on the cosmological parameters and on the data set (because a given data set tells how constrained is the large scale instability, i.e. how small can be the denominator $[1 + \beta\rho_\nu(1 - 3w_\nu)]$, i.e. how small should the interaction rate remain with respect to the dilution rate). The perturbations are amplified when the denominator is much smaller than one, so A should be a number much greater than one. Intuitively, the condition (4.33) will lead to the rejection of models with small values of (w_ϕ, Δ) and large values of μ_-. Indeed, the interaction rate is too large when the mass variation is significant (large μ_-) and rapid (small Δ). The dilution rate is too small when w_ϕ is small (close to the cosmological constant limit). Because of that, it seems that when the dark energy equation of state is allowed to vary one can obtain a larger number of viable models if $w_\phi > -0.8$ early on in the cosmological evolution [Majerotto et al., 2010; Väliviita et al., 2010].

We ran CosmoMC with our full data set in order to see how much this mass-varying scenario can depart from a standard cosmological model with a fixed dark energy equation of state and massive neutrinos. In our parameter basis, this standard model corresponds to the limit $\log\mu_- \to -\infty$, with whatever value of $\log\Delta$. The observational signature of a neutrino mass variation during dark energy or matter domination is encoded in well-known effects, such as:

(i) a modification of the small-scale matter power spectrum [due to a different free-streaming history], or

(ii) a change in the time of matter/radiation equality [due to a different correspondence between the values of (ω_b, ω_m, ω_ν) today and the actual matter density at the time of equality].

On top of that, the neutrino and dark energy perturbations can approach the regime of large-scale instability discussed above.

Our final results - namely, the marginalized 1D and 2D parameter probabilities - are shown in figures 4.4 and 4.5. The shape of the contours in $(\log\mu_-, \log\Delta)$ space is easily understandable with analytic approximations. The necessary condition (4.33) for avoiding the large-scale instability reads in terms of our model parameters

$$\mu_- \left[\frac{1+\Delta(1+\Gamma)}{\Delta}\right] < A \left[\frac{1}{(1-\Gamma)(1-f)}\right] \frac{3\Omega_\phi(1+w_\phi)}{\Omega_\nu(1-3w_\nu)} \,, \tag{4.34}$$

where we expressed the mass variation as

$$\frac{d\ln m_\nu}{du} = \left(\frac{\mu_-}{1-\mu_-\Gamma}\right)\left(\frac{1+\Delta}{\Delta}\right)(1-\Gamma)(1-f) \ . \tag{4.35}$$

Two limits can be clearly seen from this equation. For $\Delta \ll 1$ (fast transitions), the upper limit on μ_- reads

$$\mu_- \lesssim A\Delta \left[\frac{1}{(1-\Gamma)(1-f)}\right] \frac{3\Omega_\phi(1+w_\phi)}{\Omega_\nu(1-3w_\nu)} \ . \tag{4.36}$$

This corresponds to the diagonal limit in the lower half of the right upper panel of figure 4.5. In fact, the appearance of the large-scale instability is seen in models localized at the edge of the allowed region, as shown in figure 4.6.

In the opposite case of a very slow transition, $\Delta \gg 1$, it is clear from eq. (4.34) that the limit on μ_- should be independent on Δ,

$$\mu_- \lesssim A \left[\frac{1}{(1-\Gamma)(1-f)}\right] \frac{3\Omega_\phi(1+w_\phi)}{\Omega_\nu(1-3w_\nu)} \ . \tag{4.37}$$

This limit corresponds to the almost vertical cut in the upper part of the plane $(\log\mu_-, \log\Delta)$ (upper right panel, fig. 4.5).

These conditions are easier to satisfy when at the time of the transition, $\Omega_\phi(1+w_\phi)$ is large. So, in order to avoid the instability, large values of w_ϕ are preferred. However, it is well-known that cosmological observables (luminosity distance relation, CMB and LSS power spectra) better fit the data for w close to -1 (cosmological constant limit). In the present model, the role of the large-scale instability is to push the best-fit value from -1 to -0.96, but $w_\phi = -1$ is still allowed at the 68% C.L.

The main result of this section is that the variation of the neutrino mass is

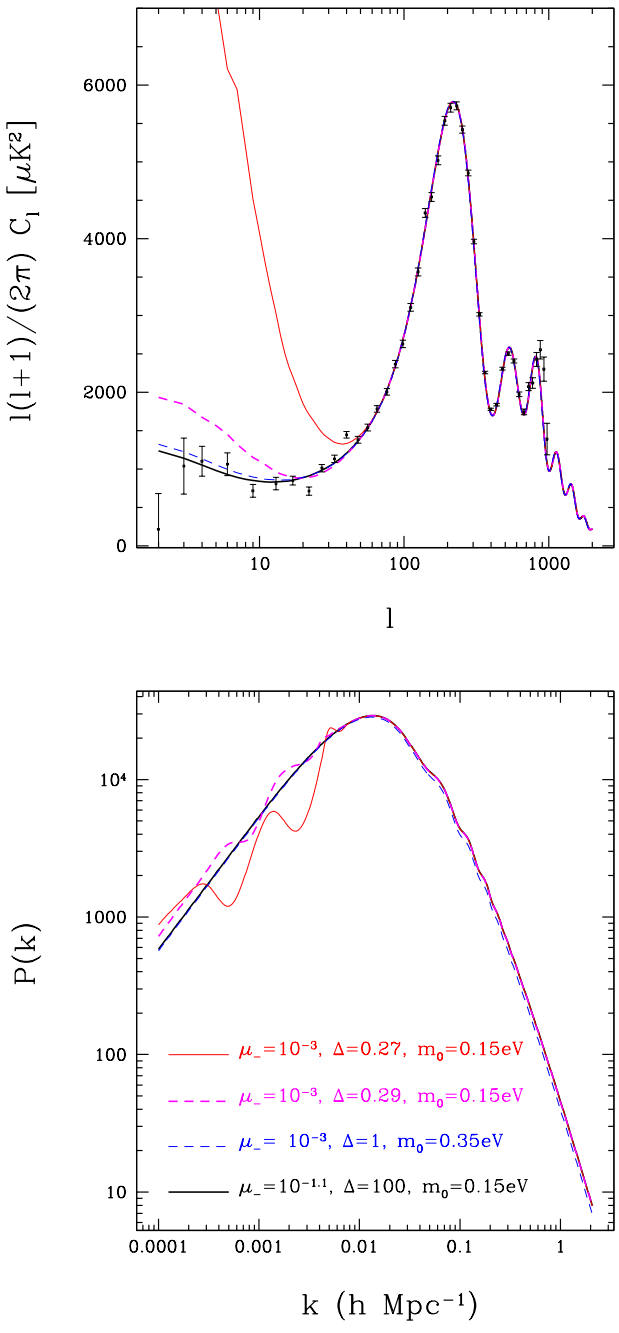

Figure 4.6: CMB anisotropies and matter power spectra for some mass varying models with increasing mass, showing the development of the large scale instability. The cosmological parameters are set to our best fit values, except for the ones shown in the plot. The data points in the CMB spectrum correspond to the binned WMAP 5yr data.

bounded to be small, not so much because of the constraining power of large-scale structure observations in the regime where neutrino free-streaming is important (i.e., small scales), but by CMB and LSS data on the largest scales, which provide limits on the possible instability in DE and neutrino perturbations.

Indeed, for the allowed models, the mass variation could be at most of order 10% for masses around 0.05 eV, and less than 1% for masses larger than 0.3 eV: this is undetectable with small scale clustering data, showing that the limit really comes from large scales.

With those results, we conclude that there is no evidence for a neutrino mass variation coming from the present data. In fact, as for most cosmological data analyses, the concordance ΛCDM model remains one of the best fits to the data, lying within the 68% interval of this analysis.

Nonetheless, better constraints will possibly be obtained with forthcoming data, especially the ones that probe patches of the cosmological "desert" between $z \simeq 1100$ and $z \simeq 1$, like CMB weak lensing [Lesgourgues et al., 2006], and/or cross-correlations of different pieces of data, like CMB and galaxy-density maps [Lesgourgues et al., 2008]. We can estimate, for instance, what is the favored redshift range for the neutrino mass variation according to our results. Taking $m_0 = 0.1$ eV and the mean likelihood values for $\log\Delta$ and $\log[m_1/m_0]$, one can see that the bulk of the mass variation takes place around $z \sim 20$, a redshift that possibly will be probed by future tomographic probes like weak lensing [Hannestad, 2006; Kitching et al., 2008] and especially 21 cm absorption lines [Loeb & Zaldarriaga, 2004; Loeb & Wyithe, 2008; Mao et al., 2008; Pritchard & Pierpaoli, 2008]. Those will help not only to disentangle some degeneracies in the parameter space, but will also allow for direct probes of the neutrino mass in different redshift slices.

4.3.3. Decreasing neutrino mass

In this case, the evolution rate of the dark energy density is still given by equation (4.32) but with an opposite sign for the interaction rate: it can be summarized as

$$\frac{\dot{\rho}_\phi}{\rho_\phi} = -\Gamma_d + \Gamma_i \ , \tag{4.38}$$

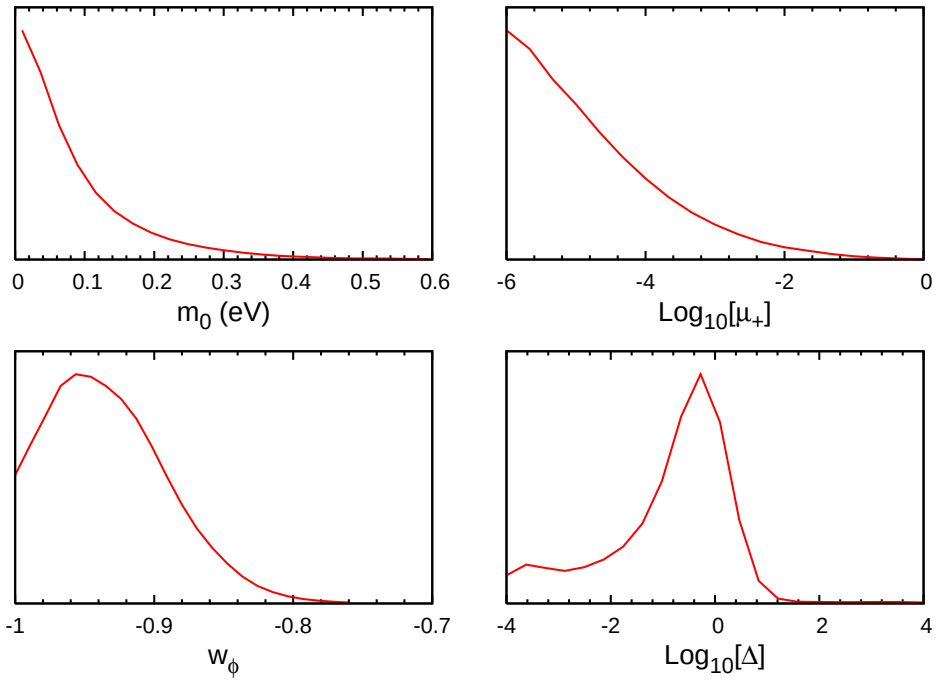

Figure 4.7: Marginalized 1D probability distribution (red/solid lines) in arbitrary scale for the decreasing mass case $m_1 > m_0$, for neutrino / dark energy parameters: m_0, $\log[\mu_+]$ (top panels), w_ϕ, and $\log \Delta$ (bottom panels).

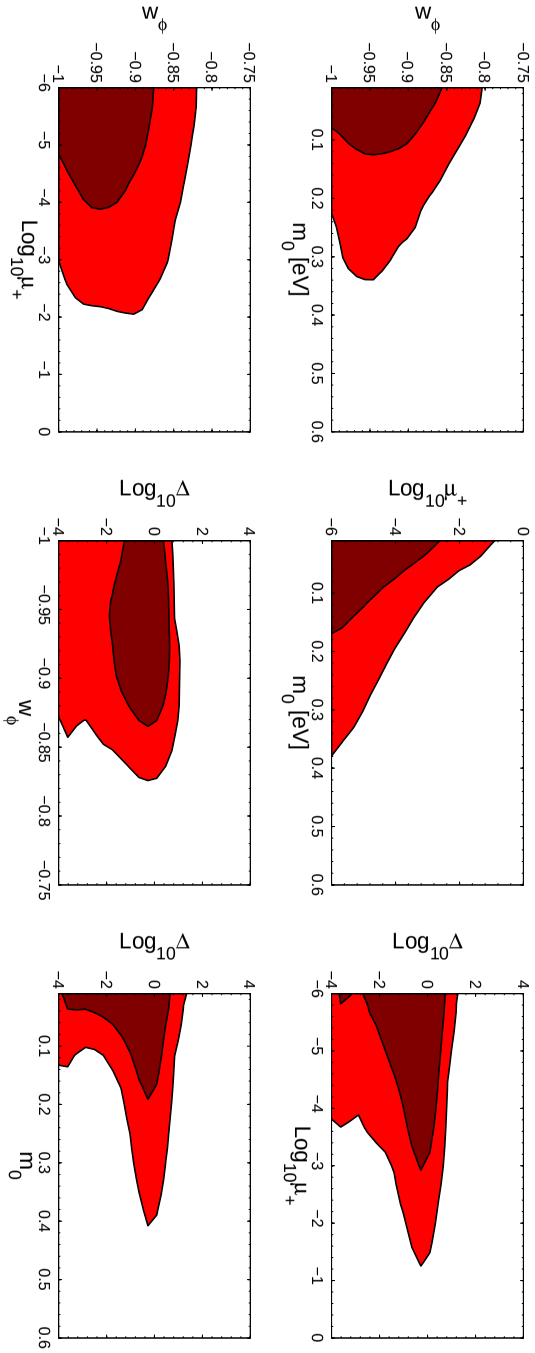

Figure 4.8: Marginalized 2D probability distribution for decreasing mass, $m_1 > m_0$.

with Γ_d and Γ_i both positive. In principle, the interaction rate could overcome the dilution rate, leading to an increase of ρ_ϕ. Hence, the integration of the dark energy evolution equation backward in time can lead to negative values of ρ_ϕ, and the prior $\rho_\phi > 0$ implemented in our CAMB version is relevant. Still, the denominator $[1+\beta\rho_\nu(1-3w_\nu)]$ can never vanish since it is equal to $\Gamma_d/(\Gamma_d-\Gamma_i)$.

Well before before the transition, the interaction rate is negligible and $\dot{\rho}_\phi$ is always negative. We conclude that $\beta = d\ln m_\nu/d\rho_\phi$ starts from small positive values and increases. If the condition

$$\Gamma_i < \Gamma_d \tag{4.39}$$

is violated during the transition, $\dot{\rho}_\phi$ will cross zero and become positive. This corresponds to β growing from zero to $+\infty$, and from $-\infty$ to some finite negative value. After Γ_i/Γ_d has reached its maximum, β undergoes the opposite evolution. Reaching $\rho_\phi = 0$ is only possible if ρ_ϕ has a non-monotonic evolution, i.e. if (4.39) is violated. However, the perturbations diverge even before reaching this singular point: when β tends to infinity, it is clear from eq. (4.26) that the neutrino perturbation derivatives become arbitrarily large. We conclude that in this model, the condition (4.39) is a necessary condition for avoiding instabilities, but not a sufficient condition: the data is expected to put a limit on the largest possible value of β, which will always be reached before $\dot{\rho}_\phi$ changes sign, i.e. before the inequality (4.39) is saturated. Hence, the condition for avoiding the instability is intuitively of the form of (4.33), but now with A being a number smaller than one.

We then ran CosmoMC with the full data set and obtained the marginalized 1D and 2D parameter probabilities shown in figures 4.7 and 4.8. The major differences with respect to the increasing mass case are: a stronger bound on m_0, a much stronger bound on μ_-, and the fact that large values of Δ are now excluded. This can be understood as follows. In order to avoid instabilities, it is necessary to satisfy the inequalities (4.36), (4.37), but with a much smaller value of A than in the increasing mass case; hence, the contours should look qualitatively similar to those obtained previously, but with stronger bounds. This turns out to be the case, although in addition, large Δ values are now excluded. Looking at the mass variation for large Δ in figure 4.2, we see that in this limit the energy transfer takes place essentially at low redhsift. Hence, the interaction rate is large close to

$z = 0$. In many models, this leads to positive values of $\dot{\rho}_\phi$ at the present time, to a non-monotonic behavior of the dark energy density, and to diverging perturbations. This can only be avoided when w is large with respect to -1, i.e. when the dilution rate is enhanced. Hence, in this model, the need to avoid diverging perturbations imposes a strong parameter correlation between w and Δ. However, values of w greater than -0.8 are not compatible with the supernovae, CMB and LSS data set; this slices out all models with large Δ.

The fact that the bound on m_0 is stronger in the decreasing mass case is also easily understandable: for the same value of the mass difference $\mu_\pm = |m_1 - m_0|/m_0$, a given m_0 corresponds to a larger mass m_1 in the decreasing mass case. It is well-known that CMB and LSS data constrain the neutrinos mass through its background effect, i.e. through its impact on the time of matter/radiation equality for a given dark matter abundance today. The impact is greater when m_1 is larger, i.e. in the decreasing mass case; therefore, the bounds on m_0 are stronger.

4.4. Concluding remarks

In this chapter we analyzed some mass-varying neutrino scenarios in a nearly model independent way, using a general and well-behaved parameterization for the neutrino mass, including variations in the dark energy density in a self-consistent way, and taking neutrino/dark energy perturbations into account.

Our results for the background, CMB anisotropies, and matter power spectra are in agreement with previous analyses of particular scalar field models, showing that the results obtained with this parameterization are robust and encompass the main features of the MaVaNs scenario.

Moreover, a comparison with cosmological data shows that only small mass variations are allowed, and that MaVaNs scenario are mildly disfavored with respect to the constant mass case, especially when neutrinos become lighter as the universe expands. In both cases, neutrinos can change significantly the evolution of the dark energy density, leading to instabilities in the dark energy and/or neutrino perturbations when the transfer of energy between the two components per unit of time is too large. These instabilities can only be avoided when the mass varies by a very small amount, especially in the case of a decreasing neutrino mass. Even in the case of increasing mass, constraining better the model with forthcoming

data will be a difficult task, since it mimics a massless neutrino scenario for most of the cosmological time.

One should keep in mind that our analysis assumes a constant equation of state for dark energy and a monotonic behavior for the mass variation. Even though those features are present in most of the simplest possible models, more complicated models surely can evade the constraints we obtained in our analysis.

Finally, those constraints will be improved with forthcoming tomographic data. If any of the future probes indicate a mismatch in the values of the neutrino mass at different redshifts, we could arguably have a case made for the mass-varying models.

4.5. Recent Results

Since the publication of this work, most of the discussion in the literature on those models were focused on the properties of the nonlinear neutrino clumps and whether the perturbations could be stabilized in the nonlinear regime, what could possibly avoid some of the constraints discussed here (a nonextensive list of papers is Wintergerst et al. [2010]; Pettorino et al. [2010]; Baldi [2011]; Baldi et al. [2011]; La Vacca & Mota [2012]).

In particular, two results are worth mentioning here concerning recent advances in this area. First, Baldi et al. [2011] have performed the first simulation of structure formation in the context of the models discussed here, although their approach is limited to $z \gtrsim 1$ for the Newtonian approximation used in the code. In particular, they observe a pulsation in the growth of structure that could potentially test those models. While the authors state that this stabilizes the fluctuations and avoids the growth of the neutrino induced gravitational potential, a full relativistic analysis is necessary to assess this question. Second, La Vacca & Mota [2012] have recently studied the impact of tomographic weak lensing from a Euclid-like experiment on specific models of MaVaNs, and show that, as expected, this kind of dataset could significantly improve the limits on the coupling between neutrinos and dark energy.

5

Dark matter and the 21-cm global signal

In chapter 2 we saw that several different cosmological and astrophysical observations seem to indicate that most matter in the Universe does not interact significantly with photons: the so-called *dark matter* [Bertone et al., 2005; Bertone, 2010], yet to be detected directly and/or indirectly, can be inferred nowadays only via its gravitational interactions.

While a gigantic list of particles has been proposed as candidates for the dark matter, probably the most studied are the *weakly-interacting massive particles* (WIMPs) [Jungman et al., 1996], particles with masses from GeV to TeV that interact very weakly with the known particles of the standard model. At high temperatures they are abundant and rapidly converting to lighter particles and vice versa. Shortly after the temperature of the Universe drops below its mass the number density of DM particles drops exponentially. At this point, they cease to annihilate, fall out of equilibrium (or *freeze-out*), and a relic cosmological abundance remains. Moreover, because those particles are basically non-interacting, they will eventually form the potentials wells at which baryons will gravitationally fall to form the first luminous sources after the dark ages as well as present day cosmological structures like galaxies and clusters.

On the other hand, understanding the physics of the sources responsible for the end of the dark ages and for the reionization of the Universe is one of the main challenges of the forthcoming decade. Although inaccessible with the current observational tools, this period presents the possibility to be probed within the next decade using 21-cm cosmology, which uses the hyperfine transition line of the neutral hydrogen to map tomographically the high redshift Universe [Furlanetto

et al., 2006a; Morales & Wyithe, 2010].

While several large collaborations are building and/or planning instruments that aim to detect the three-dimensional fluctuations in the 21-cm brightness temperature (such as LOFAR [1], MWA[2], PAPER[3], and SKA[4]), some recent experimental effort has been put on looking for the so-called global, *i.e.* sky-averaged, 21-cm signal [Furlanetto, 2006]. The EDGES experiment [Bowman et al., 2008], for instance, has recently been able to place some weak limits on the duration of the reionization epoch [Bowman & Rogers, 2010; Pritchard & Loeb, 2010b], a first step in the direction of using the 21-cm signal to probe the high-redshift universe. In particular, since the 21-cm signal directly probes the physical state of the intergalactic medium at high-redshifts, it is a very sensitive probe for mechanisms that inject energy into it, like dark matter annihilation. This extra energy is released in the form of gamma ray and other particles, like electrons and positrons, that will cool rapidly due to the inverse Compton effect with the cosmic microwave background, producing a spectrum of upscattered CMB photons that play an important role in the evolution of the Intergalactic Medium (IGM).

In this chapter, based upon a preliminary version of a paper in preparation [França et al., 2012], we discuss the impact that DM could have had in the IGM during the epoch in which the first generation of stars were formed in the Universe. For that, we will focus on the modifications of the 21-cm global signal arising from the annihilation of DM particles at those epochs. Our goals are, first, to check whether one could distinguish the effects of DM annihilation from the impact on the IGM of the first luminous sources with the 21-cm global signal; and second, to learn if we could use those observation to probe some properties of the DM particles.

For that, in Section 5.1 we review the physics behind the global 21-cm signal, including the modeling of the first luminous sources. We then discuss the dark matter annihilation in Section 5.2, focusing on the mechanisms that shape the final photon spectrum at a given redshift. In Section 5.3 we discuss the impact of this extra energy injection in the global 21-cm signal, along with the prospects of constraining dark matter properties with global experiments. Finally, in Section

[1] http://www.lofar.org
[2] http://www.MWAtelescope.org
[3] http://astro.berkeley.edu/∼dbacker/eor/; see [Parsons et al., 2010] for some early results.
[4] http://www.skatelescope.org

5.4 we discuss the current state of our results and some future possibilities of extending them. Throughout this chapter we use the cosmological parameters of the ΛCDM model consistent with Komatsu et al. [2011]: $\Omega_\Lambda = 0.72$, $\Omega_M = 0.28$, $\Omega_b = 0.045$, $h = 0.7$, $n_s = 0.95$, and $\sigma_8 = 0.8$.

5.1. The global 21-cm signal with dark matter annihilation

The hyperfine or *spin-flip* transition of the hydrogen atom occurs because the triplet state when the proton and electron spins are aligned is slightly more energetic than the singlet state when they are opposite (see figure 5.1). When the atom undergoes a transition from the upper state, it releases a a photon of frequency $\nu_{21} \approx 1420.2$ MHz, corresponding to a wavelength of approximately 21-cm (see, for instance, Peebles [1992]).

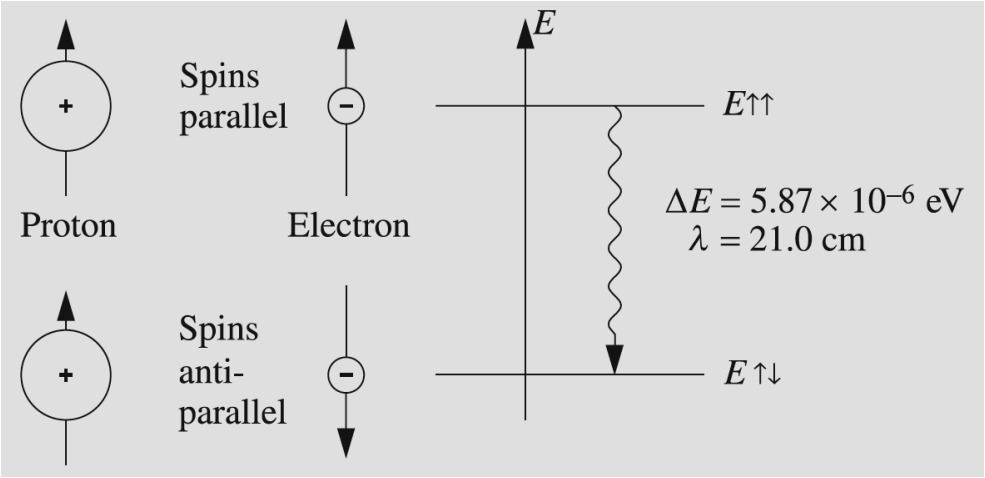

Figure 5.1: In a hydrogen atom the spins of the electron and the proton may be either parallel or opposite. The energy of the former state is slightly larger. The wavelength of a photon corresponding to a transition between these states is 21-cm. From Karttunen et al. [2007].

However, the 21-cm line from gas during the first billion years of the Universe, when the first structures start forming, redshifts to radio frequencies 30-200 MHz making it a prime target for a new generation of radio interferometers currently being built.

In the language of radioastronomers, the redshift dependent sky-averaged signal is observed in terms of the differential brightness temperature $T_b(z)$ with respect to the CMB temperature T_γ [Rohlfs et al., 2009], and can be written as

$$T_b(z) = 27(1 - x_i)\left(\frac{T_S - T_\gamma}{T_S}\right)\left(\frac{1+z}{10}\right)^{1/2} \text{mK} \ , \tag{5.1}$$

where x_i is the hydrogen ionized fraction, and T_S is the so-called spin temperature, defined by the number densities of hydrogen atoms in each of the hyperfine levels,

$$\frac{n_1}{n_0} = \frac{g_1}{g_0}\exp\left[-\frac{T_\star}{T_S}\right] = 3 \ \exp\left[-\frac{68 \text{ mK}}{T_S}\right], \tag{5.2}$$

where the subscripts 1 and 0 correspond to the excited (triplet) and ground (singlet) states of the H atom, g_i is the spin degeracy factor of each hyperfine level (3 and 1 for the triplet and singlet, respectively), and $T_\star$ is the temperature that corresponds to the energy difference between the levels, $T_\star = (E_1 - E_0)/k_B$.

The redshift evolution of the spin temperature in equilibrium can be written as

$$\begin{aligned} T_S^{-1} &= \frac{T_\gamma^{-1} + x_\alpha T_\alpha^{-1} + x_c T_K^{-1}}{1 + x_\alpha + x_c} \\ &\approx \frac{T_\gamma^{-1} + (x_\alpha + x_c) T_K^{-1}}{1 + x_\alpha + x_c} \ , \end{aligned} \tag{5.3}$$

where T_α is the effective color temperature of the Lyα field [Hirata, 2006], that is expected to relax quickly to T_K in the optically thick regime. The collisional coupling coefficient x_c can be written as

$$x_c = x_c^{HH} + x_c^{eH} = \frac{4\,T_\star}{3A_{10}\,T_\gamma}\left[\kappa_{10}^{HH}(T_K) n_H + \kappa_{10}^{eH}(T_K) n_e\right] \ , \tag{5.4}$$

where the first term refers to the collisions between neutral hydrogen atoms [Allison & Dalgarno, 1969; Zygelman, 2005], and the second one is the collisional coupling due to the collisions between electrons and neutral H atoms [Furlanetto & Furlanetto, 2007]. Finally, the ultraviolet scattering coefficient is [Chen &

Miralda-Escudé, 2004; Hirata, 2006],

$$x_\alpha = \frac{16\pi^2 T_\star e^2 f_{S,\alpha}}{27 A_{10} T_\gamma m_e c} S_\alpha J_\alpha \ , \tag{5.5}$$

where $f_{S,\alpha} = 0.4162$ is the oscillator strength of the Lyα transition, S_α is a correction factor of the order of unity that describes the photon distribution around the Lyα resonance [Furlanetto & Pritchard, 2006], and J_α is the angle-averaged specific intensity of Lyα photons calculated in detail by Pritchard & Furlanetto [2007]. A useful approximation for S_α can be found in Chuzhoy & Shapiro [2007].

For most of the redshifts that are likely to be observationally probed in the near future collisional coupling of the 21 cm line is inefficient. However, once star formation begins, resonant scattering of Lyα photons provides a second channel for coupling. This process is generally known as the *Wouthuysen-Field effect* [Wouthuysen, 1952; Field, 1959] and is illustrated in Figure 5.2, which shows the hyperfine structure of the hydrogen 1S and 2P levels.

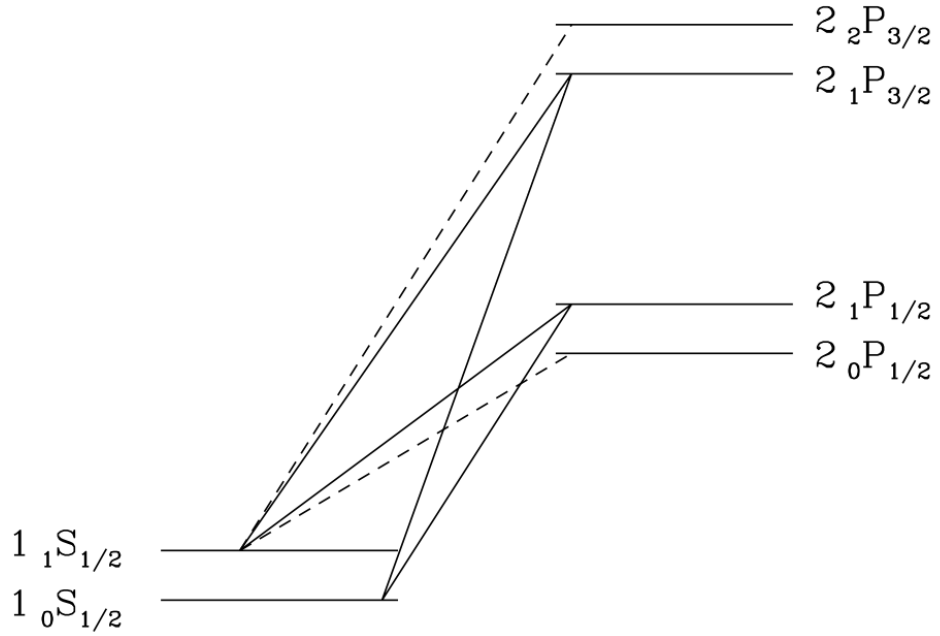

Figure 5.2: Illustration of the Wouthuysen-Field effect. Solid line transitions allow spin flips, while dashed transitions are allowed but do not contribute to spin flips. From Pritchard & Loeb [2012].

To have a qualitative grasp of the physics behind this effect, suppose that

hydrogen is initially in the hyperfine singlet state. Absorption of a Lyα photon will excite the atom into any of the central 2P hyperfine states (the dipole selection rules make the other two hyperfine levels inaccessible). From here emission of a Lyα photon can relax the atom to either of the two ground state hyperfine levels. If relaxation takes the atom to the ground level triplet state then a spin-flip has occurred. Hence, resonant scattering of Lyα photons can produce a spin-flip. This effect, when calculated in detail [Chen & Miralda-Escudé, 2004; Hirata, 2006] results in the coupling shown in eq. (5.5).

5.1.1. The thermal evolution

The evolution of the IGM kinetic temperature T_K can be written as

$$\begin{aligned} \frac{dT_K}{dt} &= \frac{x_i}{1+f_{\rm He}+x_i}\frac{8u_\gamma(z)\sigma_T}{3m_e c}(T_\gamma - T_K) \\ &- 2H(z)T_K + \frac{2}{3k_B}\frac{\epsilon_X+\epsilon_\alpha+f_{\chi,{\rm h}}\epsilon_\chi}{n_A} \ , \end{aligned} \tag{5.6}$$

where $f_{\rm He}$ is the Helium fraction in number, $u_\gamma(z)$ is the CMB energy density, m_e is the electron mass, $\sigma_T = 6.652\times10^{-25}$ cm^2 is the Thomson cross-section, $n_{\rm A} = n_{\rm H} + n_{\rm He}$ is the number density of atoms at z, and $f_{\chi,{\rm h}}$ is the fraction of the energy released in DM annihilations that goes into heating the IGM [Shull & van Steenberg, 1985], that can be approximated by [Chen & Kamionkowski, 2004],

$$f_{\chi,{\rm h}} = \frac{1+2x_i}{3} \ . \tag{5.7}$$

The first term on the right-hand side of eq. (5.6) corresponds to Compton heating, responsible for coupling T_K to T_γ at $z \gtrsim 150$. The different heating rates per unit volume, ϵ_χ and ϵ_α, are due to X-ray and Lyα photons from the first luminous sources [Furlanetto, 2006], and the extra energy input from DM annihilations is [Cirelli et al., 2009]

$$\epsilon_\chi(z) = c\int_0^{m_\chi} dE_\gamma \ E_\gamma \frac{dN_\gamma}{dE_\gamma}(E_\gamma,z)\alpha(E_\gamma,z) \ , \tag{5.8}$$

where $dN_\gamma/dE_\gamma(E_\gamma,z)$ is the final spectrum of photons from DM annihilation at

redshift z that will be discussed in further detail in Section 5.2, and $\alpha(E_\gamma, z)$ is the absorption coefficient of the different photon interactions, namely [Slatyer et al., 2009]: (*i*) photoionization, (*ii*) Compton scattering, (*iii*) pair production on H and He, (*iv*) pair production on the CMB, and (*v*) photon-photon scattering.

Moreover, the evolution of the ionized fraction, given by

$$\frac{dx_i}{dt} = (1 - x_i)\Lambda_i - \alpha_A C_e x_i^2 n_H + \frac{I(z)}{n_H} \ , \tag{5.9}$$

where Λ_i is the rate of production of ionizing photons per unit time per baryon, and it is proportional to the evolution of the gas fraction inside collapsed objects at z; $\alpha_A = 4.2 \times 10^{-13}$ cm^{3}s^{-1} is the case A recombination coefficient, adequate for the optical thin limit where no photons are reabsorbed [Draine, 2011; Osterbrock & Ferland, 2006], and $C_e \equiv \langle n_e^2 \rangle / \langle n_e \rangle^2$ [Pritchard & Furlanetto, 2007]. The last term takes into account the ionizations produced by DM annihilations [Cirelli et al., 2009], for which rate of ionization per unit volume $I(z)$ is given by

$$I(z) = \int_{E_{H,i}}^{m_\chi} dE_\gamma \frac{dN_\gamma}{dE_\gamma}(E_\gamma, z) P(E_\gamma, z) N_i(E_\gamma) \ , \tag{5.10}$$

where $E_{H,i} = 13.6$ eV is the H ionization energy, and the probability of a primary ionization per second is given by

$$P(E_\gamma, z) = n_H (1 - x_i) \sigma_{\rm i}(E_\gamma) c \ , \tag{5.11}$$

where σ_i is the photoionization cross-section [Zdziarski & Svensson, 1989], and the number of ionizations induced by the energy transferred from the photon to the scattered electron is

$$\begin{aligned} N_i(E_\gamma) &= f_{\chi,{\rm i}} E_\gamma \left[\frac{n_{\rm H}}{E_{{\rm H},i} n_{\rm A}} + \frac{n_{\rm He}}{E_{{\rm He},i} n_{\rm A}} \right] \\ &\approx 7.1 \times 10^7 f_{\chi,{\rm i}} \left(\frac{E_\gamma}{\rm GeV} \right) \end{aligned} \tag{5.12}$$

where $E_{{\rm He},i} = 24.6$ eV is the ionization energy of the Helium atom, and the fraction of the absorbed energy that goes into ionizations can be approximated by [Chen

& Kamionkowski, 2004]

$$f_{\chi,\mathrm{i}} \approx \frac{1 - x_i}{3} \ , \tag{5.13}$$

although we use the numerical fits given by Shull & van Steenberg [1985].

5.1.2. Astrophysical parameters

Before proceeding to the calculation of the spectrum from DM annihilation in the next section, we discuss briefly the astrophysical parameters that describe the modeling of the first luminous sources. We follow the approach of [Pritchard & Loeb, 2008], in which one must specify a luminosity for sources of ionizing, Lyα, and X-ray photons.

For the ionizing photons, we define the number of photons produced per baryon in stars that contribute to ionizing the IGM,

$$N_{\mathrm{ion,IGM}} = f_{\mathrm{esc}} N_{\mathrm{ion}} \ , \tag{5.14}$$

where f_{esc} is the fraction of ionizing photons that escape the host halo. Using this model, the conventional definition of ionizing efficiency [Robertson et al., 2010], for instance, can be written as

$$\zeta = N_{\mathrm{ion,IGM}} f_\star \ , \tag{5.15}$$

where $f_\star$ is the efficiency of star formation. Moreover, we specify the number of Lyα photons produced per baryon in stars N_α, which for convenience will be parametrized as $N_\alpha = f_\alpha N_{\alpha,\mathrm{ref}}$, where $N_{\alpha,\mathrm{ref}} = 6590$ for normal (*i.e.*, Population II) stars, and we expect the value of f_α to be close to unity. In the case of very massive stars (*i.e.*, Population III), for instance, $f_\alpha = 0.46$.

Finally, we fix the energy in X-rays produced per baryon in stars, ε_X, which we also parametrize as $\varepsilon_X = f_X \varepsilon_{X,\mathrm{ref}}$. We take starburst galaxies as the source for the X-rays [Pritchard & Furlanetto, 2007], with a power-law spectrum with index $\alpha_S = 1.5$, and $\varepsilon_{X,\mathrm{ref}} = 560$ eV. The dependence of the global signal on the X-ray and Lyα emissivities is showed on Figure 5.3 for a variation of 5 orders of magnitude on each one.

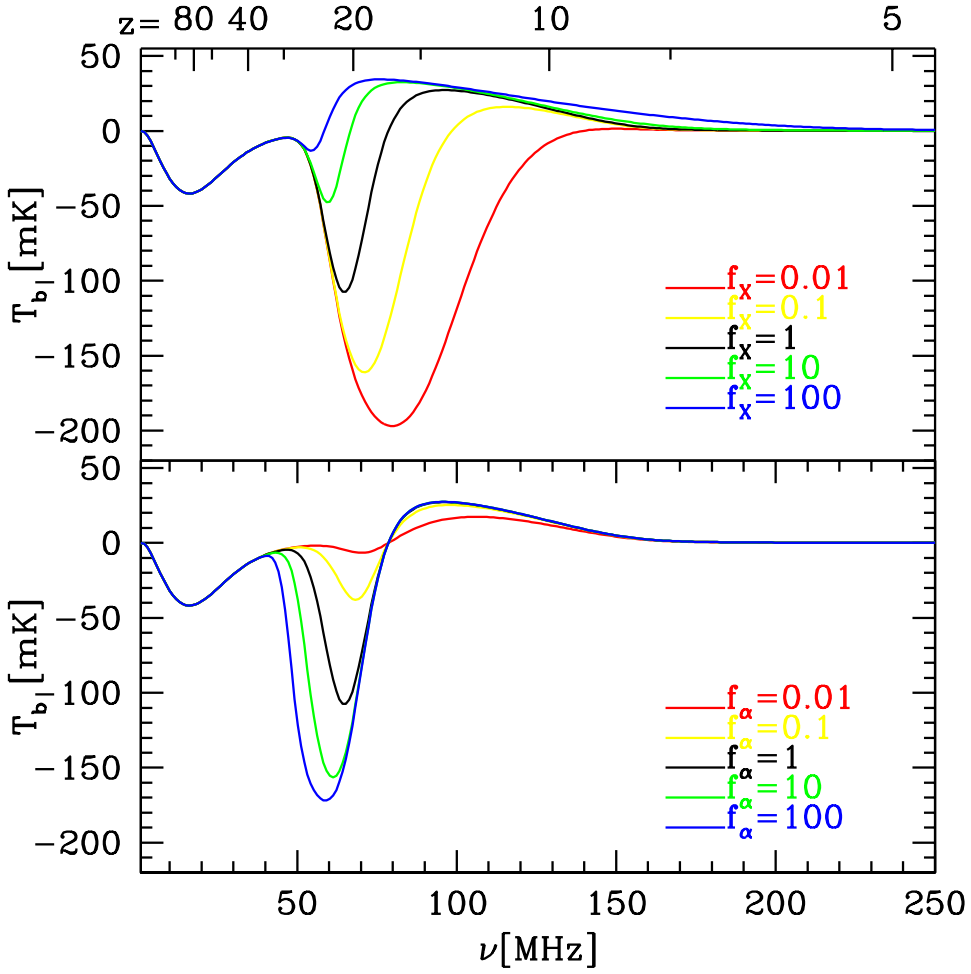

Figure 5.3: Dependence of the 21-cm signal on the X-ray (top panel) and Lyα (bottom panel) emissivity. In each case, the emissivity is reduced or increased by a factor of up to 100. From Pritchard & Loeb [2010a].

5.2. Dark matter annihilation

Different authors have discussed the consequences of dark matter annihilation/decay in the 21-cm signal [Furlanetto et al., 2006b; Valdés et al., 2007; Finkbeiner et al., 2008; Chuzhoy, 2008; Cumberbatch et al., 2010; Natarajan & Schwarz, 2009; Yuan et al., 2010]. The earlier papers, however, have neglected the annihilation inside halos [Furlanetto et al., 2006b; Valdés et al., 2007; Finkbeiner et al., 2008], considering only the annihilation due to the smooth background. That is a good approximation for redshifts $z \gtrsim 60$, but at lower redshifts the annihilation inside DM halos boosts the effect by several orders of magnitude. Chuzhoy [2008] pointed out the importance of the clumpy component, and Cumberbatch et al. [2010] studied the enhancement due to the annihilation in subhalos. The analysis of Natarajan & Schwarz [2009] studied the 21-cm signal considering only the effect of the annihilation, but ignoring the star component, although they qualitatively discussed the influence of astrophysical sources on the global brightness temperature, and Yuan et al. [2010] analyzes two specific sets of parameters for the dark matter model. In our work we take a different approach: we use the state of the art models for the first sources [Pritchard & Loeb, 2010a, 2012], and use as an example the DM annihilation spectra from neutralinos of Cirelli et al. [2011], which take into account the electroweak corrections important for annihilation of particles with masses larger than the electroweak scale [Ciafaloni et al., 2011].

The only missing component for describing the evolution of the IGM is the final spectrum of photons from DM annihilation. Notice that there are two components for it that we need to take int account: the smooth background annihilation, dominant at early epochs, and the annihilation of the DM clustered component that takes place at the halos once the structures start forming.

The smooth background annihilation rate is given by

$$R_{\rm bkg}(z) = \frac{\langle \sigma_A v \rangle}{2 m_\chi^2} \bar{\rho}_{\chi 0}^2 (1+z)^6 \ , \tag{5.16}$$

with m_χ being the mass of the dark matter particles, $\langle \sigma_A v \rangle$ is the thermally averaged annihilation cross-section, and $\bar{\rho}_{\chi 0}$ is the present energy density of the dark matter component. This is the dominant annihilation component before the formation of the first structures at $z \lesssim 100$, when the annihilation in denser strutures

starts taking place. The rate of annihilation will then depend on the number density of dark matter halos and on the density distribution inside them,

$$R_{\rm halos}(z) = \frac{\langle\sigma_A v\rangle}{2m_\chi^2}\int_{M_{\rm min}}^{\infty} dM \frac{dn}{dM}(M,z)(1+z)^3 \times \int dr\ \rho^2(r,M)4\pi r^2\ . \quad (5.17)$$

For the purposes of understanding the DM impact on the global 21-cm signal, we can consider the annihilation in halos as a "boost" factor over the background annihilation [Cirelli et al., 2009; Arina & Tytgat, 2011] and write the full annihilation rate as

$$R(z) = \frac{\langle\sigma_A v\rangle}{2m_\chi^2}\bar{\rho}_{\chi 0}^2(1+z)^6\left[1+B(z,M_{\rm min})\right]\ , \quad (5.18)$$

with

$$B(z,M_{\rm min}) = 1+\frac{\Delta_c(z)}{3\bar{\rho}_\chi(z)}\int_{M_{\rm min}}^{\infty} dM\ M\frac{dn}{dM}(M,z) \times f[c(M,z)]\ , \quad (5.19)$$

where $\bar{\rho}_\chi(z)=\bar{\rho}_{\chi 0}(1+z)^3$ is the background DM density at z, and $\Delta_c(z)$, for a flat ΛCDM model, is given by [Ullio et al., 2002]

$$\Delta_c(z) = \frac{18\pi^2+82[\Omega_M(z)-1]-39[\Omega_M(z)-1]^2}{\Omega_M(z)}\ , \quad (5.20)$$

with $\Omega_M(z)$ calculated at the collapse redshift. In the case of a NFW density profile [Navarro et al., 1996, 1997] the function $f[c(M,z)]$ reads

$$f(c) = \frac{\frac{c^3}{3}\left[1-\frac{1}{(1+c^3)}\right]}{\left[\ln(1+c)-\frac{c}{1+c}\right]^2}\ . \quad (5.21)$$

Finally, following the discussion of Subsection 2.4.3, according to the Press-Schechter formalism the comoving number density distribution of dark matter halos

is given by

$$\frac{dn}{dM}(M,z) = \frac{\rho_\chi}{M}\nu f(\nu)\frac{d\ln\nu}{dM} \ , \tag{5.22}$$

where $\nu \equiv [\delta_{\rm sc}(z)/\sigma(M,z)]^2$, $\delta_{\rm sc}(z) = 1.686/D(z)$ is the critical density required for spherical collapse at z, $D(z)$ is the linear growth factor normalized to unit at $z = 0$, and the variance of the linear field is

$$\sigma^2(M,z) = D^2(z)\int_0^\infty \frac{dk}{2\pi^2}P(k)W^2(kr) \ . \tag{5.23}$$

Here $W(y) = 3(\sin y - y\cos y)/y^3$ is the top-hat window function, r is the radius of the volume enclosing the mass M, $r = (3M/4\pi\rho_m)^3$, and $P(k)$ is the matter power spectrum. Moreover, in equation (5.22) we use the Sheth-Tormen multiplicity function,

$$\nu f(\nu) = A\left[1 + (a\nu)^{-p}\right](a\nu)^{1/2}\frac{e^{-a\nu/2}}{\sqrt{2\pi}} \ . \tag{5.24}$$

with $A = 0.322$, $p = 0.3$, and $a = 0.75$ [Sheth & Tormen, 2002].

With those ingredients, the spectrum of photons at redshift z is given by

$$\begin{aligned}\frac{dN_\gamma}{dE_\gamma}(E_\gamma,z) &= \int_z^\infty \frac{dz'}{H(z')(1+z')}\left(\frac{1+z}{1+z'}\right)^3 R(z) \\ &\times \left[\frac{dN'_\gamma}{dE'_\gamma}(E'_\gamma) + \frac{dN'_{\rm IC}}{dE'_\gamma}(E'_\gamma,z')\right] \\ &\times \exp[-\tau(z,z',E'_\gamma)] \ ,\end{aligned} \tag{5.25}$$

where $\tau(z,z',E'_\gamma)$ is the optical depth describing the absorption of the photons between redshift z and z',

$$\tau(z,z',E'_\gamma) = c\int_z^{z'} dz''\frac{\alpha(E''_\gamma,z'')}{H(z'')(1+z'')} \ , \tag{5.26}$$

where $E'' = E'(1+z'')/(1+z')$.

5.2.1. Inverse Compton Scattering

When the annihilation products include electrons and positrons, they rapidly cool with the CMB radiation field, upscattering CMB photons to energies that can play a role in the evolution of the temperature and ionization state of the Universe. Following [Profumo & Jeltema, 2009; Yuan et al., 2010], the spectrum of the inverse Compton (IC) photons at a given redshift is,

$$\frac{dN_{\rm IC}}{dE}(E,z) = \int_{m_e}^{m_\chi} dE_e \frac{dn_e}{dE_e}(E_e,z) P_{\rm IC}(E,E_e,z) \ , \tag{5.27}$$

where we defined

$$\frac{dn_e}{dE_e}(E_e,z) = \frac{1}{b(E_e,z)} \int_{E_e}^{m_\chi} dE' \frac{dN_e}{dE'}(E') \ , \tag{5.28}$$

with $b(E_e,z) \approx 2.67\times10^{-17}(1+z)^4(E_e/\mathrm{GeV})^2$ GeV s^{-1} being the electron/positron energy loss rate due to the IC scattering, and $dN_e/dE'(E')$ is the electron/positron spectrum per WIMP annihilation.

Moreover, the IC power is defined as

$$P_{\rm IC}(E,E_e,z) = c \int_{1/4\gamma^2}^{1} d\epsilon \ n_\gamma(\epsilon,z) \ \sigma_{\rm KN}(E,E_e,\epsilon) \ , \tag{5.29}$$

where $n_\gamma(\epsilon,z)$ is the CMB photon spectrum at redshift z, and $\sigma_{\rm KN}(E,E_e,\epsilon)$ is the Klein-Nishima cross-section,

$$\sigma_{\rm KN}(E,E_e,\epsilon) = \frac{3\sigma_T}{4\epsilon\gamma^2} G(q,\Gamma) \ , \tag{5.30}$$

with

$$G(q,\Gamma) \equiv 2q\ln q + (1+2q)(1-q) + \frac{(\Gamma q)^2(1-q)}{2(1+\Gamma q)}, \tag{5.31}$$

$$\Gamma \equiv \frac{4\epsilon\gamma}{m_e c^2} \ , \qquad q \equiv \frac{E}{\Gamma(\gamma m_e c^2 - E)} \ , \qquad \gamma = \frac{E_e}{m_e c^2} \ , \tag{5.32}$$

Therefore, we can use the spectra of direct photons and eq. (5.27) into eq. (5.25), and with that obtain the total photon injection of the annihilation of dark matter at a given z. Examples of such spectra are shown in Figure 5.4.

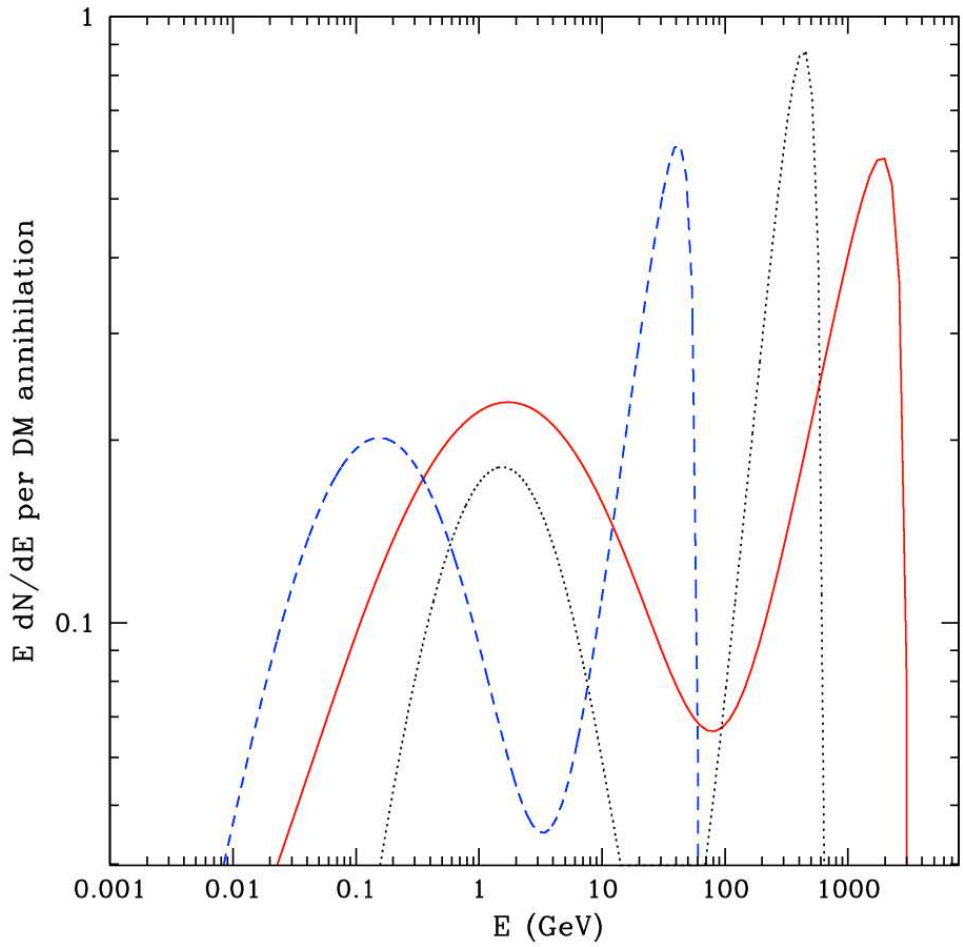

Figure 5.4: Final photon spectra including direct and inverse Compton photons as discussed in the text, for different dark matter models.

5.3. Results and discussion

With all the tools in place, we can calculate the impact of DM in the 21-cm signal. On the contrary to the previous chapters, the results discussed on this section are preliminary and somewhat brief, outlining the main technical current and expected results.

To analyze the impact of DM annihilation in the 21-cm global signal, we need first to calculate the changes in the brightness temperature given by eq. (5.1). For that, we can use eqs. (5.3) and (5.6) for the changes in the spin temperature (and IGM temperature), as well as eq. (5.9) for the changes in the ionization state of the Universe (see, for instance, Fig. 5.5).

Our goals are to check whether it is possible to distinguish between the effects of DM annihilation and the first luminous sources with the 21-cm global signal, and to learn if we could use those observation to probe some properties of the DM particles. For that, we initially discuss the signal produced by the first galaxies (following Pritchard & Loeb [2010a]), which generate an early background of Lyα and X-ray photons.

Models for the signal during the formation of the first structures exist [Furlanetto, 2006; Pritchard & Loeb, 2008], but for our purposes it will be useful to focus on physical features of the signal that are both observable and model independent. With this in mind, one can parameterize the signal using the *turning points* of the signal. Figure 5.6 shows the evolution of T_b and its frequency derivative. There are four turning points associated with [Pritchard & Loeb, 2010a]:

(0) a minimum during the dark ages where collisional coupling begins to become ineffective,

(1) a maximum at the transition from the dark ages to the Lyα pumping regime as Lyα pumping begins to be effective,

(2) an absorption minimum as X-ray heating begins to raise the signal towards emission,

(3) an emission maximum as the signal becomes saturated and starts to decrease with the cosmic expansion,

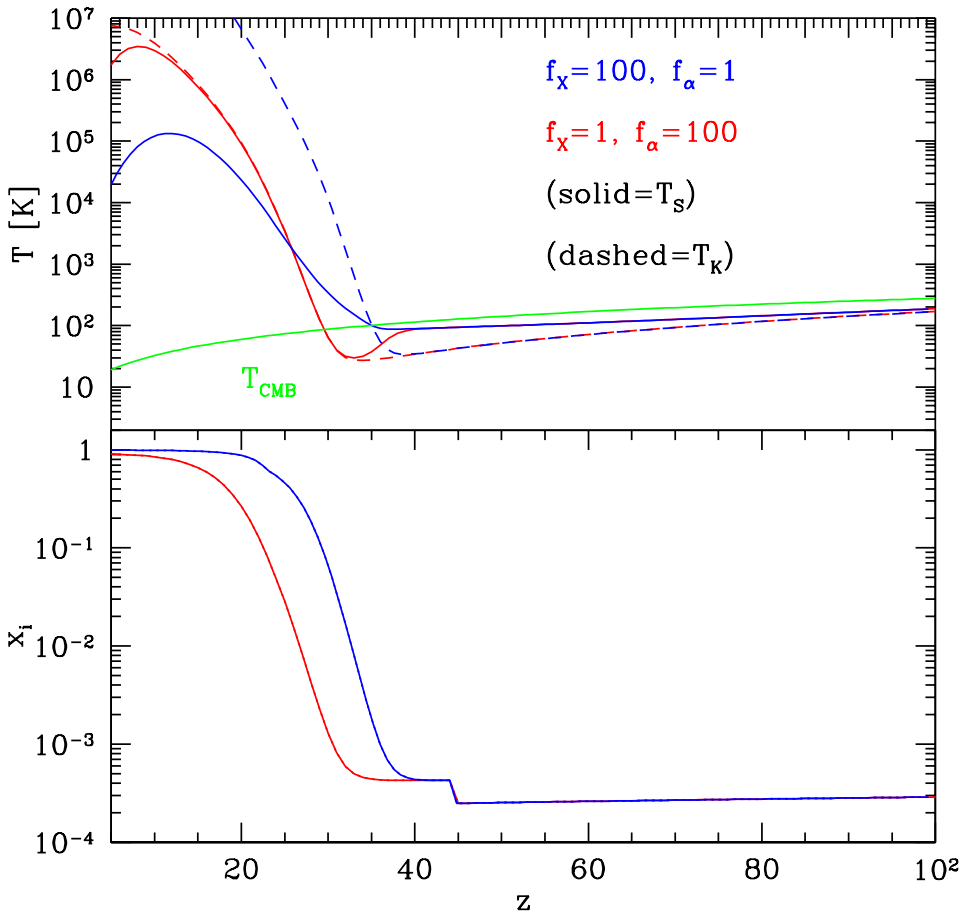

Figure 5.5: IGM temperature T_K (and the corresponding spin temperature T_S) (top panel) and ionized fraction (bottom panel) as a function of redshift for different X-ray and Lyα emissivities.

(4) the end of reionization, where asymptotically the signal goes to zero at very low and high frequencies.

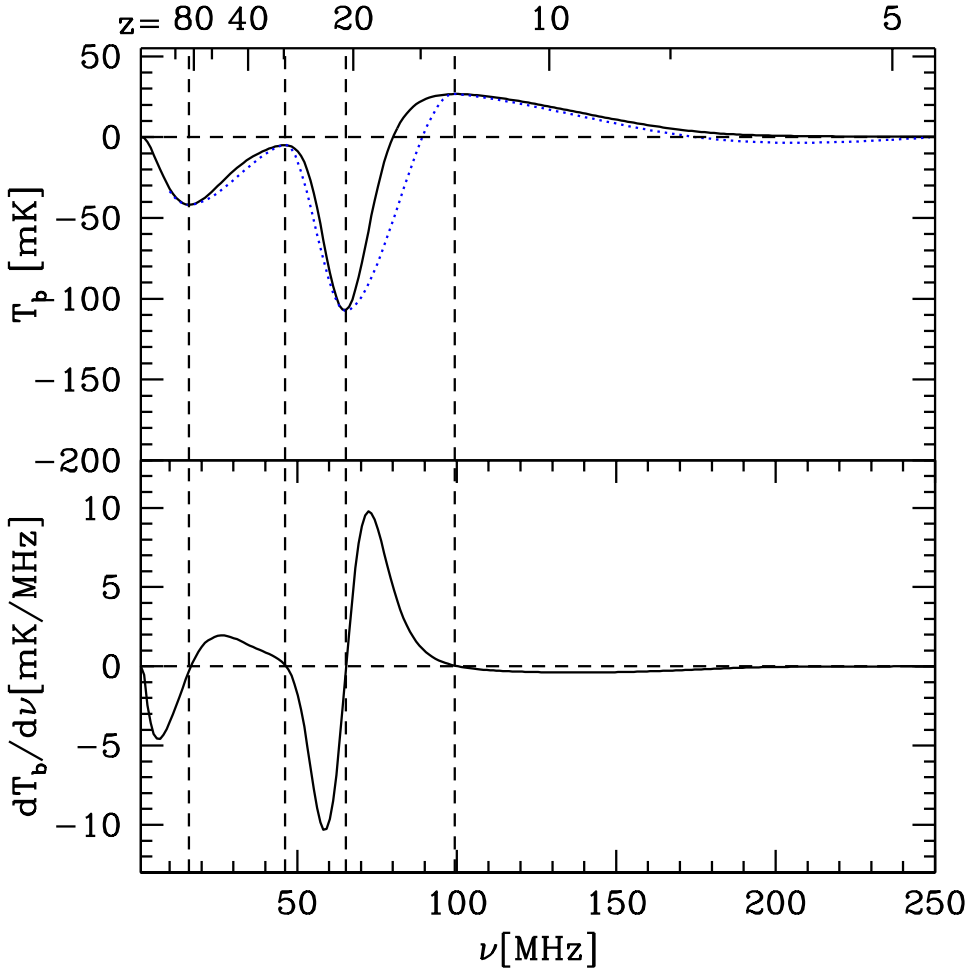

Figure 5.6: Evolution of the 21 cm global signal and its derivative. Vertical dashed lines indicate the locations of the turning points. In the top panel, we also show a cubic spline fit to the turning points (blue dotted curve) as described in the text. From Pritchard & Loeb [2010a].

A simple model for the evolution of the signal can be obtained by adopting the parameters (ν_0, T_{b0}), (ν_1, T_{b1}), (ν_2, T_{b2}), (ν_3, T_{b3}), and ν_4 for the frequency and amplitude of the turning points and the frequency at the end of reionization.

Following the conventional notation, these points are labelled as $\mathbf{x}_i = (\nu_i, T_{bi})$ (with $\mathbf{x}_4 = (\nu_4, 0\,\mathrm{mK})$). We then model the signal with a simple cubic spline

between these points with the additional condition that the derivative should be zero at the turning points (enforced by doubling the data points at the turning points and offsetting them by $\Delta\nu = \pm 1$ MHz). Moreover, for this work we generalize the procedure of Pritchard & Loeb [2010a] for allowing models with less than four turning points, as in the case of DM annihilation some models can heat the Universe early (compared to models with only stars), and suppress the trough (ν_2, T_{b2}), for instance (see Fig. 5.7).

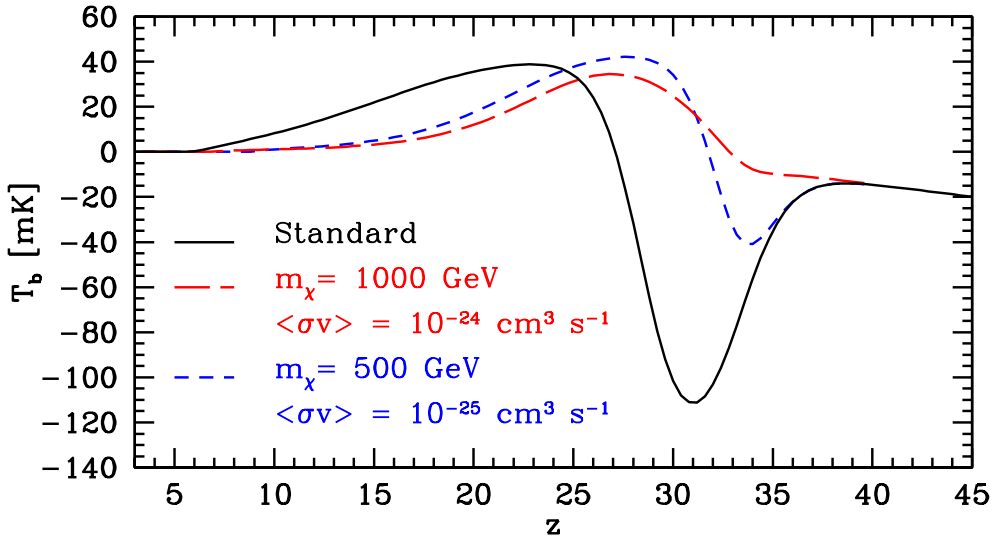

Figure 5.7: Evolution of the global 21-cm signal with redshift in different scenarios. The black (solid) curve shows the a typical evolution in a "standard" scenario in which the intergalactic medium is heated and ionized by Population III stars. The blue (short dashed) and red (long dashed) curves show two different scenarios for dark matter annihilation (parameterized by the dark matter particle mass m_χ and annihilation cross-section $\langle\sigma v\rangle$) and their impact on the global signal [França, 2012].

We adopt the same fiducial parameter set of Pritchard & Loeb [2008], assuming a star forming efficiency $f_\star = 0.1$, a Lyα emissivity expected for Population II stars $f_\alpha = 1$, and X-ray emissivity appropriate for extrapolating the locally observed X-ray-FIR correlation, $f_X = 1$. This gives turning points $\mathbf{x}_0$=(16.1 MHz, -42 mK), $\mathbf{x}_1$=(46.2 MHz, -5 mK), $\mathbf{x}_2$=(65.3 MHz, -107 mK), $\mathbf{x}_3$=(99.4 MHz, 27 mK), and $\mathbf{x}_4$=(180 MHz, 0 mK). The resulting spline fit is shown in the top panel of Fig. 5.6. The model does a good job of capturing the general features of the 21 cm signal, although there are clear differences in the detailed shape. Since global experiments are unlikely to constrain more than the sharpest features, this approach should be

adequate for our purposes.

There is considerable uncertainty in the parameters of this model, and so to gauge the likely model dependence of the turning points, we make use of the model of Pritchard & Loeb [2008]. Varying the Lyα , X-ray, and UV emissivity by two orders of magnitude on either side of their fiducial values we find the position and amplitude of the turning points to give the parameter space shown in Figure 5.8. Concerning the annihilation of DM, we are interested in models whose signal shape *can not* be reproduced by the first sources only, *i.e.*, models that lie out of the regions shown in Fig. 5.8. Those models are the ones that can be distinguished from the signal of the first stars, therefore allowing one to constrain properties of the DM models using the observed signal.

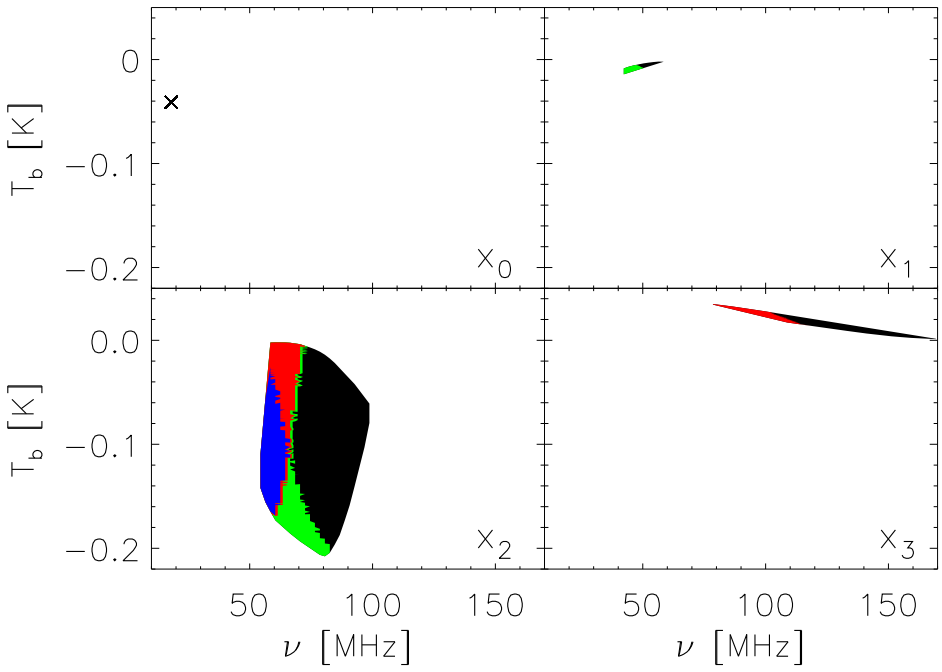

Figure 5.8: Parameter space for the frequency and brightness temperature of the four turning points of the 21 cm signal calculated by varying parameters over the range $f_X = [0.01, 100]$ and $f_\alpha = [0.01, 100]$ for fixed cosmology and star formation rate $f_* = 0.1$. Green region indicates $f_\alpha > 1$, red region indicates $f_X > 1$, blue regions indicates both $f_\alpha > 1$ and $f_X > 1$, while the black region has $f_\alpha < 1$ and $f_X < 1$. From Pritchard & Loeb [2010a].

Because in this case the cosmology is fixed, $\mathbf{x}_0$ appears as a single point. The

locations of $\mathbf{x}_1$ and $\mathbf{x}_3$ are controlled by the Lyα and X-ray emissivity respectively. Only $\mathbf{x}_2$ shows significant dependence on both Lyα and X-ray emissivity leading to a large uncertainty in its position. This is good news for observations, because even a poor measurement of the position of $\mathbf{x}_2$ is likely to rule out a wide region of parameter space. Since $\mathbf{x}_2$ is the feature with both the largest amplitude and sharpest shape, one expects that this is the best target for observation and makes experiments covering $\nu = 50 - 100\,\mathrm{MHz}$ of great interest. This is the range expected to be covered by the second generation of global experiments, like improvements of EDGES.

Lastly, we show in Fig. 5.9 a preliminary version of the parameter space $(m_\chi, \langle\sigma_A v\rangle)$ of DM models whose signal cannot be mimicked by first stars. For comparison, we show the current limits coming from CMB annihilation (WMAP limits) and the forecasted region that will be probed by Planck [Galli et al., 2011]. As one can see, we expect next generation of global signal experiments to be competitive with the most recent CMB experiments for constraining DM properties, and the exact quantitative comparison will be discussed elsewhere [França et al., 2012].

5.4. Next steps

In this chapter we have discussed the methods and some preliminary results of an analysis of the impact of DM on the 21-cm global signal. In the short-term, our plan is to scan in more details the whole parameter space of Fig. 5.9 to quantify with more precision the constraints that the next generations of 21-cm all-sky experiments can place on DM properties. Moreover, we also plan to compare those limits with other high-z probes, as for instance CMB spectral distortions, to have a more general picture of what kind of cosmological constraints we can place on the parameter space of the simpler DM models.

In the long-term, we plan to extend the current analysis for the power spectrum of the 21-cm fluctuations, since a lot of the experimental efforts is also being done in this direction. Generalizing the tools of the current work to include for instance the clumpling of DM and the relative velocity between baryons and DM particles at early redshifts will be crucial, as well as using state-of-the-art results of semi-numerical simulations like 21cmFAST [Mesinger et al., 2011]. That will allow us

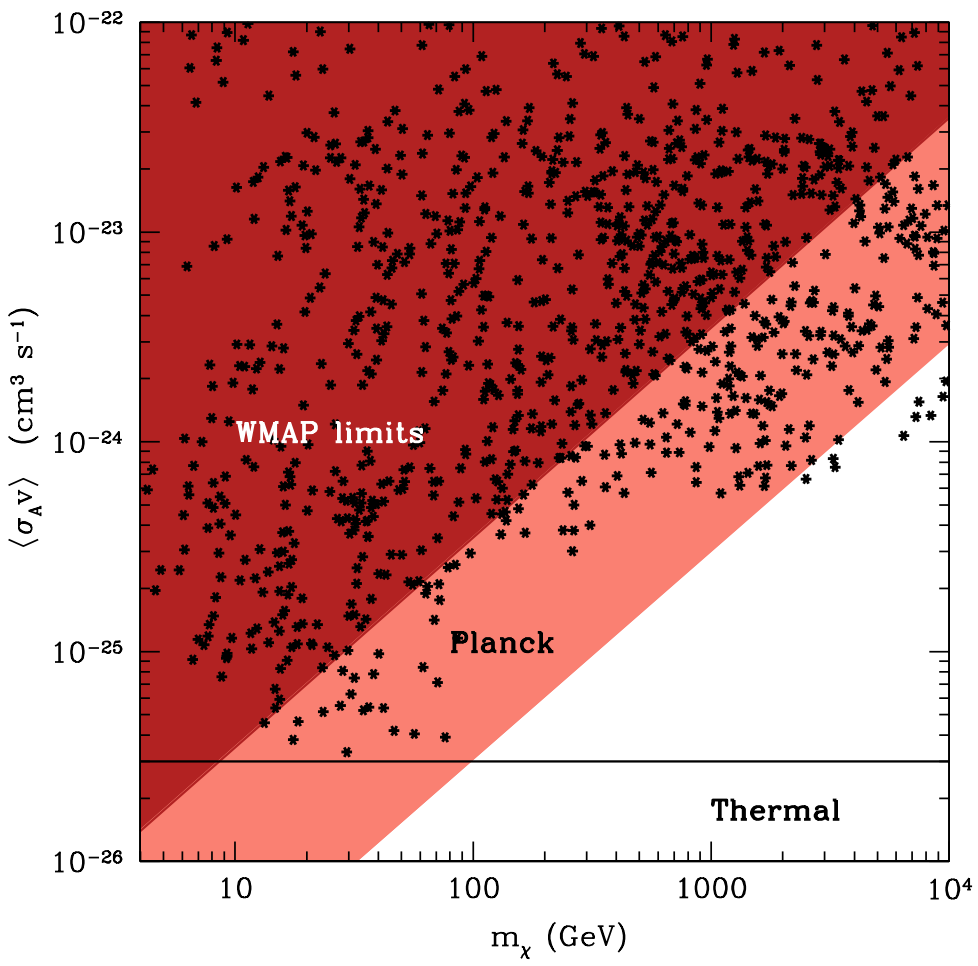

Figure 5.9: A preliminary version of the parameter space of DM models considered here. The stars refer to models whose brightness temperature can be distinguished from the first luminous sources. Also shown are the current limits from WMAP and the forecasted exclusion region for the Planck satellite discussed by Galli et al. [2011].

to have a more detailed picture of the effects of the annihilation and probably to constrain more severely the DM models under discussion.

6 Conclusions

Currently all cosmological observations seem to point towards the standard cosmological model, in which around 96% of the contribution to the current energy density of Universe has not yet been detected directly, and all we learn about them is known only because of its gravitational effects.

However, the very fact that nowadays one can speak about a cosmological standard model is a remarkable success of the scientific enterprise, as less than a century has passed since Einstein published his theory of gravitation, and Hubble discovered the expansion of the Universe.

In this thesis we discussed three components of the cosmic recipe that still have to be better understood, namely the nature of dark energy and dark matter, as well as the role played by neutrinos in the Universe.

In chapter 3 (based on Castorina et al. [2012]) we discussed the possibility that the neutrino sector store large cosmological asymmetries when compared to the baryonic one. In particular, since the origin of the matter-antimatter is still an open question in cosmology, it is important to keep an open mind for theories that predict large lepton asymmetries. In that case, constraining total and flavor neutrino asymmetries using cosmological data is a way to test and constrain some of the possible particle physics scenarios at epochs earlier than the BBN.

For that, we initially used current cosmological data to constrain not only the asymmetries, but also to understand the robustness of the cosmological parameters (such as the limits on the sum of the neutrino masses) for two different values of the mixing angle θ_{13} to account for the evidences of a nonzero value for this angle. Our results confirm the fact that at present the limits on the cosmological lepton

asymmetries are dominated by the abundance of primordial elements generated during the BBN, in particular the abundance of ^{4}He, currently the most sensitive "leptometer" available. However, future CMB experiments might be able to compete with BBN data in what concerns constraining lepton asymmetries, although BBN will always be needed in order to get information on the sign of the η's. We took as an example the future CMB mission COrE, proposed to measure with unprecedent precision the lensing of CMB anisotropies, and our results indicate that it has the potential to significantly improve over current constraints and, at the same time placing limits on the sum of the neutrino masses that are of the order of the neutrino mass differences. Finally, we notice that for the values of θ_{13} measured by the Daya Bay and RENO experiments the limits on the cosmological lepton asymmetries and on its associated effective number of neutrinos are quite strong, so that lepton asymmetries cannot increase $N_{\rm eff}$ significantly above 3.1. Under those circumstances, if the cosmological data (other than BBN) continues to push for large values of $N_{\rm eff}$, new pieces of physics such as sterile neutrinos will be necessary to explain that excess.

In chapter 4 (based on França et al. [2009]) we focused on a class of models for explaining the acceleration of the Universe, the so-called Mass-Varying Neutrino models. Our analysis is nearly model independent, for it uses a general and well-behaved parameterization for the neutrino mass, including variations in the dark energy density in a self-consistent way, and taking neutrino/dark energy perturbations into account.

Our results for the background, CMB anisotropies, and matter power spectra are in agreement with previous analyses of particular scalar field models, showing that the results obtained with this parameterization are robust and encompass the main features of the MaVaN scenarios. Moreover, a comparison with cosmological data shows that only small mass variations are allowed, and that MaVaNs scenario are mildly disfavored with respect to the constant mass case, especially when neutrinos become lighter as the Universe expands. In both cases, neutrinos can change significantly the evolution of the dark energy density, leading to instabilities in the dark energy and/or neutrino perturbations when the transfer of energy between the two components per unit of time is too large. These instabilities can only be avoided when the mass varies by a very small amount, especially in the case of a decreasing neutrino mass. Even in the case of increasing mass, constraining

better the model with forthcoming data will be a difficult task, because it mimics a massless neutrino scenario for most of the cosmological time.

One should keep in mind that our analysis assumes a constant equation of state for dark energy and a monotonic behavior for the mass variation. Even though those features are present in most of the simplest possible models, more complicated models surely can evade the constraints we obtained in our analysis. Moreover, recently it has been discussed in the literature the possibility that non-linearities stabilize the instabilities we discussed here, although one should keep in mind that the nonlinear treatment of perturbations in this models are a complicated task, and it is still not clear whether the instability problems can be cured. Finally, those constraints will improve with forthcoming tomographic data. If any of the future probes indicate a mismatch in the values of the neutrino mass at different redshifts, we could arguably have a case made for the mass-varying models.

Finally, in chapter 5 (based on França et al. [2012]) we showed some of our results for the impact of DM annihilation on the global 21-cm signal and the possibility of using this technique to obtain constraints on DM properties. This technique has the potential to significantly improve the measurements of cosmological parameters, besides being the only known observations that can have access to the period when the first stars and galaxies formed. The high redshifted 21-cm transition of the hydrogen atom has the potential to probe those epochs, opening a window in redshift that most probably will allow us to explore not only the astrophysical processes taking place during the early Universe when the first stars and galaxies form, but also the fundamental physics that might play some role at those early times.

Our work builds upon previous ones, but we use the current knowledge of the IGM and particle physics in order to obtain more reliable results: we use the state-of-the-art models for the first sources, and use DM annihilation spectra that take into account the electroweak corrections important for annihilation of particles with masses larger than the electroweak scale. Their importance arises from the fact that thanks to them the energy of the self-annihilations is distributed among several final products, including electrons and positrons. The energetic electrons and positrons redistribute their energy mostly via the inverse Compton scattering with CMB photons, which can be upscattered to energies that heat and ionize the gas, changing the 21-cm signal. It is clear that any extra radiation injection

that alters the X-ray and Lyα fraction can change significantly the brightness temperature. In the case of the modifications due to dark matter annihilation, the signal is sensitive to the mass of the dark matter particle and to the self-annihilation cross-section, as the former controls the energy that will be ultimately available for upscattering the CMB photons and the latter sets the number of annihilations at a given density. Finally, our preliminary results seem to indicate that at least in principle this technique could distinguish the contribution of the first stars from the one from DM annihilation for a reasonable region of the parameter space (m_χ vs. $\langle \sigma v \rangle$) as the DM annihilation products affect the IGM at earlier epochs than the first stars. The next step will be to understand the impact of DM not only on the sky-averaged global signal, but also on the fluctuations of this signal.

In summary, we discussed here three astroparticle physics topics that still need to be better understood. For that, more data is necessary. Thankfully, a large amount of data is expected to come from several cosmological observations that are currently running, and many others that are already funded and planned. Moreover, terrestrial experiments, like particle accelerators, are expected to help gluing together some of the pieces of the standard particle physics model or even finally discover the nature of the dark matter that dominates the dynamics of the galaxies.

One should keep in mind that history of science teachs us to expect future observations and experiments to bring not only answers to our current questions, but also to give us new interesting puzzles to play with in order to understand the Universe we live in. That is the hope we all share.

Bibliography

Abazajian, K. N., Beacom, J. F., & Bell, N. F. 2002, Phys. Rev. D, 66, 013008, [arXiv:astro-ph/0203442]

Abe, K. et al. 2011, Phys. Rev. Lett., 107, 041801, [arXiv:1106.2822]

Abe, Y. et al. 2012, Phys. Rev. Lett., 108, 131801, [arXiv:1112.6353]

Adamson, P. et al. 2011, Phys. Rev. Lett., 107, 181802, [arXiv:1108.0015]

Adelberger, E. G., Gundlach, J. H., Heckel, B. R., Hoedl, S., & Schlamminger, S. 2009, Prog. Part. Nucl. Phys., 62, 102

Adelberger, E. G., et al. 2007, Phys. Rev. Lett., 98, 131104, [arXiv:hep-ph/0611223]

Afshordi, N., Zaldarriaga, M., & Kohri, K. 2005, Phys. Rev. D, 72, 065024, [arXiv:astro-ph/0506663]

Ahn, J. K. et al. 2012, Phys. Rev. Lett., 108, 191802, [arXiv:1204.0626]

Albrecht, A., & Bernstein, G. 2007, Phys. Rev. D, 75, 103003, [arXiv:astro-ph/0608269]

Albrecht, A. et al. 2006, Report of the Dark Energy Task Force, [arXiv:astro-ph/0609591]

Albrecht, A., & Steinhardt, P. J. 1982, Phys. Rev. Lett., 48, 1220

Allison, A. C., & Dalgarno, A. 1969, Astrophys. J., 158, 423

Alpher, R. A., & Herman, R. 1948, Nature, 162, 774

——. 1950, Rev. Mod. Phys., 22, 153

——. 1988, Phys. Today, 41, 24

Alpher, R. A., Herman, R., & Gamow, G. A. 1948, Phys. Rev., 74, 1198

Amendola, L. 1999, Phys. Rev. D, 60, 043501, [arXiv:astro-ph/9904120]

——. 2000, Phys. Rev. D, 62, 043511, [arXiv:astro-ph/9908023]

——. 2003, Mon. Not. R. Astron. Soc., 342, 221, [arXiv:astro-ph/0209494]

Amendola, L., Baldi, M., & Wetterich, C. 2008, Phys. Rev. D, 78, 023015, [arXiv:0706.3064]

Amendola, L., Gasperini, M., & Piazza, F. 2006, Phys. Rev. D, 74, 127302, [arXiv:astro-ph/0610574]

Amendola, L., & Tocchini-Valentini, D. 2001, Phys. Rev. D, 64, 043509, [arXiv:astro-ph/0011243]

Amendola, L., & Tsujikawa, S. 2010, *Dark Energy: Theory and Observations* (Cambridge, UK: Cambridge University Press, 506 p.)

An, F. P. et al. 2012, Phys. Rev. Lett., 108, 171803, [arXiv:1203.1669]

Anderson, G. W., & Carroll, S. M. 1998, in COSMO-97, First International Workshop on Particle Physics and the Early Universe, ed. L. Roszkowski, 227, [arXiv:astro-ph/9711288]

Archidiacono, M., Calabrese, E., & Melchiorri, A. 2011, Phys. Rev. D, 84, 123008, [arXiv:1109.2767]

Arina, C., & Tytgat, M. H. G. 2011, JCAP, 01, 011, [arXiv:1007.2765]

Armendariz-Picon, C., Mukhanov, V., & Steinhardt, P. J. 2000, Phys. Rev. Lett., 85, 4438, [arXiv:astro-ph/0004134]

——. 2001, Phys. Rev. D, 63, 103510, [arXiv:astro-ph/0006373]

Aver, E., Olive, K. A., & Skillman, E. D. 2010, JCAP, 05, 003, [arXiv:1001.5218]

——. 2011, JCAP, 03, 043, [arXiv:1012.2385]

——. 2012, JCAP, 04, 004, [arXiv:1112.3713]

Bahcall, N. A., Ostriker, J. P., Perlmutter, S., & Steinhardt, P. J. 1999, Science, 284, 1481, [arXiv:astro-ph/9906463]

Baldi, M. 2011, [arXiv:1110.2173]

Baldi, M., Pettorino, V., Amendola, L., & Wetterich, C. 2011, Mon. Not. R. Astron. Soc., 418, 214, [arXiv:1106.2161]

Barkana, R., & Loeb, A. 2001, Phys. Rept., 349, 125, [arXiv:astro-ph/0010468]

Bartolo, N., Komatsu, E., Matarrese, S., & Riotto, A. 2004, Phys. Rept., 402, 103, [arXiv:astro-ph/0406398]

Bassett, B. A., Tsujikawa, S., & Wands, D. 2006, Rev. Mod. Phys., 78, 537, [arXiv:astro-ph/0507632]

Beacom, J. F., Bell, N. F., & Dodelson, S. 2004, Phys. Rev. Lett., 93, 121302, [arXiv:astro-ph/0404585]

Bean, R., & Doré, O. 2004, Phys. Rev. D, 69, 083503, [arXiv:astro-ph/0307100]

Bean, R., Flanagan, É. É., Laszlo, I., & Trodden, M. 2008a, Phys. Rev. D, 78, 123514, [arXiv:0808.1105]

Bean, R., Flanagan, É. É., & Trodden, M. 2008b, Phys. Rev. D, 78, 023009, [arXiv:0709.1128]

——. 2008c, New J. Physics, 10, 033006, [arXiv:0709.1124]

Benson, B. A. et al. 2011, [arXiv:1112.5435]

Bernardini, A. E., & Bertolami, O. 2008, Phys. Lett. B, 662, 97, [arXiv:0802.4449]

Bertone, G. 2010, *Particle Dark Matter: Observations, Models and Searches* (Cambridge, UK: Cambridge University Press, 762 p.)

Bertone, G., Hooper, D., & Silk, J. 2005, Phys. Rept., 405, 279, [arXiv:hep-ph/0404175]

Beutler, F. et al. 2011, Mon. Not. R. Astron. Soc., 416, 3017, [arXiv:1106.3366]

Blas, D., Lesgourgues, J., & Tram, T. 2011, JCAP, 07, 034, [arXiv:1104.2933]

Bouchet, F. et al. 2011, COrE (Cosmic Origins Explorer) A White Paper, [arXiv:1102.2181]

Bowman, J. D., & Rogers, A. E. E. 2010, Nature, 468, 796

Bowman, J. D., Rogers, A. E. E., & Hewitt, J. N. 2008, Astrophys. J., 676, 1, [arXiv:0710.2541]

Brax, P., van de Bruck, C., Davis, A.-C., Khoury, J., & Weltman, A. 2004, Phys. Rev. D, 70, 123518, [arXiv:astro-ph/0408415]

Brookfield, A. W., van de Bruck, C., Mota, D. F., & Tocchini-Valentini, D. 2006a, Phys. Rev. D, 73, 083515, [arXiv:astro-ph/0512367]

——. 2006b, Phys. Rev. Lett., 96, 061301, [arXiv:astro-ph/0503349]

Brown, M. L. et al. 2009, Astrophys. J., 705, 978, [arXiv:0906.1003]

Brush, S. G. 1992, Sci. Am., 267, 62

Burbidge, E. M., Burbidge, G. R., Fowler, W. A., & Hoyle, F. 1957, Rev. Mod. Phys., 29, 547

Caldwell, R. R., Dave, R., & Steinhardt, P. J. 1998, Phys. Rev. Lett., 80, 1582, [arXiv:astro-ph/9708069]

Caldwell, R. R., & Kamionkowski, M. 2009, Ann. Rev. Nucl. Part. Sci, 59, 397

Carroll, S. M. 2001, Living Rev. Rel., 4, 1, [arXiv:astro-ph/0004075]

Carroll, S. M., Press, W. H., & Turner, E. L. 1992, Ann. Rev. Astron. Astrophys., 30, 499

Casas, A., Cheng, W. Y., & Gelmini, G. 1999, Nucl. Phys. B, 538, 297, [arXiv:hep-ph/9709289]

Casas, J., Garcia-Bellido, J., & Quiros, M. 1992, Class. Quant. Grav., 9, 1371, [arXiv:hep-ph/9204213]

Castorina, E., França, U., Lattanzi, M., Lesgourgues, J., Mangano, G., Melchiorri, A., & Pastor, S. 2012, Phys. Rev. D, 86, 023517, [arXiv:1204.2510]

Chang, T.-C., Pen, U.-L., Peterson, J. B., & McDonald, P. 2008, Phys. Rev. Lett., 100, 091303, [arXiv:0709.3672]

Chen, X., & Kamionkowski, M. 2004, Phys. Rev. D, 70, 043502, [arXiv:astro-ph/0310473]

Chen, X., & Miralda-Escudé, J. 2004, Astrophys. J., 602, 1, [arXiv:astro-ph/0303395]

Chevallier, M., & Polarski, D. 2001, Int. J. Mod. Phys. D, 10, 213, [arXiv:gr-qc/0009008]

Chuzhoy, L. 2008, Astrophys. J. Lett., 679, L65, [arXiv:0710.1856]

Chuzhoy, L., & Shapiro, P. R. 2007, Astrophys. J., 655, 843, arXiv:astro-ph/0604483

Ciafaloni, P., Cirelli, M., Comelli, D., De Simone, A., Riotto, A., & Urbano, A. 2011, JCAP, 06, 18, [arXiv:1104.2996]

Cirelli, M. et al. 2011, JCAP, 03, 51, [arXiv:1012.4515]

Cirelli, M., Iocco, F., & Panci, P. 2009, JCAP, 10, 009, [arXiv:0907.0719]

Clifton, T., Clarkson, C., & Bull, P. 2012, Phys. Rev. Lett., 109, 051303, [arXiv:1111.3794]

Cole, S. et al. 2005, Mon. Not. R. Astron. Soc., 362, 505, [arXiv:astro-ph/0501174]

Comelli, D., Pietroni, M., & Riotto, A. 2003, Phys. Lett. B, 571, 115, [arXiv:hep-ph/0302080]

Conley, A. et al. 2011, Astrophys. J. Suppl. Ser., 192, 1, [arXiv:1104.1443]

Copeland, E. J., Lee, S.-J., Lidsey, J. E., & Mizuno, S. 2005, Phys. Rev. D, 71, 023526, [arXiv:astro-ph/0410110]

Copeland, E. J., Liddle, A. R., & Wands, D. 1998, Phys. Rev. D, 57, 4686, [arXiv:gr-qc/9711068]

Copeland, E. J., Nunes, N. J., & Pospelov, M. 2004, Phys. Rev. D, 69, 023501, [arXiv:hep-ph/0307299]

Copeland, E. J., Sami, M., & Tsujikawa, S. 2006, Int. J. Mod. Phys. D, 15, 1753, [arXiv:hep-th/0603057]

Corasaniti, P. S., & Copeland, E. J. 2003, Phys. Rev. D, 67, 063521, [arXiv:astro-ph/0205544]

Corasaniti, P. S., Kunz, M., Parkinson, D., Copeland, E. J., & Bassett, B. A. 2004, Phys. Rev. D, 70, 083006, [arXiv:astro-ph/0406608]

Cumberbatch, D. T., Lattanzi, M., & Silk, J. 2010, Phys. Rev. D, 82, 103508, [arXiv:0808.0881]

Cunha, C., Huterer, D., & Frieman, J. A. 2009, Phys. Rev. D, 80, 063532, [arXiv:0904.1589]

Das, S., Corasaniti, P. S., & Khoury, J. 2006, Phys. Rev. D, 73, 083509, [arXiv:astro-ph/0510628]

De Bernardis, F., Pagano, L., Serra, P., Melchiorri, A., & Cooray, A. 2008, JCAP, 06, 013, [arXiv:0804.1925]

Dent, T., Stern, S., & Wetterich, C. 2009, JCAP, 01, 038, [arXiv:0809.4628]

di Valentino, E., Lattanzi, M., Mangano, G., Melchiorri, A., & Serpico, P. 2012, Phys. Rev. D, 85, 043511, [arXiv:1111.3810]

Dicke, R. H., Peebles, P. J. E., Roll, P. G., & Wilkinson, D. T. 1965, Astrophys. J., 142, 414

Dicus, D. A., Kolb, E. W., Gleeson, A., Sudarshan, E., Teplitz, V. L., et al. 1982, Phys. Rev. D, 26, 2694

Dodelson, S. 2003, *Modern cosmology* (Amsterdan: Academic Press, 440 p.)

Dodelson, S., Kinney, W. H., & Kolb, E. W. 1997, Phys. Rev. D, 56, 3207, [arXiv:astro-ph/9702166]

Dodelson, S., & Turner, M. S. 1992, Phys. Rev. D, 46, 3372

Dolgov, A. D., Hansen, S. H., Pastor, S., Petcov, S. T., Raffelt, G. G., & Semikoz, D. V. 2002, Nucl. Phys. B, 632, 363, [arXiv:hep-ph/0201287]

Doran, M., & Jäckel, J. 2002, Phys. Rev. D, 66, 043519, [arXiv:astro-ph/0203018]

Douspis, M., Zolnierowski, Y., Blanchard, A., & Riazuelo, A. 2008, Astron. & Astrophys., 488, 47

Draine, B. T. 2011, *Physics of the Interstellar and Intergalactic Medium* (Princeton, NJ: Princeton University Press, 540 p.)

Dunkley, J. et al. 2011, Astrophys. J., 739, 52, [arXiv:1009.0866]

——. 2009, Astrophys. J. Suppl. Ser., 180, 306, [arXiv:0803.0586]

Dvorkin, C., & Hu, W. 2010, Phys. Rev. D, 82, 043513, [arXiv:1007.0215]

Eggers Bjælde, O., Brookfield, A. W., van de Bruck, C., Hannestad, S., Mota, D. F., Schrempp, L., & Tocchini-Valentini, D. 2008, JCAP, 01, 026, [arXiv:0705.2018]

Ellis, J., Kalara, S., Olive, K. A., & Wetterich, C. 1989, Phys. Lett. B, 228, 264

Fan, X. 2008, in American Institute of Physics Conference Series, Vol. 990, First Stars III, ed. B. W. O'Shea & A. Heger, 437–441

Fan, X., Carilli, C. L., & Keating, B. 2006, Ann. Rev. Astron. Astrophys., 44, 415, [arXiv:astro-ph/0602375]

Fardon, R., Nelson, A. E., & Weiner, N. 2004, JCAP, 10, 005, [arXiv:astro-ph/0309800]

Farrar, G. R., & Peebles, P. J. E. 2004, Astrophys. J., 604, 1, [arXiv:astro-ph/0307316]

Ferreira, P. G., & Joyce, M. 1998, Phys. Rev. D, 58, 023503, [arXiv:astro-ph/9711102]

Field, G. B. 1959, Astrophys. J., 129, 536

Fields, B. D. 2011, Ann. Rev. Nucl. Part. Sci, 61, 47, [arXiv:1203.3551]

Fields, B. D., & Sarkar, S. 2012, *in* J. Beringer *et al.*(PDG), Phys. Rev. D, 86, 010001, `http://pdg.lbl.gov`, [arXiv:0806.2649]

Finkbeiner, D. P., Padmanabhan, N., & Weiner, N. 2008, Phys. Rev. D, 78, 063530, [arXiv:0805.3531]

Fixsen, D. J., Cheng, E. S., Gales, J. M., Mather, J. C., Shafer, R. A., & Wright, E. L. 1996, Astrophys. J., 473, 576, [arXiv:astro-ph/9605054]

Fogli, G. L., Lisi, E., Marrone, A., Montanino, D., Palazzo, A., & Rotunno, A. M. 2012, Phys. Rev. D, 86, 013012, [arXiv:1205.5254]

Fogli, G. L., Lisi, E., Marrone, A., Palazzo, A., & Rotunno, A. M. 2011, Phys. Rev. D, 84, 053007, [arXiv:1106.6028]

Forero, D. V., Tórtola, M., & Valle, J. W. F. 2012, [arXiv:1205.4018]

França, U. 2006, Phys. Lett. B, 641, 351, [arXiv:astro-ph/0509177]

——. 2012, AIP Conf. Proc., 1420, 102

França, U., Lattanzi, M., Lesgourgues, J., & Pastor, S. 2009, Phys. Rev. D, 80, 083506, [arXiv:0908.0534]

França, U., Pritchard, J. R., & Loeb, A. 2012, to be submitted

França, U., & Rosenfeld, R. 2002, JHEP, 10, 15, [arXiv:astro-ph/0206194]

——. 2004, Phys. Rev. D, 69, 063517, [arXiv:astro-ph/0308149]

Freedman, W. L. et al. 2001, Astrophys. J., 553, 47, [arXiv:astro-ph/0012376]

Freedman, W. L., & Turner, M. S. 2003, Rev. Mod. Phys., 75, 1433, [arXiv:astro-ph/0308418]

Frieman, J., Turner, M., & Huterer, D. 2008, Ann. Rev. Astron. Astrophys., 46, 385, [arXiv:0803.0982]

Frieman, J. A., Hill, C. T., Stebbins, A., & Waga, I. 1995, Phys. Rev. Lett., 75, 2077, [arXiv:astro-ph/9505060]

Furlanetto, S. R. 2006, Mon. Not. R. Astron. Soc., 371, 867, [arXiv:astro-ph/0604040]

Furlanetto, S. R., & Furlanetto, M. R. 2007, Mon. Not. R. Astron. Soc., 374, 547, [arXiv:astro-ph/0608067]

Furlanetto, S. R., Oh, S. P., & Briggs, F. H. 2006a, Phys. Rept., 433, 181, [arXiv:astro-ph/0608032]

Furlanetto, S. R., Oh, S. P., & Pierpaoli, E. 2006b, Phys. Rev. D, 74, 103502, [arXiv:astro-ph/0608385]

Furlanetto, S. R., & Pritchard, J. R. 2006, Mon. Not. R. Astron. Soc., 372, 1093, [arXiv:astro-ph/0605680]

Galli, S., Iocco, F., Bertone, G., & Melchiorri, A. 2011, Phys. Rev. D, 84, 027302, 1106.1528

Gamow, G. 1948a, Nature, 162, 680

——. 1948b, Phys. Rev., 74, 505

——. 1970, *My world line: An informal autobiography* (New York, NY: Viking Press, 178 p.)

Gavela, M. B., Hernández, D., Lopez Honorez, L., Mena, O., & Rigolin, S. 2009, JCAP, 07, 034, [arXiv:0901.1611]

Gelmini, G. B. 2005, Phys. Scripta T, 121, 131, [arXiv:hep-ph/0412305]

Gilks, W., Richardson, S., & Spiegelhalter, D. 1996, *Markov Chain Monte Carlo in Practice* (London, UK: Chapman & Hall / CRC, 486 p.)

Giusarma, E., Corsi, M., Archidiacono, M., de Putter, R., Melchiorri, A., Mena, O., & Pandolfi, S. 2011, Phys. Rev. D, 83, 115023, [arXiv:1102.4774]

Gordon, C., & Malik, K. A. 2004, Phys. Rev. D, 69, 063508, [arXiv:astro-ph/0311102]

Gu, P., Wang, X., & Zhang, X. 2003, Phys. Rev. D, 68, 087301, [arXiv:hep-ph/0307148]

Gunn, J. E., & Peterson, B. A. 1965, Astrophys. J., 142, 1633

Guth, A. H. 1981, Phys. Rev. D, 23, 347

Gutperle, M., Kallosh, R., & Linde, A. D. 2003, JCAP, 07, 001, [arXiv:hep-th/0304225]

Hamann, J., Hannestad, S., Raffelt, G. G., & Wong, Y. Y. Y. 2011, JCAP, 09, 034, [arXiv:1108.4136]

Hamann, J., Lesgourgues, J., & Mangano, G. 2008, JCAP, 03, 004, [arXiv:0712.2826]

Hannestad, S. 2005, Phys. Rev. D, 71, 103519, [arXiv:astro-ph/0504017]

——. 2006, Ann. Rev. Nucl. Part. Sci, 56, 137, [arXiv:hep-ph/0602058]

Hansen, S. H., Mangano, G., Melchiorri, A., Miele, G., & Pisanti, O. 2002, Phys. Rev. D, 65, 023511, [arXiv:astro-ph/0105385]

Hirata, C. M. 2006, Mon. Not. R. Astron. Soc., 367, 259, [arXiv:astro-ph/0507102]

Hlozek, R. et al. 2012, Astrophys. J., 749, 90, [arXiv:1105.4887]

Hoffman, M. B. 2003, PhD thesis, The University of Chicago, [arXiv:astro-ph/0307350]

Hu, W. 1998, Astrophys. J., 506, 485, [arXiv:astro-ph/9801234]

Hubble, E. 1929, Proc. Natl. Acad. Sci. USA, 15, 168

Huey, G., & Wandelt, B. D. 2006, Phys. Rev. D, 74, 023519, [arXiv:astro-ph/0407196]

Huterer, D. 2002, Phys. Rev. D, 65, 063001, [arXiv:astro-ph/0106399]

Ichiki, K., & Keum, Y.-Y. 2008, JCAP, 06, 005, [arXiv:0705.2134]

Iocco, F., Mangano, G., Miele, G., Pisanti, O., & Serpico, P. D. 2009, Phys. Rept., 472, 1, [arXiv:0809.0631]

Izotov, Y. I., & Thuan, T. X. 2010, Astrophys. J. Lett., 710, L67, [arXiv:1001.4440]

Jimenez, R., Verde, L., Treu, T., & Stern, D. 2003, Astrophys. J., 593, 622, [arXiv:astro-ph/0302560]

Jungman, G., Kamionkowski, M., & Griest, K. 1996, Phys. Rept., 267, 195, [arXiv:hep-ph/9506380]

Kallosh, R., Linde, A., Prokushkin, S., & Shmakova, M. 2002, Phys. Rev. D, 66, 123503, [arXiv:hep-th/0208156]

Kang, H.-S., & Steigman, G. 1992, Nucl. Phys. B, 372, 494

Kapner, D. J., Cook, T. S., Adelberger, E. G., Gundlach, J. H., Heckel, B. R., Hoyle, C. D., & Swanson, H. E. 2007, Phys. Rev. Lett., 98, 021101, [arXiv:hep-ph/0611184]

Karttunen, H., Kroeger, P., Oja, H., Poutanen, M., & Donner, K. J. 2007, *Fundamental astronomy, 5th ed.* (Berlin: Springer, 510 p.)

Keisler, R. et al. 2011, Astrophys. J., 743, 28, [arXiv:1105.3182]

Kessler, R. et al. 2009, Astrophys. J. Suppl. Ser., 185, 32, [arXiv:0908.4274]

Khoury, J., & Weltman, A. 2004a, Phys. Rev. D, 69, 044026, [arXiv:astro-ph/0309411]

——. 2004b, Phys. Rev. Lett., 93, 171104, [arXiv:astro-ph/0309300]

Kitching, T. D., Heavens, A. F., Verde, L., Serra, P., & Melchiorri, A. 2008, Phys. Rev. D, 77, 103008, [arXiv:0801.4565]

Kneller, J. P., & Strigari, L. E. 2003, Phys. Rev. D, 68, 083517, [arXiv:astro-ph/0302167]

Koivisto, T., & Mota, D. F. 2006, Phys. Rev. D, 73, 083502, [arXiv:astro-ph/0512135]

Kolb, E. W., & Turner, M. S. 1990, *The Early Universe* (Front. Phys., Vol. 69, Reading, MA: Addison-Wesley, 547 p.)

Komatsu, E. et al. 2009, Astrophys. J. Suppl. Ser., 180, 330, [arXiv:0803.0547]

——. 2011, Astrophys. J. Suppl. Ser., 192, 18, [arXiv:1001.4538]

Kowalski, M. et al. 2008, Astrophys. J., 686, 749, [arXiv:0804.4142]

Krauss, L. M. 2004, Astrophys. J., 604, 481, [arXiv:astro-ph/0212369]

Krauss, L. M., & Chaboyer, B. 2003, Science, 299, 65

Krauss, L. M., & Turner, M. S. 1995, Gen. Relativ. Gravit., 27, 1137, [arXiv:astro-ph/9504003]

——. 1999, Gen. Relativ. Gravit., 31, 1453, [arXiv:astro-ph/9904020]

Kunz, M., Corasaniti, P.-S., Parkinson, D., & Copeland, E. J. 2004, Phys. Rev. D, 70, 041301, [arXiv:astro-ph/0307346]

Kuo, C. L. et al. 2004, Astrophys. J., 600, 32, [arXiv:astro-ph/0212289]

La Vacca, G., Kristiansen, J. R., Colombo, L. P. L., Mainini, R., & Bonometto, S. A. 2009, JCAP, 04, 007, [arXiv:0902.2711]

La Vacca, G., & Mota, D. F. 2012, ArXiv e-prints, 1205.6059

Laine, M., & Shaposhnikov, M. 2008, JCAP, 06, 031, [arXiv:0804.4543]

Lattanzi, M., Ruffini, R., & Vereshchagin, G. V. 2005, Phys. Rev. D, 72, 063003, [arXiv:astro-ph/0509079]

Lattanzi, M., & Valle, J. W. F. 2007, Phys. Rev. Lett., 99, 121301, [arXiv:0705.2406]

Lesgourgues, J., Mangano, G., Miele, G., & Pastor, S. 2012, *Neutrino Cosmology*, (Cambridge, UK: Cambridge University Press, *in press*)

Lesgourgues, J., & Pastor, S. 1999, Phys. Rev. D, 60, 103521, [arXiv:hep-ph/9904411]

——. 2006, Phys. Rept., 429, 307, [arXiv:astro-ph/0603494]

Lesgourgues, J., Perotto, L., Pastor, S., & Piat, M. 2006, Phys. Rev., D73, 045021, [arXiv:astro-ph/0511735]

Lesgourgues, J., Valkenburg, W., & Gaztañaga, E. 2008, Phys. Rev. D, 77, 063505, [arXiv:0710.5525]

Lewis, A., & Bridle, S. 2002, Phys. Rev. D, 66, 103511, [arXiv:astro-ph/0205436]

Lewis, A., Challinor, A., & Lasenby, A. 2000, Astrophys. J., 538, 473, [arXiv:astro-ph/9911177]

Liddle, A. R., & Scherrer, R. J. 1999, Phys. Rev. D, 59, 023509, [arXiv:astro-ph/9809272]

Lidsey, J. E., Liddle, A. R., Kolb, E. W., Copeland, E. J., Barreiro, T., & Abney, M. 1997, Rev. Mod. Phys., 69, 373, [arXiv:astro-ph/9508078]

Linde, A. D. 1982, Phys. Lett. B, 108, 389

——. 1983, Phys. Lett. B, 129, 177

Linden, S., & Virey, J.-M. 2008, Phys. Rev. D, 78, 023526, [arXiv:0804.0389]

Linder, E. V. 2003, Phys. Rev. Lett., 90, 091301, [arXiv:astro-ph/0208512]

——. 2008a, Rept. Prog. Phys., 71, 056901, [arXiv:0801.2968]

——. 2008b, Gen. Relativ. Gravit., 40, 329, [arXiv:0704.2064]

Loeb, A. 2010, *How Did the First Stars and Galaxies Form?* (Princeton, NJ: Princeton University Press, 216 p.)

Loeb, A., & Furlanetto, S. R. 2012, *The First Galaxies* (Princeton, NJ: Princeton University Press, *in press*)

Loeb, A., & Wyithe, J. S. B. 2008, Phys. Rev. Lett., 100, 161301, [arXiv:0801.1677]

Loeb, A., & Zaldarriaga, M. 2004, Phys. Rev. Lett., 92, 211301, [arXiv:astro-ph/0312134]

Lyth, D. H., & Liddle, A. R. 2009, *The Primordial Density Perturbation* (Cambridge, UK: Cambridge University Press, 497 p.)

Lyth, D. H., Ungarelli, C., & Wands, D. 2003, Phys. Rev. D, 67, 023503, [arXiv:astro-ph/0208055]

Lyth, D. H. D. H., & Riotto, A. A. 1999, Phys. Rept., 314, 1, [arXiv:hep-ph/9807278]

Ma, C.-P., & Bertschinger, E. 1995, Astrophys. J., 455, 7, [arXiv:astro-ph/9506072]

Majerotto, E., Väliviita, J., & Maartens, R. 2010, Mon. Not. R. Astron. Soc., 402, 2344, [arXiv:0907.4981]

Mangano, G., Miele, G., Pastor, S., & Peloso, M. 2002, Phys. Lett. B, 534, 8, [arXiv:astro-ph/0111408]

Mangano, G., Miele, G., Pastor, S., Pinto, T., Pisanti, O., et al. 2005, Nucl. Phys. B, 729, 221, [arXiv:hep-ph/0506164]

Mangano, G., Miele, G., Pastor, S., Pisanti, O., & Sarikas, S. 2011, JCAP, 03, 035, [arXiv:1011.0916]

——. 2012, Phys. Lett. B, 708, 1, [arXiv:1110.4335]

Mangano, G., Miele, G., & Pettorino, V. 2003, Mod. Phys. Lett. A, 18, 831, [arXiv:astro-ph/0212518]

Mangano, G., & Serpico, P. D. 2011, Phys. Lett. B, 701, 296, [arXiv:1103.1261]

Mao, Y., Tegmark, M., McQuinn, M., Zaldarriaga, M., & Zahn, O. 2008, Phys. Rev. D, 78, 023529, [arXiv:0802.1710]

March-Russell, J., Riotto, A., & Murayama, H. 1999, JHEP, 11, 015, [arXiv:hep-ph/9908396]

Masui, K. W., McDonald, P., & Pen, U.-L. 2010, Phys. Rev. D, 81, 103527, [arXiv:1001.4811]

Mather, J. C. et al. 1994, Astrophys. J., 420, 439

McDonald, J. 2000, Phys. Rev. Lett., 84, 4798, [arXiv:hep-ph/9908300]

McKellar, B. H. J., & Thomson, M. J. 1994, Phys. Rev. D, 49, 2710

Meiksin, A. A. 2009, Rev. Mod. Phys., 81, 1405, [arXiv:0711.3358]

Mesinger, A., Furlanetto, S., & Cen, R. 2011, Mon. Not. R. Astron. Soc., 411, 955, 1003.3878

Michney, R. J., & Caldwell, R. R. 2007, JCAP, 01, 014, [arXiv:astro-ph/0608303]

Morales, M. F., & Wyithe, J. S. B. 2010, Ann. Rev. Astron. Astrophys., 48, 127, [arXiv:0910.3010]

Mortonson, M. J., Peiris, H. V., & Easther, R. 2011, Phys. Rev. D, 83, 043505, [arXiv:1007.4205]

Mota, D. F., Kristiansen, J. R., Koivisto, T., & Groeneboom, N. E. 2007, Mon. Not. R. Astron. Soc., 382, 793, [arXiv:0708.0830]

Mota, D. F., & Shaw, D. J. 2006, Phys. Rev. Lett., 97, 151102, [arXiv:hep-ph/0606204]

——. 2007, Phys. Rev., D75, 063501, [arXiv:hep-ph/0608078]

Natarajan, A., & Schwarz, D. J. 2009, Phys. Rev. D, 80, 043529, [arXiv:0903.4485]

Navarro, J. F., Frenk, C. S., & White, S. D. M. 1996, Astrophys. J., 462, 563, [arXiv:astro-ph/9508025]

——. 1997, Astrophys. J., 490, 493, [arXiv:astro-ph/9611107]

Olive, K. A., Pospelov, M., Qian, Y.-Z., Coc, A., Cassé, M., & Vangioni-Flam, E. 2002, Phys. Rev. D, 66, 045022, [arXiv:hep-ph/0205269]

Osterbrock, D. E., & Ferland, G. J. 2006, *Astrophysics of gaseous nebulae And active galactic nuclei* (2nd ed., Sausalito, CA: University Science Books, 650 p.)

Ostriker, J. P., & Steinhardt, P. J. 1995, Nature, 377, 600

Padmanabhan, N., Xu, X., Eisenstein, D. J., Scalzo, R., Cuesta, A. J., Mehta, K. T., & Kazin, E. 2012, [arXiv:1202.0090]

Padmanabhan, T. 1993, *Structure Formation in the Universe* (Cambridge, UK: Cambridge University Press, 500 p.)

Parsons, A. R. et al. 2010, Astron. J., 139, 1468

Pastor, S., Pinto, T., & Raffelt, G. G. 2009, Phys. Rev. Lett., 102, 241302, [arXiv:0808.3137]

Pearson, T. J. et al. 2003, Astrophys. J., 591, 556, [arXiv:astro-ph/0205388]

Peccei, R. D. 2005, Phys. Rev. D, 71, 023527, [arXiv:hep-ph/0411137]

Peebles, P. J. E. 1992, *Quantum mechanics* (Princeton, N.J.: Princeton University Press, 444 p.)

Peebles, P. J. E., Page, L. A., & Partridge, R. B. 2009, *Finding the Big Bang* (Cambridge, UK: Cambridge University Press, 596 p.)

Peebles, P. J. E., & Ratra, B. 1988, Astrophys. J. Lett., 325, L17

Peebles, P. J. E., & Ratra, B. 2003, Rev. Mod. Phys., 75, 559, [arXiv:astro-ph/0207347]

Penzias, A. A., & Wilson, R. W. 1965, Astrophys. J., 142, 419

Perlmutter, S. et al. 1999, Astrophys. J., 517, 565, [arXiv:astro-ph/9812133]

Perotto, L., Lesgourgues, J., Hannestad, S., Tu, H., & Y Y Wong, Y. 2006, JCAP, 10, 013, [arXiv:astro-ph/0606227]

Pettini, M., & Cooke, R. 2012, [arXiv:1205.3785]

Pettorino, V., Wintergerst, N., Amendola, L., & Wetterich, C. 2010, Phys. Rev. D, 82, 123001, [arXiv:1009.2461]

Popa, L. A., & Vasile, A. 2008, JCAP, 06, 028, [arXiv:0804.2971]

Press, W. H., & Schechter, P. 1974, Astrophys. J., 187, 425

Pritchard, J. R., & Furlanetto, S. R. 2007, Mon. Not. Roy. Astron. Soc., 376, 1680, [arXiv:astro-ph/0607234]

Pritchard, J. R., Furlanetto, S. R., & Kamionkowski, M. 2007, Mon. Not. R. Astron. Soc., 374, 159, [arXiv:astro-ph/0604358]

Pritchard, J. R., & Loeb, A. 2008, Phys. Rev. D, 78, 103511, [arXiv:0802.2102]

——. 2010a, Phys. Rev. D, 82, 023006, [arXiv:1005.4057]

——. 2010b, Nature, 468, 772

——. 2012, Rept. Prog. Phys., 75, 086901, [arXiv:1109.6012]

Pritchard, J. R., & Pierpaoli, E. 2008, Phys. Rev. D, 78, 065009, [arXiv:0805.1920]

Profumo, S., & Jeltema, T. E. 2009, JCAP, 07, 020, [arXiv:0906.0001]

Quartin, M., Calvão, M. O., Jorás, S. E., Reis, R. R. R., & Waga, I. 2008, JCAP, 05, 007, [arXiv:0802.0546]

Ratra, B., & Peebles, P. J. E. 1988, Phys. Rev. D, 37, 3406

Ratra, B., & Vogeley, M. S. 2008, Publ. Astron. Soc. Pac., 120, 235, [arXiv:0706.1565]

Reichardt, C. L. et al. 2009, Astrophys. J., 694, 1200, [arXiv:0801.1491]

Reid, B. A. et al. 2010, Mon. Not. R. Astron. Soc., 404, 60, [arXiv:0907.1659]

Riess, A. G. et al. 1998, Astron. J., 116, arXiv:1009, [arXiv:astro-ph/9805201]

——. 2011, Astrophys. J., 730, 119, [arXiv:1103.2976]

——. 2009, Astrophys. J., 699, 539, [arXiv:0905.0695]

Robertson, B. E., Ellis, R. S., Dunlop, J. S., McLure, R. J., & Stark, D. P. 2010, Nature, 468, 49, [arXiv:1011.0727]

Rohlfs, K., Wilson, T. L., & Hüttemeister, S. 2009, *Tools of Radio Astronomy* (5th ed., Berlin: Springer, 536 p.)

Rosenfeld, R. 2005, Phys. Lett. B, 624, 158, [arXiv:astro-ph/0504121]

——. 2007, Phys. Rev. D, 75, 083509, [arXiv:astro-ph/0701213]

Sanchez, A. G., Scoccola, C., Ross, A., Percival, W., Manera, M., et al. 2012, [arXiv:1203.6616]

Schwarz, D. J., & Stuke, M. 2009, JCAP, 11, 025, [arXiv:0906.3434]

Schwetz, T., Tórtola, M., & Valle, J. W. F. 2011, New J. Phys., 13, 063004, [arXiv:1103.0734]

Scott, P. F. et al. 2003, Mon. Not. R. Astron. Soc., 341, 1076, [arXiv:astro-ph/0205380]

Seljak, U., Slosar, A., & McDonald, P. 2006, JCAP, 10, 014, [arXiv:astro-ph/0604335]

Seljak, U., & Zaldarriaga, M. 1996, Astrophys. J., 469, 437, [arXiv:astro-ph/9603033]

Semikoz, V. B., Sokoloff, D. D., & Valle, J. W. F. 2009, Phys. Rev. D, 80, 083510, [arXiv:0905.3365]

Sendra, I., & Smith, T. L. 2012, Phys. Rev. D, 85, 123002, [arXiv:1203.4232]

Seo, H.-J., & Eisenstein, D. J. 2003, Astrophys. J., 598, 720, [arXiv:astro-ph/0307460]

——. 2007, Astrophys. J., 665, 14, [arXiv:astro-ph/0701079]

Serpico, P. D., & Raffelt, G. G. 2005, Phys. Rev. D, 71, 127301, [arXiv:astro-ph/0506162]

Shapiro, C., & Turner, M. S. 2006, Astrophys.J., 649, 563, [astro-ph/0512586]

Sheth, R. K., & Tormen, G. 1999, Mon. Not. R. Astron. Soc., 308, 119, [arXiv:astro-ph/9901122]

——. 2002, Mon. Not. R. Astron. Soc., 329, 61, [arXiv:astro-ph/0105113]

Shi, X., & Fuller, G. M. 1999, Phys. Rev. Lett., 83, 3120, [arXiv:astro-ph/9904041]

Shiraishi, M., Ichikawa, K., Ichiki, K., Sugiyama, N., & Yamaguchi, M. 2009, JCAP, 07, 005, [arXiv:0904.4396]

Shull, J. M., & van Steenberg, M. E. 1985, Astrophys. J., 298, 268

Sigl, G., & Raffelt, G. 1993, Nuclear Physics B, 406, 423

Slatyer, T. R., Padmanabhan, N., & Finkbeiner, D. P. 2009, Phys. Rev. D, 80, 043526, [arXiv:0906.1197]

Smoot, G. F. et al. 1992, Astrophys. J. Lett., 396, L1

Springel, V., Frenk, C. S., & White, S. D. M. 2006, Nature, 440, 1137, [arXiv:astro-ph/0604561]

Steinhardt, P. J., Wang, L., & Zlatev, I. 1999, Phys. Rev. D, 59, 123504, [arXiv:astro-ph/9812313]

Stiavelli, M. 2009, *From First Light to Reionization: The End of the Dark Ages* (New York, NJ: Wiley, 218 p.)

Stuke, M., Schwarz, D. J., & Starkman, G. 2012, JCAP, 03, 040, [arXiv:1111.3954]

Tegmark, M. et al. 2006, Phys. Rev. D, 74, 123507, [arXiv:astro-ph/0608632]

Trotta, R., & Melchiorri, A. 2005, Phys. Rev. Lett., 95, 011305, [arXiv:astro-ph/0412066]

Tseliakhovich, D., & Hirata, C. 2010, Phys. Rev. D, 82, 083520, [arXiv:1005.2416]

Turner, M. S., Steigman, G., & Krauss, L. M. 1984, Phys. Rev. Lett., 52, 2090

Turner, M. S., & Tyson, J. A. 1999, Rev. Mod. Phys. Suppl., 71, 145, [arXiv:astro-ph/9901113]

Ullio, P., Bergström, L., Edsjö, J., & Lacey, C. 2002, Phys. Rev. D, 66, 123502, [arXiv:astro-ph/0207125]

Upadhye, A., Hu, W., & Khoury, J. 2012, Phys. Rev. Lett., 109, 041301, [arXiv:1204.3906]

Uzan, J.-P. 2003, Rev. Mod. Phys., 75, 403, [arXiv:hep-ph/0205340]

——. 2011, Living Rev. Rel., 14, 2, [arXiv:1009.5514]

Valdés, M., Ferrara, A., Mapelli, M., & Ripamonti, E. 2007, Mon. Not. R. Astron. Soc., 377, 245, [arXiv:astro-ph/0701301]

Väliviita, J., Maartens, R., & Majerotto, E. 2010, Mon. Not. R. Astron. Soc., 402, 2355, [arXiv:0907.4987]

Väliviita, J., Majerotto, E., & Maartens, R. 2008, JCAP, 07, 020, [arXiv:0804.0232]

Vanderveld, R. A., Mortonson, M. J., Hu, W., & Eifler, T. 2012, Phys. Rev. D, 85, 103518, [arXiv:1203.3195]

Visbal, E., Barkana, R., Fialkov, A., Tseliakhovich, D., & Hirata, C. M. 2012, Nature, 487, 70, [arXiv:1201.1005]

Weinberg, S. 1989, Rev. Mod. Phys., 61, 1

Weller, J., & Lewis, A. M. 2003, Mon. Not. R. Astron. Soc., 346, 987, [arXiv:astro-ph/0307104]

Wetterich, C. 1988, Nuc. Phys. B, 302, 668

——. 2007, Phys. Lett. B, 655, 201, [arXiv:0706.4427]

Wintergerst, N., Pettorino, V., Mota, D. F., & Wetterich, C. 2010, Phys. Rev. D, 81, 063525, [arXiv:0910.4985]

Wong, Y. Y. 2002, Phys. Rev. D, 66, 025015, [arXiv:hep-ph/0203180]

Wouthuysen, S. A. 1952, Astron. J., 57, 31

Wright, E. L. et al. 1992, Astrophys. J. Lett., 396, L13

Wyithe, J. S. B., Loeb, A., & Geil, P. M. 2008, Mon. Not. R. Astron. Soc., 383, 1195

Xu, X., Cuesta, A. J., Padmanabhan, N., Eisenstein, D. J., & McBride, C. K. 2012, [arXiv:1206.6732]

Yuan, Q., Yue, B., Bi, X., Chen, X., & Zhang, X. 2010, JCAP, 10, 023, [arXiv:0912.2504]

Zdziarski, A. A., & Svensson, R. 1989, Astrophys. J., 344, 551

Zhan, H., Knox, L., & Tyson, J. A. 2009, Astrophys. J., 690, 923, [arXiv:0806.0937]

Zhao, G.-B., Xia, J.-Q., & Zhang, X. 2007, JCAP, 7, 10, [arXiv:astro-ph/0611227]

Zlatev, I., Wang, L., & Steinhardt, P. J. 1999, Phys. Rev. Lett., 82, 896, [arXiv:astro-ph/9807002]

Zygelman, B. 2005, Astrophys. J., 622, 1356